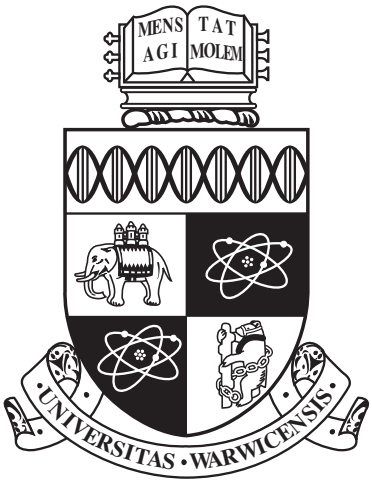

Unmanned Aerial Vehicles (UAVs) for Wireless Communication and Networks: Potentials and Design Challenges

by

Aziz Altaf Khuwaja

Thesis

Submitted to the University of Warwick

for the degree of

Doctor of Philosophy

School of Engineering

May 2021

THE UNIVERSITY OF WARWICK

Contents

Acknowledgments

First and foremost, I thank Almighty Allah for giving me strength and potential to complete this thesis. I owe my sincere and deepest gratitude to my supervisor, Dr Yunfei Chen, for his continuous support, guidance, and suggestions during my PhD study. His inspiring advice, immense knowledge, and experience helps me to conduct research in a very productive manner by publishing impactful papers on UAV communications. I would like to thank him for his time, efforts, and ideas to find the right path for my future career.

I would like to sincerely acknowledge the efforts of Dr Gan Zheng for providing me constructive suggestions and feedback related to the research work during PhD study. His valuable comments helped me to significantly improve the quality of research work throughout my PhD study.

I would like to thank the academic staff of Connected Systems Group to foster conducive environment for research. Also, I would like to thank the members of my progress review panel, Dr Mark Leeson (chair) and Dr Christos Mias (member) for their insightful comments and suggestions. Their expert knowledge has helped me to improve the quality of this thesis significantly. I am very grateful to all the PhD and MScR students of the ComSys Lab for their help and support. In particular, I offer gratitude to my friends, Syed Bilal Tirmizi and Mir Muhammad Lodro.

Most importantly, I am greatly thankful to my family members, Altaf Hussain Khuwaja, Zarina Altaf, Imtiaz Ali, Khairunissa, Razia Ameer Ali, Ghulam Nabi Soomro, Irsa Khuwaja, Izaan Ali Khuwaja, Qurat ul ain, Noor ul ain, Zohra, Ayeza, Shazain, and Naeem Hussain for their sustained encouragement and unconditional love. Specially,

I want to sincerely acknowledge the unconditional sacrifices of my beloved wife, Irsa Khuwaja. Indeed, without her support, I could have never finish this thesis. I would like to dedicate this thesis to them.

Last, but not least, words are not enough to express how thankful I am to Late Prof. Nisar Ahmed Siddique (Founder Vice Chancellor, Sukkur IBA University), Prof. Dr Mir Muhammad Shah (Vice Chancellor, Sukkur IBA University), and Dr Zahid Hussain Khand (Registrar, Sukkur IBA University) to provide financial support and be a constant source of inspiration throughout my career.

Declarations

This thesis is submitted in partial fulfilment for the degree of Doctor of Philosophy under the regulations set out by the Graduate School at the University of Warwick. This thesis is solely composed of research completed by Aziz Altaf Khuwaja, except where stated, under the supervision of Dr. Yunfei Chen between the dates of June 2017 and May 2021. This thesis has not previously been presented in identical or similar form to any other examination board.

Aziz Altaf Khuwaja

May, 2021

Abstract

Unmanned aerial vehicles (UAVs) are mostly considered by the military for surveillance and reconnaissance operations, and by hobbyists for aerial photography. However, in recent years, the UAV operations have been extended for civilian and commercial purposes due to their agile and cost-effective deployment. UAVs appear to be more prolific platforms to enable wireless communication due to their better line-of-sight (LOS) channel conditions as compared with the fixed base stations (BSs) in terrestrial communication which suffer from severe path loss, shadowing, and multipath fading in more challenging propagation environments. In UAV-enabled wireless communications, the UAV can either act as a complementary aerial BS to provide on-demand communication or as an aerial user equipment (UE) which is operated by the existing cellular network. Several challenges exist in the design of UAV communications which include but not limited to channel modeling, optimal deployment, interference generation, performance analysis, limited on-board battery lifetime, trajectory optimization, and unavailability of regulations and standards which are specific for UAV communication and networking.

This thesis particularly investigates some important design challenges for safe and reliable functionalities of UAV for wireless communication and networking. UAV communication has its own distinctive channel characteristics compared to the widely used cellular or satellite systems. However, several challenges exist in UAV channel modeling. For example, the propagation characteristics of UAV channels are under explored for spatial and temporal variations in non-stationary channels. Therefore, first and foremost, this thesis provides an extensive review of the measurement methods proposed for UAV channel modeling and discusses channel modeling efforts for air-to-ground and

air-to-air channels. Furthermore, knowledge-gaps are identified to realize accurate UAV channel models.

The efficient deployment strategy is imperative to compensate the adverse impact of interference on the coverage area performance of multiple UAVs. As a result, this thesis proposes an optimal deployment strategy for multiple UAVs in presence of downlink co-channel interference in the worst-case scenario. In particular, this work presents coordinated multi-UAV strategy in two schemes. In the first scheme, symmetric placement of UAVs is assumed at a common optimal altitude and transmit power. In the second scheme, asymmetric deployment of UAVs with different altitudes and transmit powers is assumed. The impact of various system parameters, such as signal-to-interference-plus-noise ratio (SINR) threshold, separation distance between UAVs, and the number of UAVs and their formations are carefully studied to achieve the maximum coverage area inside and to reduce the unnecessary coverage expansion outside the target area.

Fundamental analysis is required to obtain the optimal trade-off between the design parameters and performance metrics of any communication systems. This thesis particularly considers two emerging scenarios for evaluating performance of UAV communication systems. In the first scenario, the uplink UAV communication system is considered where the ground user follows the random waypoint (RWP) model for user mobility, the small-scale channel fading follows the Nakagami-m model, and the uplink interference is modeled by Gamma approximation. Specifically, the closed-form expressions for the probability density function (PDF), the cumulative distribution function (CDF), the outage probability, and the average bit error rate (BER) of the considered UAV system are derived as performance metrics. In the second scenario, the downlink hybrid caching system is considered where UAVs and ground small-cell BSs (SBSs) are distributed according to two independent homogeneous Poisson point processes (PPPs), and downlink interference is modeled by the Laplace transforms. Specifically, the analytical expressions of the successful content delivery probability and energy efficiency of the considered network are derived as performance metrics. In both scenarios, results are presented to demonstrate the interplay between the communication performance

and the design parameters.

List of Publications

Journal Publication:

1. **Aziz Altaf Khuwaja**, Yunfei Chen, Nan Zhao, Mohamed-Slim Alouini and Paul Dobbins, "A Survey of Channel Modeling for UAV Communications," in **IEEE Communications Surveys & Tutorials**, vol. 20, no. 4, pp. 2804-2821, Fourthquarter 2018.

2. **Aziz Altaf Khuwaja**, Gan Zheng, Yunfei Chen and Wei Feng, "Optimum Deployment of Multiple UAVs for Coverage Area Maximization in the Presence of Co-Channel Interference," in **IEEE Access**, vol. 7, pp. 85203-85212, 2019.

3. **Aziz Altaf Khuwaja**, Yunfei Chen and Gan Zheng, "Effect of User Mobility and Channel Fading on the Outage Performance of UAV Communications," in **IEEE Wireless Communications Letters**, vol. 9, no. 3, pp. 367-370, 2020.

4. **Aziz Altaf Khuwaja**, Yongxu Zhu, Gan Zheng, Yunfei Chen and Wei Liu, "Performance Analysis of Hybrid UAV Networks for Probabilistic Content Caching," in **IEEE Systems Journal**, 2020.

Conference Publication:

1. **Aziz Altaf Khuwaja**, Gan Zheng, Wei Feng and Yunfei Chen, "Coverage Area Performance for Multiple Interfering UAVs," **IEEE Global Communications Conference (GLOBECOM)**, Waikoloa, HI, USA, 2019, pp. 1-6.

List of Tables

List of Figures

Abbreviations

1D One-dimensional

2D Two-dimensional

3D Three-dimensional

3GPP 3rd generation partnership project

3G Third generation

4G Fourth generation

5G Fifth generation

AFD Average fade duration

AOA Angle of arrival

AP Access point

ATC Air traffic control

BER Bit error rate

BFSK Binary frequency-shift keying

BPSK Binary phase-shift keying

BS Base station

CAD Computer-aided design

CASA Civil aviation safety authority

CD Content diversity

CDF Cumulative distribution function

CE2R Curved earth two-ray

CNPC Control and non-payload communication

CNR Carrier-to-noise ratio

CoMP Coordinated multipoint

CW Continuous wave

D2D Device-to-device

EDGE Enhanced data rates for GSM evolution

FAA Federal aviation administration

FANET Flying ad hoc network

FE2R Flat earth two-ray

FD Fade depth

GSM Global system for mobile

GPS Global positioning system

HAP High altitude platform

HF High frequency

IMU Inertial measurement unit

IP Internet protocol

ITU International telecommunication union

LAP Low altitude platform

LCR Level crossing rate

LiFi Light-fidelity

LOS Line-of-sight

LTE Long term evolution

MIMO Multiple-input multiple-output

MMSE Minimum mean squared error

mmWave Milli-meter wave

MRC Maximal ratio combining

NASA National aeronautics and space administration

NLOS Non-LOS

NOMA Non-orthogonal multiple access

OFDM Orthogonal frequency-division multiplexing

OLOS Obstructed-LOS

PDF Probability density function

PDP Power delay profile

PLE Path loss exponent

PN Pseudonoise

PPP Poisson point process

QoS Quality-of-service

RF Radio frequency

RIS Reconfigurable intelligent surface

RMS Root mean square

RTCA Radio technical commission for aeronautics

RWP Random waypoint

SBS Small-cell base station

SC Special committee

SDR Software defined radio

SINR Signal-to-interference-plus-noise ratio

SISO Single-input single-output

SIR Signal-to-interference ratio

SNR Signal-to-noise ratio

TDL Tapped delay line

UAV Unmanned aerial vehicle

UE User equipment

UMTS Universal mobile telecommunications service

US United States

USC UAV-based small cell

USRP Universal software radio peripheral

UTM UAS traffic management

UWB Ultra-wideband

VANET Vehicular ad hoc network

VHF Very high frequency

VLC Visible light communication

WLAN Wireless local area network

WSSUS Wide-sense stationary uncorrelated scattering

Chapter 1

Introduction

1.1 Unmanned Aerial Vehicles (UAVs)

Unmanned aerial vehicles (UAVs) colloquially referred to as 'drones' are continuously shaping the future of smart city applications and revolutionizing commercial operations. For example, DJI's Agras T20 hexacopter can be used for agriculture and crop protection. Traditionally, UAVs are used by military for surveillance and security operations. However, the UAV-based applications ranging from entertainment to telecommunication led to a paradigm shift in realization of UAVs in the civilian domain. Particularly, in the field of telecommunication, the operation of the UAV mounted with wireless equipment is considered as an ingenious solution by both academia and industry to meet the ever increasing communication demand of end users in a variety of scenarios.

Compatibility of the UAV to operate in different applications and environments warrants the selection of an appropriate type of UAV which must take in to account the requirements compelled by the application, environment, and civil aviation regulations. In fact, the efficacy of the UAV-based applications depends on the suitable flying altitude or aerial platform of the UAV. In general, UAVs can be categorized according to their altitudes as the low altitude platform (LAP) and the high altitude platform (HAP). LAPs have the capability to move quickly, and have flexible deployment up to few km. On the other

hand, HAPs are typically quasi-stationary and can attain altitude above 17 km. In comparison with HAPs, LAPs can be more desirable for time-critical applications due to their rapid deployment, for example, the need of communication services in the emergency situations or natural disasters. However, HAPs can be preferable for long-term operations due to their longer endurance, such as Facebook Aquila project and Google Loon flight system, which provides ubiquitous connectivity in the unserved regions.

UAVs can also be classified based on their design, into rotary-wing and fixed-wing UAVs. In rotary-wing UAVs, multiple horizontally-spinning rotors are used to supply the vertical lift and thrust. This allow the rotary-wing UAVs to take off and land, to fly in forward, backward and lateral direction, and to hover. These attributes allow the UAV to be used in congested urban areas which cannot be reached by the fixed-wing UAV. In contrast, the fixed-wing UAVs have outstretched wings to remain aloft in the forward direction. Examples of different UAV types are illustrated in Fig. 1.1 and their attributes are listed in Table 1.1

1.2 Basic Communication Requirements

UAV communications requirement for different applications can be classified into payload communication, and control and non-payload communication (CNPC).

1.2.1 Payload Communication

This type of communication refers to the transmission of the actual intended data or information between the UAV and ground user, such as back-hauling, relaying transmission, sensor data, images, and real-time videos. For example, in aerial photography applications, the captured images need to be transmit to the end user in a timely manner using payload communication. The UAV payload communication mostly occur at much higher data rate with relaxed latency of the order of hundreds of ms. For instance, a data rate of several Mbps is required to assist the transmission of high-definition video, while

Table 1.1: Attributes of different UAV types.

Model	Spreading Wings S1000 DJI	H520E/520 Yuneec	Parrot Disco	MQ-9 Reaper (Predator B)
Ref.	[1]	[2]	[3]	[4]
UAV type	rotary-wing (octocopter)	rotary-wing (hexacopter)	fixed-wing	fixed-wing
Weight	4.2 kg	1.86 kg	750 g	2223 kg
Payload	6.8 kg	500 g	N/A	1746 kg
Range	N/A	up to 3.5-7 km	2 km	1852 km
Endurance	15 minutes (@ 15000 mAh & 9.5 kg take-off weight)	25-30 minutes	45 minutes	27 hours
Altitude	N/A	500 m	N/A	15.24 km
Speed	N/A	72 kph	80 kph	445 kph
Power supply	LiPo (6S, 10000mAh 20000mAh)	LiPo (4s, 6200 mAh)	LiPo (2700 mAh 3-cells)	Honeywell TPE331-10 turboprop engine
Power consumption	Maximum: 4 kw, Hover: 1.5 kw (@ 9.5 kg take-off weight)	N/A	N/A	Engine: 712 kw
Applications	Aerial photography, appropriate to transport packages, and to support cellular BSs and UEs	Aerial photography, and suitable to carry sensors	Recreation	Airborne surveillance, armed reconnaissance, and target acquisition

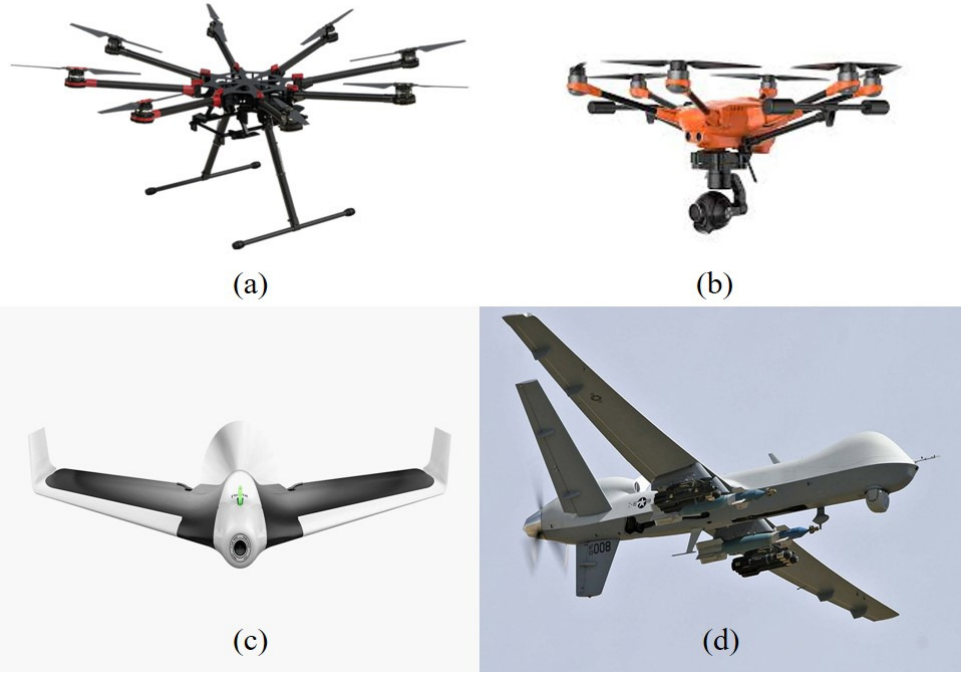

Figure 1.1: Illustrative examples of different UAV types, (a) DJI-Spreading Wings S1000 [1], (b) Yuneec-H520E/520 [2], (c) Parrot Disco [3], (d) MQ-9 Reaper (Predator B). [4]

higher than 30 Mbps is desired for 4K resolution video, and even higher rates i.e. up to tens of Gbps for wireless back-hauling in UAV-enabled communication.

1.2.2 Control and Non-Payload Communication (CNPC)

This type of communication refers to the bi-directional transmission of critical and safety messages between the UAV and ground control station to ensure reliable and effective flight operations. In this regard, the International Telecommunication Union (ITU) has outlined the essential CNPC guidelines to accomplish safe UAV operations as [5]:

- **CNPC for UAV Command and Control**: This consists of navigation database, telemetry report (velocity and flight altitude), real-time UAV control for piloting, identity and flight authorization, and flying course updates for autonomous UAVs.
- **CNPC for Air Traffic Control (ATC) Relay**: It is important to ensure that UAV mis-

sions and applications do not cause any disruption or safety concerns to the operation of the manned aircraft, especially near airports. To this end, the connectivity between the ATC and the ground controller via the UAV, known as ATC relay, is needed.

- **CNPC Supporting 'Sense and Avoid'**: The potential of CNPC to assist 'Sense and Avoid' enables the UAV to maintain safe distance with nearby UAVs, obstacles, and terrain.

Communication and spectrum requirements for CNPC differ from the payload communication. Specifically, the data rate requirement to establish CNPC link is usually low i.e. up to hundreds of kbps, but rather require stringent check on high security, ultra-reliability, and low latency. According to the technical report (release 15) published by 3rd generation partnership project (3GPP) in 2018 [6], the data rate requirement for the command and control of aerial vehicles to support enhanced Long Term Evolution (LTE) is between 60-100 kbps in both uplink and downlink directions, reliability of less than 10^{-3} packet error rate, and a latency of less than 50 ms.

1.3 UAV-Enabled Wireless Networks

The recent advancement in microelectronic technology shrinks the size and thus reduces the weight of wireless network equipment, allowing new ways to employ wireless network infrastructure. From a networking perspective, UAV-mounted wireless modules can provide more flexibility in terms of easy deployment and offer cost-effectiveness. In general, the aerial communication platform can be categorized, based on the functionality of the UAV, into aerial base station (BS) and aerial user equipment (UE). In the former case, an aerial BS can be used in the UAV-assisted networks to support the future wireless technologies and also provide on-demand wireless communication services. In the latter case, an aerial UE can be used in the cellular-connected UAV networks to communicate with the ground UEs by using the cellular core networks, where the inter-

connectivity is performed by the licensed spectrum of the existing mobile networks.

Future wireless networks need to satisfy the demands of the ubiquitous coverage and reliable high-speed communication. Despite these benefits, the establishment of new wireless networks confronts many challenges, such as spectrum scarcity, limited space to setup new infrastructure, and high deployment cost. Another problem arises when the communication resources are overwhelmed or existing ground networks fails to satisfy the demand of wireless connectivity. To this end, the use of the UAV as an alternative aerial communication platform can complement the future wireless network that can provide seamless connectivity to the ground users. Moreover, the agility of UAV deployment make it possible to effectively address the objectives of future wireless networks. The benefits of UAV-assisted networks and cellular-connected UAV networks are further discussed next.

1.3.1 UAV-Assisted Communication Networks

During unexpected events or temporary situations, it is infeasible to invest in installation of the terrestrial infrastructure that will generate revenue for a very short duration. A plausible solution to this problem is using LAP-UAV as an aerial BS that provide communication services to the end users in the form of 'UAV-cells' as shown in Fig. 1.2. Furthermore, UAVs are used as aerial relays to overcome the hurdles of deploying terrestrial relays. The benefits of using aerial BSs in UAV-assisted networks includes but not limited to:

- **Ubiquitous Coverage**: Aerial BS featured with robust deployment, flexible configuration, and line-of-sight (LOS) links, have capability to facilitate the ubiquitous wireless coverage in presence of the existing communication infrastructure. Two example scenarios are the traffic offloading from the ground BSs in the extremely crowded events and rapid formation of ad hoc networks due to partial or complete damage of infrastructure in case of natural calamity.

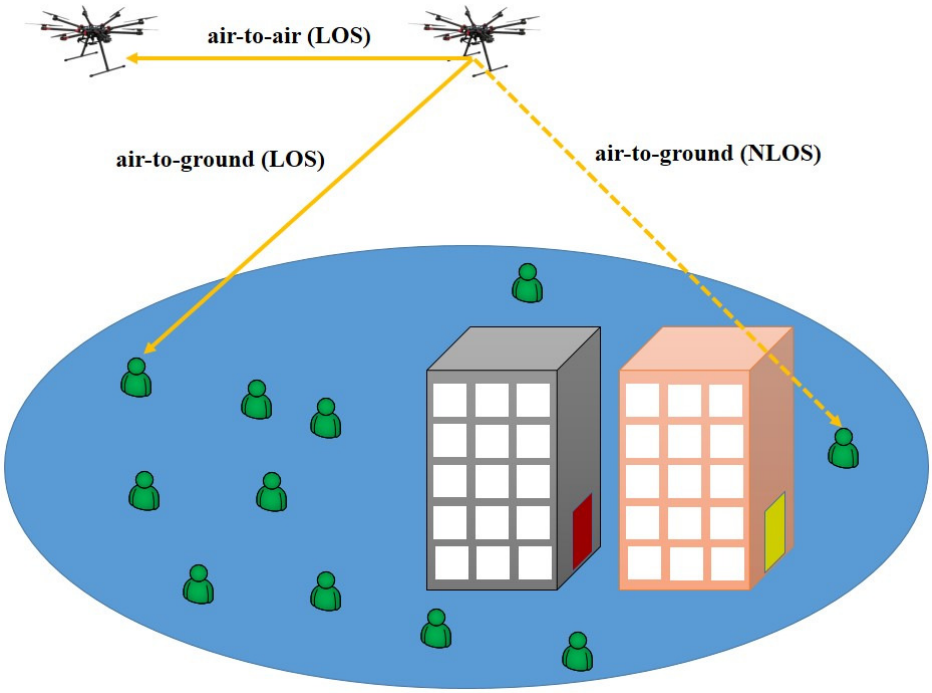

Figure 1.2: Illustration of the deployment of an aerial BS in the UAV-assisted network to serve the multiple ground users.

- **Supporting Future Wireless Technologies**: The new wireless technologies, such as milli-meter wave (mmWave) communications, massive multiple-input multiple-output (MIMO), and ultra-dense small-cell networks have emerged to enhance capacity in high-mobility environment. In this case, aerial BSs can be used as an integral component of the future wireless network if they are properly operated and deployed. Furthermore, the communication performance can be further improved by jointly designing the adaptive communication with the UAV mobility control. For instance, when UAV encounters better air-to-ground channel conditions, it can lower its altitude to attain higher transmission rate and sustain good wireless connectivity with the ground user to transmit more data.

- **Aerial Relaying**: In absence of the reliable point-to-point communication link, UAVs are deployed to establish long-haul wireless connectivity between two or more remotely located ground terminals. For instance, this could be distant ter-

restrial BSs.

These evident benefits may not be possible with a fixed infrastructure. Consequently, Ericsson and China Mobile have initiated field measurements to develop a fifth generation (5G) prototype enabled by drone UAVs [7]. In another example, Qualcomm is interested to deploy the 5G networks by using LAP-UAVs [8].In addition, AT&T roll-out temporary LTE cell site with the help of helicopter in Puerto Rico, where the infrastructure was completely destroyed by hurricane Maria in 2017. Thus, an aerial BS can serve as an independent communication platform in UAV-assisted networks to incorporate the needs of future wireless networks and complement the existing ground infrastructure to provide on-demand communications.

1.3.2 Cellular-Connected UAV Networks

UAVs have been envisioned as an innovative way of deploying new aerial UEs that utilizes cellular networks for their operations, as depicted in Fig. 1.3, where UAVs are used for aerial wireless relaying, parcel delivery, and photography. Wireless cellular network is intrinsic technology to serve the UAV because of its ability to provide wider coverage, continuous connectivity, high throughput, and low latency. Some appealing advantages of the cellular-connected UAV networks are discussed as follows :

- **Ubiquitous Accessibility**: Aerial UEs are controlled remotely by the ground pilot due to the worldwide availability of the cellular networks, which enable the UAV to collect and transmit data from virtually unlimited operational range. Also, it effectively maintains the wireless connectivity between the UAV and end user, regardless of its location. For instance, live videos can be sent directly from the UAV to the worldwide audience.

- **Enhanced Privacy and Security**: Advance authentication mechanism in cellular technologies make it possible to protect un-authorized access control of aerial UEs in the cellular-connected networks.

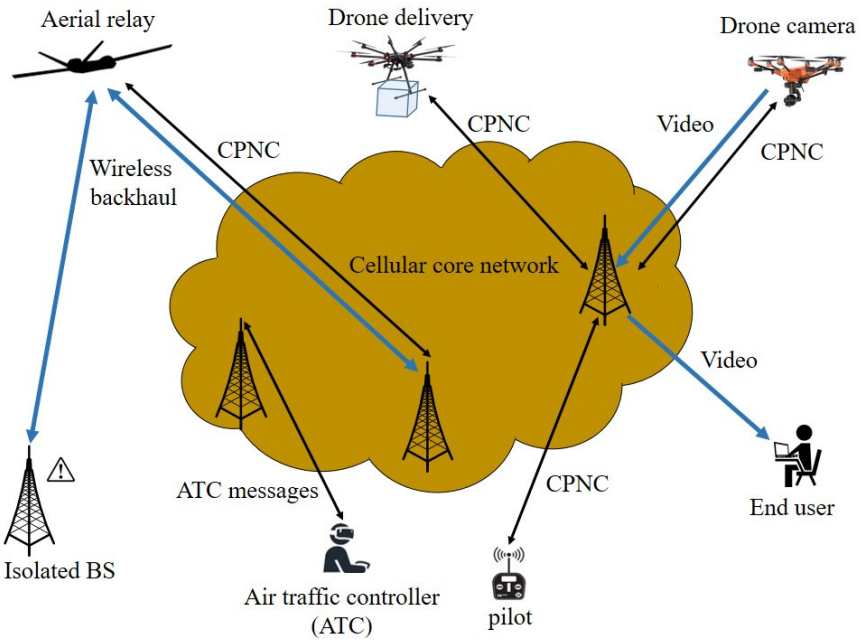

Figure 1.3: A Schematic of three use cases of cellular-connected UAV network: aerial wireless relaying, drone delivery, and drone camera.

- **Cost-Effectiveness**: Aerial UEs in the cellular-connected networks can utilize the licensed mobile spectrum for payload communication. Consequently, the well placed mobile spectrum can support widespread, high quality, and affordable UAV connectivity with sufficient capacity to allow competitive services. Trials have been conducted to exhibit that the existing mobile network can support the UAV connectivity up to the altitude of 122 m [8]. This means that the rapid growth of the UAV market can be supported by the mobile spectrum and no new network or technology investment is needed.

- **Facilitate Monitoring and Management**: Dense air traffic monitoring and management can be effectively achieved through aerial UEs of the cellular-connected networks. For example, with proper legislation and regulation, whenever mandatory, the ATC could legally take control of the UAV to avoid any foreseen safety threat in timely manner.

- **Robust Navigation**: Cellular-connected aerial UE enables robust navigation. Usu-

ally, UAV navigation depends on the satellite-based global positioning system (GPS). However, it is susceptible to disruption due to the atmospheric conditions or blockage from the high-rise buildings. One promising solution to get rid of this problem is to consider differential GPS in cellular-connected aerial UE, where the UAV navigation is achieved through the cellular networks.

Despite the above-mentioned advantages of the cellular-connected aerial UEs, the propagation conditions for air-to-ground channels are completely different from the terrestrial channels. The down-tilted terrestrial BSs are intended to provide communication services to the ground UEs and may not to the aerial UEs. Moreover, the ground UEs are less dynamic than the aerial UEs. Another issue is that the cumulative co-channel interference increases as the UAV altitude increases due to the better aerial connectivity and thus aggravate the uplink performance. Therefore, a new three-dimensional (3D) paradigm has to be adopted for the services and techniques to access the classical wireless networks via aerial UEs.

1.4 Design Challenges

Beside many advantages of UAVs, several key challenges must need to be addressed for the effective utilization of aerial BSs and UEs for communication and networking. The key challenges discussed in this section are channel characteristics, optimal deployment of UAVs, performance evaluation, interference generation, and the limited on-board UAV energy. Other challenges pertinent to UAV communications include but not limited to the airframe shadowing, trajectory optimization, security in case of cyber-physical attacks, back-haul connectivity, and standardizations and regulations.

1.4.1 Unique Channel Characteristics

The propagation channel in any wireless communication network is the air interface between the transmitter and the receiver for the transmission of the electromagnetic

waves, such as radio waves. The design of UAV-enabled networks is impractical without the proper understanding of the wireless channel. Therefore, radio characterization and channel modeling in the UAV network architecture becomes of the utmost importance.

The vast majority of the work related to channel modeling has been carried out for terrestrial radio channels. However, these models may not be applicable for the UAV-enabled wireless communication. UAV communications consist of air-to-ground propagation to provide services to the ground users and air-to-air propagation to connect multiple airborne UAVs. A distinctive feature of the air-to-ground channel implies an altitude-dependent probability for the LOS propagation. As a result, at higher altitudes, the communication performance improves with the higher link reliability and requires lower transmission power. Even with non-LOS (NLOS) propagation, received power variations are comparatively less severe in UAV communications because only the ground-base side of the air-to-ground link is mostly surrounded by the obstacles that affect the propagation. On the other hand, air-to-air channels are mostly experiencing strong LOS propagation similar to the high-altitude air-to-ground channels. Fig. 1.2 depicts the air-to-ground and air-to-air propagation scenarios using aerial BS in the UAV-assisted network.

The choice of an appropriate channel model depends on the application requirements and expected outcomes. When an estimated result is required for the large set of area, it is more practical to consider a simple channel model to recapture general propagation trends. For example, the log-distance with a constant path loss exponent (PLE) is an appropriate choice. However, a complex channel model is needed in case of more specific environments. The most complete air-to-ground channel model must consider:

- Path loss effects, and large-scale and small-scale fading mechanisms
- air-to-ground propagation segment (high-altitude air-to-ground, obstructed air-to-ground, only ground)
- Different types of environment (rural, suburban, urban, dense urban)

- Separate parameters for LOS and NLOS propagation
- UAV dynamics (Doppler shift)

1.4.2 Optimal Deployment

One of the key design challenges in the practicability of UAV-enabled wireless networks is the proper deployment of the UAV in the 3D space to cater for the instantaneous traffic demand. In fact, the potential of UAV mobility offers extra degrees of freedom for effective deployment. For a single qausi-stationary LAP-UAV acting as an aerial BS, optimal deployment aims to achieve a maximum ground coverage while meeting a specific threshold and to fulfil certain quality-of-service (QoS) requirements. In this regard, UAV altitude is one of the most important design parameters to control the propagation distance and consequently, the average path loss. To find the optimal altitude, it is necessary to simultaneously consider the impact of both the LOS probability and propagation distance. However, it is possible that the radio frequency (RF) section of the UAV consists of the tilted directional antenna. In this case, antenna tilt angle and antenna beam-width should be taken in to account to formulate the optimization problem for the UAV deployment.

Multiple UAVs provide more flexibility in terms of performing different tasks at the same time and if necessary, re-position themselves. However, the placement optimization problem of multiple UAVs becomes even more challenging due to the received co-channel interference from different UAVs during downlink transmission. Thus, the effect of co-channel interference must be taken in to account to analyze the coverage performance. To this end, beyond the optimal altitude, the optimal separation distance between UAVs should also be determined to mitigate the impact of co-channel interference. The propagation environment can also influence the strategy to optimally deploy UAV in order to cover maximum ground users. In general, the propagation environment is classified on the basis of terrain features namely, flat, mountainous or hilly, and over water body. A specific terrain can have covering in the form of tree canopy,

forest, and buildings. The ITU has further categorized urban terrain as rural, suburban, urban, dense urban, and high-rise buildings [9]. In this case, UAVs can adjust their altitude based on the urban scenario. For instance, in suburban environment the UAV may fly at the lower to attain the higher LOS probability and the lower path loss. In contrast, UAVs may fly above the rooftop level in the urban environment to maintain higher LOS connectivity.

1.4.3 Performance Analysis

In any communication network, it is important to provide fundamental analysis to evaluate the effect of resource constraints on performance limits. However, the salient features of the UAV-enabled networks are the UAV mobility in 3D space and the altitude-dependant channels, which complicates the overall system modeling and consequently, its performance analysis. In both UAV-enabled and terrestrial communications, performance analysis depends on the QoS requirements and similar performance metrics can be used, such as signal-to-interference-plus-noise ratio (SINR), coverage probability, throughput, latency, spectral efficiency, and energy efficiency. Furthermore, in UAV-enabled networks, new performance metrics, such as energy consumption and mission completion time, are of practical interest. Such performance evaluations can shed new light on the inherent trade-offs between the different system parameters and the expected performance while designing the UAV-enabled networks for a particular mission or application.

1.4.4 Interference Generation

One major design consideration of the UAV-enabled networks is the severe interference during downlink and uplink communications, which is illustrated in Fig. 1.4 and Fig. 1.5 for the UAV-assisted network and cellular-connected UAV network, respectively. In comparison with conventional terrestrial networks, the interference in UAV-enabled networks is more aggravated due to the dominant LOS channel between the ground user

and the UAV at higher altitude. For the downlink communications in UAV-assisted networks, the intended ground user may receive severe interference from a number of the neighbouring aerial BSs that are not linked with it. Moreover, downlink communications in the cellular-connected UAV networks, aerial UE receive extreme levels of interference from the large number of ground BSs due to the strong LOS channel. As a result, it is expected that the ground UE would have superior performance to an aerial UE. On the other hand, for the uplink communications in the UAV-assisted networks, the desired UAV receives strong interference from non-associated ground users. In the cellular-connected networks, the aerial UE could also pose strong interference to many adjacent but non-associated BSs and result in a new 'exposed BS' interference issue. Thus, the unique air-to-ground and air-to-air channels constitute distinct interference characteristics, which requires effective interference mitigation techniques to design the UAV-assisted and cellular-connected UAV networks.

1.4.5 Energy Limitations

Commercial UAVs are usually battery operated and thus have a finite amount of onboard energy to power circuits for communication purposes, such as transmission and data processing, and also propulsion energy to support mobility and maintain UAV's airborne. Propulsion energy (mostly of the order of a kilowatt) is generally several orders of magnitude higher than the communication energy (mostly of the order of watts).

In conventional wireless communication, the trade-off between the throughput and energy is basically rooted in the Shannon's capacity theorem, which explicitly determine that the channel capacity or achievable throughput increases monotonically with the transmission power. One useful performance metrics emerge from the throughput-energy trade-off is the energy efficiency that defines the number of bits transmission by using a Joule of RF circuit energy. In UAV-enabled communication, the impact of propulsion energy on the UAV trajectory determines the throughput-energy trade-off. For example, to increase the throughput, and considering that the UAV transmits at its

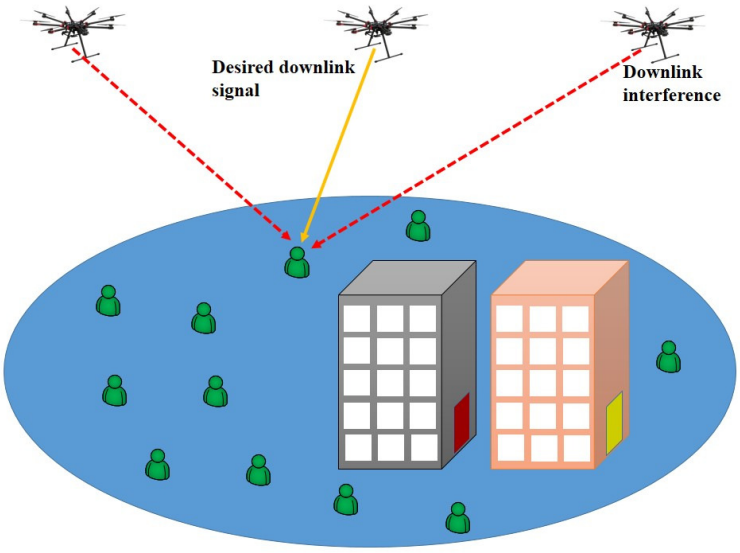

(a) Downlink interference

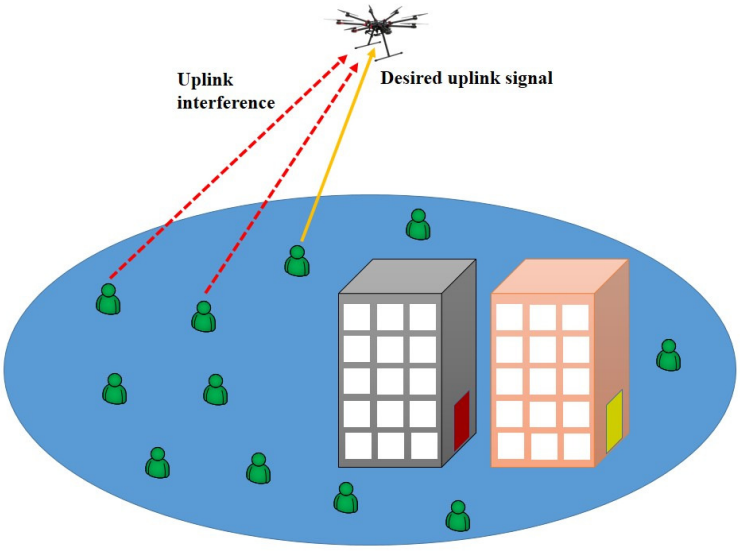

(b) Uplink interference

Figure 1.4: Illustration of interference generation in the UAV-assisted network.

maximum power, each UAV needs to fly at a faster speed in order to reach sufficiently close to the serving ground users and stay their as long as possible (given a limited flight time) to establish dominant LOS channels with them. In addition, each UAV may require to abruptly change its altitude and make sharp turns to avoid blockage. All these will contribute to the consumption of the substantial amount of propulsion energy. There-

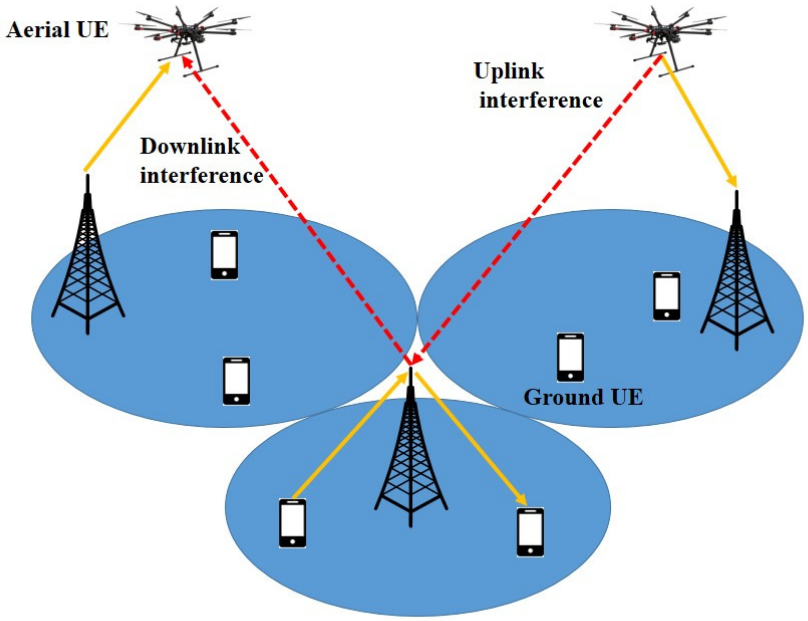

Figure 1.5: Illustration of interference in the cellular-connected UAV network.

fore, energy efficiency for UAV communications is the measure of information bit transmission per Joule of propulsion energy. This new measure has a critical significance to design the UAV-enabled networks because it will determine the duration of the mission, where maximum number of information bits need to be transmitted by consuming finite amount of on-board energy. The UAV energy consumption also depends on the weather conditions, for instance, UAVs may requires more propulsion energy in case of air turbulence to keep them hovering.

1.5 Scope of the Thesis

1.5.1 Research Motivation

Although UAV-based technologies have been extensively studied as a promising candidate for the future wireless networks and to provide on-demand communication, there are still some design challenges listed in Section 1.4 that require further investigation.

The first and foremost challenge of the UAV-enabled communication network is channel modeling due to the UAV dynamics. Specifically, any variations in the position of the UAV can affect the channel characteristics. In addition, the air-to-ground propagation channel is overly dependent on the altitude of the UAV and the type of the propagation environment. There are number of studies that organize and summarize recent research efforts related to UAV communications. For instance, the survey in [10] discussed the utilization of HAPs for wireless broadband communication. Furthermore, it presented the major benefits of HAPs compared to satellite and terrestrial networks. References [11] and [12] reported some of the outstanding issues to deploy UAVs as flying ad hoc networks (FANETs). From a communication and networking viewpoint, [13] surveyed the requirements and characteristics of UAV networks. Reference [14] presented a survey on the challenges related to the UAV-based IoT services. In [15], the authors presented the research efforts related to the space-air-ground integrated networks for 5G and beyond 5G technologies. Key challenges and the open research problems regarding networking and security, collision avoidance, and UAV charging were outlined and identified in [16]. The work in [17] provided important issues of UAV-enabled cellular networks, such as UAV types, standardization efforts by 3GPP, vendor prototypes of aerial BSs, regulations, and cyber-security. In [18], the authors provided a comprehensive overview of the UAV networks from the cyber-physical system view-point. These surveys address the important problems of UAV communications. However, they mostly limit their discussion on the issues and use cases of UAV-enabled wireless networking and overlooked channel models for UAVs. Therefore, there is a need to gather largely fragmented and sparse studies related to the channel modeling of UAV communications, which will provide comprehensive overview of the potential opportunities and major challenges in deploying UAVs as aerial BSs and aerial UEs in UAV-assisted and cellular-connected UAV networks, respectively.

Another challenging task is the optimal deployment of UAVs, which depends on many factors, such as the objective of deployment (e.g. to achieve maximum coverage

and thus accommodate many ground users), position of ground users, and altitude-dependent channel characteristics. As a result, significant attention has been devoted to the optimal deployment of UAVs. In [19], the authors found the optimal altitude to achieve a maximum coverage with a single UAV. In this work, the average path loss was compared with a specified threshold to determine the deterministic coverage range. As shown in [19], the LOS probability between UAV and ground user decreases at very low altitudes due to the shadowing. On the other hand, high LOS probability exists at very high altitudes. However, due to the large propagation distance, the path loss increases and consequently, degrades the coverage performance. Thus, the effect of both propagation distance and LOS probability should be considered together to obtain the optimal altitude. The deployment of multiple UAVs is even more challenging due to the co-channel interference. Reference [20] extended the results of [19] while considering two interfering UAVs and derived optimal separation distance between them to mitigate the impact of interference. The work in [21] determined the efficient 3D deployment of multiple aerial BSs while minimizing the number of UAVs required to serve all the ground users within a target area. In [22], the authors analyzed the 3D placement of UAVs with a objective to accommodate maximum number of ground users by the UAV. The work in [23] studied the impact of the UAV altitude on the maximization of sum-rate in the UAV-assisted ground network. For the disaster relief scenario in [24], the authors proposed evolutionary algorithms to find the optimal deployment of LAPs and portable BSs. As found in [24], the required number of portable BSs significantly reduces as the number of LAPs increases. However, high interference induces due to the large number of LAPs, which degrade the overall coverage performance. Despite the notable number of studies on the deployment of UAVs as aerial BSs, they mostly ignore the problem of coverage maximization in presence of the co-channel interference while utilizing the minimum transmit power. In case of multiple UAVs, the separation distance between them is an important design parameter which should be optimized to mitigate the interference effect and consequently provide the maximum ground coverage within a specific target

area.

In any wireless communication technology, fundamental evaluation needs to be done to determine its intrinsic trade-off and thus devise effective methods to improve the overall performance. However, different from the conventional terrestrial networks, performance analysis in the UAV-enabled system mostly depends upon the UAV mobility and distinct air-to-ground channel characteristics. The work in [25], considered the use of a stand-alone UAV as an aerial BS. Specifically, the authors provided a tractable analytical framework for the average coverage probability and sum-rate of the UAV that coexists with the under-laid device-to-device (D2D) communication network. As observed in [25], the optimal UAV altitude exists to maximize the coverage and the system sum-rate. The authors in [25], derived the closed-form expressions for the coverage probability for the downlink transmission between multiple UAVs and ground users. In particular, the work in [25] used the tools from stochastic geometry to analyze the coverage performance of a finite UAV network that considered a Nakagami-m fading channel for air-to-ground communications. In [26], the analytical expressions for the outage probability were derived for air-to-ground cooperative communication networks that consist of a single UAV and the randomly distributed relays on the ground. Moreover, [26] considered the Rician distribution to characterize the small-scale fading between the UAV and any ground node. In [27], the authors investigated the coverage performance of multiple mobile UAVs moving randomly in a 3D cylindrical region while serving a reference ground UE in a finite network. In particular, the work in [27] used the mixed mobility model for mobile UAVs, free-space path loss model for capturing large-scale effects, and a Nakagami-m distribution for representing small-scale fading. In [28], the authors evaluated the coverage performance of the UAV-assisted cellular networks while considering the limited on-board battery of UAVs. The works in [25–28] mostly considered the static ground users and ignored the impact of ground user mobility on the performance evaluation. It is evident from the literature [29, 30] that the ground user mobility effects the performance of different communication systems, for instance, a visible light commu-

nication (VLC) system in [31] and indoor Light-fidelity (LiFi) system in [32]. Therefore, there is a need to study the impact of ground user mobility on the performance of UAV-enabled communication systems.

The combination of UAV communications and edge-caching is a promising solution for off-loading telecommunication traffic in the hot-spot areas and dissemination of information in the wireless networks. In this case, the end user can directly receive the requested content from the UAV acting as an aerial caching node. As a result, the traffic load from the back-haul connectivity will be reduced. However, the aspects of caching and UAV are often studied sparsely in the literature. Moreover, the recent studies [33, 34] on caching in the UAV-enabled networks, largely ignored the performance analysis and energy efficiency of such networks in presence of the cache-enabled small-cell ground networks. Therefore, it is important to formulate the design guidelines for the practicability of the UAV-enabled network that coexists with the samll-cell network in the form of cache-enabled hybrid network.

1.5.2 Chapter Outlines

Motivated by the above observations, this thesis aims to present a comprehensive overview of the channel modeling efforts for UAV communications. Furthermore, the impact of multiple UAVs and their co-channel interference on the coverage area performance is studied for optimal multi-UAV deployment. Performance of the UAV-enabled networks is analytically evaluated in this thesis for two compelling scenarios. First, when the mobile ground users access a stand-alone aerial BS in uplink transmission and uplink interference is generated by them. Second, when multiple UAVs are acting as cache-enabled aerial nodes. Each chapter consists of the introduction and conclusion sections in order to get better insight of the research problem and to understand the overall summary of the chapters. The rest of this thesis is organized as follows:

Chapter 2 presents a comprehensive overview of the channel characterization efforts for UAV communications. Specifically, the empirical channel models obtained from

measurement campaigns are presented and consequently reported with their large-scale and small-scale fading statistics for both the air-to ground and air-to-air channels. Moreover, this chapter reviews the analytical channel models for air-to-ground propagation and categorizes them into deterministic, stochastic, and geometry–based stochastic models. Finally, the key issues related to the advancement of the UAV channel modeling are discussed.

Chapter 3 proposes the optimal deployment strategy for the multiple UAVs acting as an aerial BSs in the presence of downlink interference. In particular, two deployment scenarios are considered. In the first scenario, symmetric placement of UAVs is assumed at a common optimal altitude and transmit power. In the second scenario, asymmetric deployment of UAVs with different altitudes and transmit powers is assumed. Then, the coverage area performance is investigated as a function of the separation distance between UAVs that are deployed in a certain geographical area to satisfy a target SINR threshold. In this case, the ground user is located at the cell boundary to represent the worst-case scenario.

Chapter 4 analytically characterizes the impact of ground user mobility, propagation environment and fading channel on the outage and error performances of UAV communications for the system model that consists of a single aerial BS. Specifically, the statistics of the signal-to-noise ratio (SNR) and signal-to-interference ratio (SIR) are derived. Moreover, the closed-form expressions for the outage probability and bit error rate (BER) are obtained in the noise-only scenario by using the random waypoint (RWP) model for ground user mobility, air-to-ground channel models for different propagation environments and the Nakagami-m model for small-scale fading. Furthermore, the outage analysis considered the effect of the co-channel interference in uplink transmission by both the stationary and mobile ground users.

Chapter 5 models a hybrid caching network which comprises of the cache-enabled multiple UAVs and ground small-cell BSs. This chapter uses the tools from the stochastic geometry to define the random deployment of cache-enabled UAVs and ground small-

cell BSs. First, the association probability for the ground user affiliated with a UAV and ground small-cell BS is derived. Then, the performance of the hybrid network is evaluated with the help of the successful content delivery probability while considering the impact of both the inter-cell and intra-cell interference during downlink transmission. Furthermore, the energy efficiency of the hybrid network is computed and compared with the stand-alone UAV and ground networks. Finally, a caching scheme is proposed to improve the successful content delivery performance by managing the content popularity. In the proposed scheme the part of the caching capacity in each UAV and ground small-cell BS is reserved to store the most popular content, while the remaining stores less popular contents.

Finally, Chapter 6 summarizes the main body of this thesis, and discusses future work on UAV communications and on some UAV-enabled applications.

Chapter 2

Channel Modeling for UAV Communications

2.1 Introduction

UAV communications have seen dramatic development in a variety of applications. Most of these deploy UAVs as LAPs. In order to ensure safety and high reliability of UAVs for wireless communication applications, it is of utmost importance to thoroughly characterize communication channels. Many research organizations and standardization bodies have worked together to establish pragmatic UAV frameworks. For example, in 2013, the special committee (SC-228) was formed by the Radio Technical Commission for Aeronautics (RTCA) to frame minimum performance standards for UAV operations [35]. In 2016, RTCA has also established the drone advisory committee to ensure the safe introduction of UAVs into the United States (US) national airspace system [36]. In January 2020, the Aeronautics Research Mission Directorate of the National Aeronautics and Space Administration (NASA) partnered with the Federal Aviation Administration (FAA) to launch the UAS Traffic Management (UTM) project with an aim to conduct research on enabling small size drones to safely access the LAP for beyond visual LOS operations [37].

The unique features that distinguish UAV communication and its channel characteristics from the conventional communication include:

1. terrestrial radio channels mostly experience severe path loss, shadowing, and multipath fading, whereas air-to-air and air-to-ground channels generally encounter dominant LOS between UAVs and ground users;

2. highly dynamic communication channel characteristics for air-to-air and air-to-ground propagation due to the UAV velocity;

3. excessive spatial and temporal variations induced in the non-stationary channels due to the mobility of both the UAV and the ground devices;

4. airframe shadowing caused by the structural design and rotation of the UAV.

In the diverse propagation environment where UAVs operate, these features become more challenging. The main difference between UAV communications with UAVs deployed in 3D space and conventional cellular communications with fixed BSs in a two-dimensional (2D) plane is that the movement of UAVs can worsen problems with coverage and connectivity by inducing severe non-stationarity. On the other hand, UAVs can be a viable solution to provide on-demand communications and form an emergency wireless network in cases of terrestrial disruption. Also, compared with satellite communication, UAV is cost-effective, having lower latency, and mostly performs better under SNR and SINR constraints. Propagation characteristics for terrestrial cellular systems are often corroborated using well-established empirical and analytical models. Satellite links for land mobile systems have also been thoroughly investigated in the literature [38, 39]. However, for different network formations and operations, these models are often not well suited for characterizing UAV channels. To this end, UAV communication is still in its infancy and no well-established standard has been proposed.

Reliable analytical models are necessary to evaluate the performances of different wireless techniques. Generally, for air-to-ground channels in UAV communications,

modeling approaches can be classified into three categories. The first approach is to develop deterministic models using environmental parameters. Such models are useful for studying large-scale fading effects in the channel [40, 41]. Hence, the propagation conditions can provide coverage analysis and indicate the optimal UAV position [19],[42–45]. The second approach is to develop a tapped delay line (TDL) model to characterize the direct path as well as the multipath components. Then wideband frequency-selective parameters can be derived from the channel impulse response [46–48]. This approach is particularly important if non-stationarity exists in the air-to-ground channel. Finally, geometric-based stochastic models are desirable for evaluating spatial-temporal characteristics in a geometric simulation environment. This approach is preferable for characterizing the air-to-ground channel in a 3D plane with less environmental parameters [49–54].

However, empirical studies are essential to authenticate or disprove theoretical models. Practically the choice of aerial platform in terms of its altitude has presented some opportunities and challenges. High altitude UAVs are capable of operating in the upper layer of the stratosphere [55] where the coverage performance is completely dependent on LOS propagation, and marginally relies on the elevation angle. Atmospheric effects and propagation delay are bottlenecks in their modeling, but multi-tier HAPs can expand the UAV coverage and provide a generic communication framework of next-generation aerial heterogeneous networks. In contrast, for LAPs, the deployment of commercial UAVs are limited by civil aviation regulations [56]. For instance, a maximum limit of 120 meters is permitted by the FAA in USA [57] and the Civil Aviation Safety Authority (CASA) in Australia [58]. In United Kingdom, according to the regulations set by the Civil Aviation Authority, the maximum allowable altitude for recreational drones that weight less than 25 kg is 120 meters above the surface [59]. This altitude range is feasible for power-limited UAVs to meet the QoS requirements of end users confined within the small-cells. In this case, optimum placement of the UAV and the characteristics of the environment determine the major channel parameters. However, the power consump-

tion and endurance time of UAVs are the performance limitation factors for both cases. Most of the work reported in the literature [60–74] is pertinent to air-to-ground channel characterization based on measurements with manned aircrafts at HAP. However, these findings cannot be directly applied to single-hop UAV networks deployed at lower altitudes due to the demand for a high data rate, low latency and continuous connectivity. It is evident from the studies in [75–111] that the impact of the UAV placement and the surrounding environments is significant for the propagation characteristics of UAV communications due to time and frequency selectivity in the dynamic UAV channels and can lead to fading. However, less research efforts have been made to tackle shadowing induced in air-to-air and air-to-ground channels by the UAV's structural design and maneuvering. In addition, the wide-sense stationary uncorrelated scattering (WSSUS) assumption may be violated in some UAV-aided applications. Thus, in order to avoid over exaggerated performance evaluation from analytical and empirical channel models, it is important to estimate the fading statistics within stationary intervals. Unlike the air-to-ground channel, the air-to-air propagation channel is predominantly important in multi-hop UAV networks for sensing and coordination applications, and for backhaul wireless connectivity to complement existing communication systems. Moreover, the propagation characteristics of air-to-air channels are similar to that in free space and largely dependent on strong LOS conditions and ground reflection effects. In the literature, the air-to-air propagation channel has been empirically characterized using low power radios based on the IEEE 802.15.4 [89–91] and IEEE 802.11 standards [92, 94]. But these studies only reported large-scale fading statistics, while the impact of antenna orientation and the Doppler spectrum of the air-to-ground channel are largely unstudied.

Despite the importance of channel modeling in UAV communications, very few survey studies are available in the literature. For instance, reference [11] identified key issues related to the formation of multi-UAV network, but that survey focuses more on the communications and especially the control of the UAV. Aerial networking characteristics and requirements were reviewed in [13] for civil applications, however, that survey

mainly discussed the communications aspects of UAVs, in particularly network layer designs. Both [11] and [13] barely touch on channel modeling. On the other hand, the physical layer characterization of the air-to-ground channel in the L and C bands was comprehensively reviewed in [112]. However, practical measurements reported in this paper were mainly for aeronautical communications and land mobile satellite systems in the L and C bands. Motivated by these observations, this chapter reviews the current advances in UAV channel characterization.

The main contributions of this chapter are summarized as follows:

- Measurement campaigns have been reported for small size UAVs at lower altitudes and these campaigns are categorized based on the channel sounding methods.
- The empirical channel models obtained from the measurement campaigns are tabulated and the large-scale and small-scale statistical parameters of air-to-ground and air-to-air channels are reported.
- The analytical channel models used for UAV communications are categorized as deterministic, stochastic, and geometry-based stochastic models.
- Some of the important issues are highlighted that are pertinent to UAV channel modeling which include, airframe shadowing, stationary interval, and multi-antenna diversity gain.
- Finally, open research challenges are thoroughly investigated for conducting UAV measurement campaigns and developing propagation channel models.

The rest of the chapter is organized as follows. Section 2.2 reviews the measurement campaigns conducted by using UAVs at LAPs. The characterization of air-to-air and air-to-ground propagation using empirical channel models is discussed in Section 2.3. Section 2.4 categorizes the analytical UAV channel models as deterministic, stochastic, and geometry-based. Section 2.5 highlights some important issues pertinent to airframe shadowing, non-stationary channels, and applicability of diversity techniques in

UAV communications. Section 2.6 discusses some open research challenges for UAV measurements and channel modeling. Section 2.7 summarizes the main conclusions of this chapter.

2.2 Measurement Campaigns

The actual behavior of the propagation channel can be better understood via field measurements. UAV channel characterization mainly depends on the operational environment, propagation scenario (air-to-air or air-to-ground), channel sounding process, antenna orientation, UAV deployment in 3D space, and flight dynamics.

In the literature, most of the measurement campaigns have been conducted using two types of aerial vehicles. The first type are small and medium sized manned aircraft. For instance, in [46–48], a S-3B Viking aircraft was used to comprehend the air-to-ground channel characteristics in the L and C bands in different environments. In [65], a Cessna-172S aircraft was used to evaluate the performance of a 4×4 MIMO enabled orthogonal frequency-division multiplexing (OFDM) system for the air-to-ground channel. In [66] and [67], a UH-1H military helicopter was used to study the air-to-ground channel in a 4×2 MIMO configuration to achieve diversity gain and to mitigate inter-symbol interference in frequency-selective channels. In [68], a news-reporting helicopter was used to attain spatial multiplexing gain and throughput for airborne communication in 2×2 MIMO settings. The logistics involved in the measurement campaigns using manned aircraft are expensive and daunting. Therefore, the second type of aerial vehicles i.e., UAVs are preferable to reduce the cost. In this case, the UAV payload is often integrated with an on-board processor to control flight dynamics and wireless equipment to collect data. In addition, the experimental setup also contains antennas to radiate and receive RF signals, a GPS system to record telemetry data, and an inertial measurement unit (IMU) to measure flight dynamics, such as pitch, yaw, and roll angles. The rest of the chapter mainly focus on measurement campaigns using UAVs.

2.2.1 Narrowband Measurement Systems

These systems evaluate the Doppler frequency shift and the channel gain experienced by narrowband continuous wave (CW) signals using a channel sounder that generates pilot tones at a single carrier frequency. Examples of narrowband measurement campaigns for characterizing the air-to-ground propagation channels in aeronautical communications for the very high frequency (VHF) band are given in [69, 70], for L band in [71] and for the high frequency (HF) band in [72].

In [75], the measurement campaign was performed in an urban area of Prague, Czech Republic, using a 2 GHz CW transmitter with a bandwidth of 12.5 kHz. The airship UAV flew between 100 to 170 meters above the ground level at a low elevation angle between 1° to 6°. The authors have statistically characterized the air-to-ground channel which fits between a purely terrestrial link and a land mobile satellite system. They have also presented a narrowband channel estimator capable of replicating the signal dynamics. Some related measurement campaigns were conducted with similar equipment in Prague for a path loss model in an urban area [76] with a flight altitude between 150 to 300 meters. Further, measurements in [77] and [78] were obtained in urban and wooded areas, respectively, to study space diversity techniques.

In [79], field experiments were performed in suburban Madrid, Spain, at frequency band of 5.76 GHz for narrowband measurements. The UAV flew at an altitude between 0 to 50 meters for the vertical flight test in ascending and descending directions and covered a distance of 210 meters for a horizontal test at altitudes of 20 meters and 30 meters in two different zones. The authors have investigated large-scale fading effects in the UAV propagation channel and computed PLE for both vertical and horizontal directions using the dual slope and the log-distance path loss models, respectively. They found that, during the vertical flight, the attenuation decreased below the break-point distance and then increased with UAV altitude. Whereas, the attenuation increased exponentially with the horizontal flight direction.

These works have studied air-to-ground propagation for variations in channel gain with respect to the elevation angle using the Loo model in [75] and the impact of the UAV during the course of vertical and horizontal flight routes on fast fading of Rician distribution in [79]. However, channel features were not addressed with regard to the geographical environment, such as the density and shape of surrounding scatterers. Also, the Doppler behavior of the air-to-ground channel was not investigated, which is the key parameter that may differentiate UAV channels from the conventional wireless channel. Therefore, more measurements are required for characterizing the air-to-ground propagation with the environmental effects and the maneuvering of UAVs. Moreover, these campaigns were conducted with narrowband measurement systems which are only appropriate for computing frequency non-selective fading parameters, as they lack the temporal resolution needed to distinguish closely arriving paths and hence, may not be suitable in a rich multipath environment.

2.2.2 Wideband Measurement Systems

These systems determine the channel impulse response (or transfer function) and frequency-selective parameters, such as delay spread. In addition, the power delay profile is acquired from the collection of channel impulse responses to determine the fading statistics for an in-depth insight into the average power carried by the multipath components with a certain delay and the available frequency diversity. As a result, different transmission schemes can be tested to combat small-scale fading in UAV channels. Wideband channel measurements for characterizing the aeronautical propagation channels are mostly conducted with a spread spectrum channel sounder. One such type is the correlative channel sounder, where a pseudonoise (PN) sequence is transmitted as the channel sounding signal, and the received signal is then correlated at the receiver with the same PN sequence. As a result, fading statistics for the time-invariant channel can be captured from the output of the receiver correlator by performing a convolution between the PN sequence and the channel impulse response. This process is usually performed

off-line using computational resources. From the perspective of aeronautical communication, a correlative channel sounder was used in [73] and [74] for measuring multipath effects. In the context of characterizing the UAV propagation channel, the wideband frequency-selective parameters are often measured using the universal software radio peripheral (USRP) hardware platform, for instance, as in [79, 80, 83]. This platform provides more flexibility in terms of low-power consumption and multiple frequency bands.

In [79], the wideband measurement campaign was performed with the channel sounding signal generated by a LTE BS at a frequency of 1.817 GHz. In this work, the small-scale variations in the UAV propagation channel were characterized with the measured channel impulse response, the estimated delay spread and power delay profile. The authors have analyzed the fading statistics, and consequently qualitative performance of the air-to-ground propagation using the empirical cumulative distribution function (CDF). They found a random behavior of the multipath components at different UAV altitudes. However, comparison analysis of empirical CDF with the fading channel distributions was not performed. Therefore, this work was extended in [80] to propose a channel modeling approach based on a machine learning and estimated channel parameters with regard to the environment. The Rician K factor (see section 2.3.3) was evaluated as a piece-wise function of altitude. However, the Doppler spread was not estimated due to the low airspeed of the UAV.

In [81], the measurement campaign was conducted for open and suburban spaces on the campus of Florida International University using an ultra-wideband (UWB) channel sounding radio. In the first scenario, the receiver was placed under the tree canopy at 1.5 meters above the ground. In the second scenario, the receiver was placed at the same height with clear LOS to the transmitter. In the third scenario, the receiver was lowered to 7 centimeters from the ground in a LOS condition. For all these three receiver settings, the UAV transmitter was raised from 4 meters to 16 meters above ground with a step size of 4 meters. In this work, the authors have characterized the air-to-ground propagation channel. They proposed the empirical path loss model for both static and

mobile UAVs. They found the worst path loss attenuation for the mobile UAV in the first scenario, whereas, the best for the static UAV in the second scenario. They characterized the fading channel as Nakagami-m distributed (see section 2.3.3) and presented a multipath propagation model.

In [83], the measurement campaign was performed in both a residential area and a mountainous desert landscape in Arizona, USA. The software defined radio (SDR) platform was tuned to 5.8 GHz. The authors have characterized the frequency-selectivity of the air-to-ground propagation by the average and RMS delay spread of the channel. Also, the time-selectivity in terms of the Doppler power spectrum was calculated by summing the entire range of the scattering function delay. They analyzed the channel statistics with the CDF and found that the desert terrain caused substantial delay spread in the air-to-ground propagation compared to the residential area. Moreover, CDF analysis followed a log-normal trend for the RMS Doppler spread. However, this work studied the variations in the channel due to time and frequency selectivity effects, and did not provide an empirical model for fading channel distributions.

These studies have characterized the air-to-ground channel for small-scale variations in hovering and mobility of the UAV in space, but did not take into account ground reflected multipath components during the landing and take-off phases. In addition, these works ignored the non-stationarity of the air-to-ground channel while estimating the fading statistics. Therefore, future wideband measurements should address these challenges for the accurate characterization of the UAV propagation channel. Due to their better multipath resolution, wideband measurements are more desirable for acquiring both time and frequency-selective fading parameters. However, additional computational capabilities are required to process the raw data collected from the measurements. Therefore, this type of measurement system may not be suitable for real-time characterization of the fading channel parameters. Also, the cost and physical dimensions of wideband channel sounding equipment are constraints that need to be considered.

2.2.3 IEEE 802.11-based UAV Measurements

UAV channel characterization using commercial off-the-shelf 802.11 radios is desirable due to their low power consumption, cost effectiveness and flexibility to be integrated with small size UAVs. Furthermore, these radios are mostly utilized to form single-hop and multi-hop UAV networks. For these reasons, single-hop UAV networks are usually desirable for characterizing the propagation channel between a single UAV and the ground station or between two UAVs. On the other hand, multi-hop UAV networks are preferable for studying inter-UAV communication either in mesh or star topologies controlled by the ground station. However, the performance of such radios is prone to interference and background noise. Fixed narrowband frequency and limited communication range are other constraints affecting the evaluation of fading channel parameters. Channel characterization efforts reported in the literature for multi-hop UAV networks were based on IEEE 802.11 in [85–88] and also IEEE 802.15.4 ZigBee devices in [89–91]. This section mainly reviews the measurement campaigns relevant to 802.11 radios for single-hop UAV networks. Section 2.3 will highlight the empirical relevance of multi-hop UAV networks from the perspective of both the air-to-air and air-to-ground channel modeling.

In [92], the measurement campaign was performed in the laboratory and outdoor environments to study, in particular, the altitude-dependent multipath propagation for air-to-air channel. The measurements were collected with 802.11 a/b/g/n wireless local area network (WLAN) devices from two different vendors and deployed in three outdoor scenarios using a hexacopter UAV. In the first scenario, the impact of flight distance followed a free space path loss model. In the second scenario, yaw angle was considered with a good signal reception attained between 170°-230° and the worst signal for an angle of 240°-260°. Finally, the effect of the ground reflected multipath components on UAV altitude was examined for a flight altitude between 10 to 40 meters and the height-dependent Rician model (see section 2.3.3) was proposed with a K factor reliant

on the UAV altitude.

In [93], the measurement campaign was performed for both an open area and a campus environment using a quadcopter UAV and an access point (AP) connected with a 802.11a WLAN interface at a frequency of 5.240 GHz, where the UAV flight altitude varied between 20 and 120 meters. Two vertically polarized omni-directional antennas were mounted on both UAV and AP. This study analyzed the impact of flight dynamics and antenna orientation on the air-to-ground propagation channel and found that the optimal antenna orientation can alleviate the impact of UAV hovering and mobility on received signal strength and throughput. On the one hand, horizontally aligned antennas reduced the effect of UAV yaw difference due to improved antenna alignment gain. On the other, a vertically aligned antenna handled the impact of UAV acceleration and deceleration against the tilting. Furthermore, they also found that the propagation condition followed that of free space for an open field. This work was extended in [94] using the 802.11a (5.240 GHz) standard to study the network performance and fading channel statistics for air-to-air and air-to-ground propagations. Measurements were collected with three horizontally aligned dipole antennas at flight altitudes between 15 and 110 meters. The authors observed that for both air-to-ground and air-to-air channels, the PLE computed by the log-distance model matched roughly with that of free space propagation. The Nakagami-m distribution (see section 2.3.3) was found to be a good fit for a multipath fading channel in air-to-ground propagation. Furthermore, the quality of UAV channels in terms of throughput variations over distance intervals was analyzed using the inter-arrival time of packet and re-transmission attempts. As a result, inter-arrival time was under 1 ms for all distances. The number of re-transmissions required for distances between 300 to 400 meters was not more than 85 % for most of the time.

In [95], the measurement campaign was conducted at a private airfield in Connecticut, USA, using a 802.11a radio mounted on a fixed-wing UAV. The UAV flew at approximately 64 kph and maintained an altitude of roughly 46 meters over the ground receiver nodes. The authors evaluated the throughput and reported the highest rates were

with a horizontal dipole, orthogonal to flight direction and parallel to the ground. In addition, they also estimated that the path loss roughly followed that of free space propagation. A related measurement campaign was performed in [96] using 2.4 GHz 802.11g and 5.8 GHz 802.11a devices. In this case, the authors computed the maximum range attained with a 802.11a radio and compared this with 802.11g. They found that a 802.11g node can provide robust communication at an altitude of approximately 183 meters. In this work, another experimental trial was conducted with a 900 MHz 802.11 radio to determine the communication range performances in comparison to 802.11a/b/g. They found a significant communication range of up to 2000 meters with throughput in Mbps by analyzing the slope of a linear regression applied to the received signal strength. In [110], the measurement campaign was performed in a farmland area surrounded by woods. In this work, air-to-ground channel characterization was determined in terms of network level diversity gain, and they found a significant enhancement in packet transmission rate by using multiple receivers.

These studies have mostly focused on measuring the attenuation of the received signal strength and throughput of the air-to-ground propagation using omni-directional antennas. It is evident from these campaigns that IEEE 802.11 low-power radios can provide opportunities for characterizing UAV propagation channels that have novel designs. Different types, orientations and placements of antenna on UAVs can be studied. Moreover, these radios are preferable for estimating the BER performance and latency in UAV networking. However, analysis of spatial and temporal variations was not comprehensively studied in these works due to a lack of frequency resolution. Also, in a complex communications environment where a UAV operates, interference from other 802.11 equipment can be challenging. In this case, one possible solution is to optimize altitude and inter-UAV distance to attain high SINR in the physical layer for a short period of time. Otherwise, interference management techniques may be needed.

2.2.4 Cellular-Connected UAV Measurements

Cellular networks can be considered as a prospective candidate to facilitate UAV applications in civil and commercial domains. The widely deployed cellular infrastructure can be utilized to provide reliable air-to-ground channels, and hence cut the cost of investing additional ground infrastructure and spectrum allocation. However, since cellular-connected UAVs depend on the cellular network and cellular infrastructure, which can collapse due to a natural disaster, a viable fail-safe mechanism is needed. Other challenges, such as down-tilted BS antennas, neighboring cell interference, handover performance, multiple access, UAV mobility and link security, also need to be addressed thoroughly before the widespread implementation of a UAV network connected to the cellular networks. This has motivated several mobile operators, telecommunication vendors and research organizations to further scrutinize the propagation channel characteristics between a cellular BS and UAV. For example, Ericsson and China Mobile have conducted measurement trials in China's Jiangsu province to develop a 5G prototype enabled by drone UAVs [7]. In another example, Qualcomm Technologies has launched field measurements in San Diego, California, to assess the LTE network performance at lower altitudes by using a quadcopter UAV [8]. However, these studies mainly focused on network planning and did not present any findings on the channel modeling.

In [97], a measurement campaign was launched in urban and rural scenarios in Germany to characterize the propagation channel between UAV and a cellular BS, using 900 MHz Global System for Mobile (GSM) network and 1.9-2.2 GHz Universal Mobile Telecommunications Service (UMTS) services. Field measurements were carried out with a fixed-wing UAV and a captive balloon at altitudes up to 500 meters. This work evaluated the overall RF coverage in terms of received signal strength for aerial users from the various ground BSs during the handover with regards to UAV altitude. To this end, the authors proposed an altitude-dependent channel model with the assumption that the attenuation was independent of frequency and distance. It was found that the

handover rate decreases due to signal degradation at UAV altitudes above 500 meters and consequently, the availability of BSs decreases. To conclude, good RF coverage was achieved for UAV altitudes upto 500 meters in a rural environment. It was less due to ground obstacles than in an urban terrain.

In [98] and [113], measurement campaigns were launched under the SAAS project (remote piloted semi-autonomous aerial surveillance system using terrestrial wireless networks) in an urban environment of Lisbon, Portugal to investigate the applicability of terrestrial cellular networks in UAV communication. In [98], the field trials were performed at GSM, UMTS and LTE cellular bands using a spectrum analyzer and an antenna on a meteorological balloon, deployed as the UAV platform. In this work, an empirical model was obtained for path loss attenuation in an outdoor urban scenario. The worst case scenario was reported due to the radiation pattern of the down-tilted BS antenna for a UAV altitude between 5 to 7 meters. Also, the distance in 3D space and the cellular frequency were the other performance degrading factors. However, handover analysis was not studied in this scenario. Additionally, reference [113] presented a multi-UAV network architecture based on cellular and internet protocol (IP) networks. They have assessed the network level performance with QoS measurements in terms of latency and jitter. In this case, the LTE network provides the best performance without relaying, and enhanced data rates for GSM evolution (EDGE) performs worst due to the relay between the UAVs and different BSs within the proposed architecture.

In [99], the measurements campaign was performed in a rural environment with 800 MHz LTE networks and two different cellular service providers in Denmark. The authors found considerable reduction in path loss component and shadowing variation as the UAV altitude increased. Therefore, their findings show that the UAV propagation channel requires altitude-dependent parameters for channel modeling. In contrast, [100] proposed an angle-dependent channel model to characterize propagation between the cellular BS and the UAV airborne platform. However, these studies have ignored connectivity disruption issues occuring in the UAV-cellular systems due to diffrac-

tion losses and nulls in the radiation pattern of the BS's antenna. Therefore, in [101], the measurement campaign was conducted for an open area and a mock village in California, USA, with a 909 MHz cellular band. In this work, the authors proposed a compositional path loss model to account for two-ray ground reflection propagation and diffraction losses. They also identified low coverage zones in cellular-connected UAV networks for beyond LOS operations, and named this phenomenon "holes in the sky". These holes produce unexpected coverage in the connectivity-reliant UAVs and could span from 10 meters to 100 meters in the coverage radius. They pointed out that the primary causes were interference caused by two-ray ground reflection, diffraction losses incurred by the Fresnel zone of the propagation path, and nulls in the antenna radiation pattern. Therefore, this study concluded that for the en-route UAV, the real-time estimation of the propagation conditions based on the geometrical information of the environment could mitigate glitches in the coverage zones of the cellular-connected UAV networks.

These measurement campaigns have mainly studied the performance of the cellular-enabled UAV network with regard to path loss attenuation. However, they did not consider the consequence of co-channel interference and did not provide in-depth handover analysis. Furthermore, the characterization of air-to-ground propagation with respect to small-scale variations and fading channel distributions were mostly overlooked. Cellular networks are not designed to provide air-to-ground propagation above the BS height due to the down-tilted sector antennas which can hinder wireless connectivity and cause significant reduction in reliability and capacity for aerial users. Therefore, optimum placement of the UAV in space and 3D features of the BS's antenna radiation patterns should be taken into consideration for channel modeling and network planning of UAV-enabled cellular systems. Also, UAV applications such as search and rescue services and disaster management may suffer from infrastructure failure. In this case, aerial heterogeneous networks can be a promising fail-safe framework for enabling coexistence between terrestrial communication networks and satellite systems. In addition, multi-tier UAV-cellular networks as suggested in [114], can be a viable solution for avoiding

traffic congestion and to restore communication services in disaster areas.

This section reviewed the measurement campaigns using UAVs as LAPs. However, in these cases, channel characteristics are mostly studied with hovering or mobile UAVs and static ground users. As a result, channel dynamics may change slowly with approximately constant statistics. Also, measurement scenarios are limited to urban, suburban and rural environment with better propagation conditions. Therefore, more measurement campaigns are required in more diverse scenarios, such as metropolitan areas with skyscrapers and over water bodies. Table 2.1 summarizes the aforementioned measurement campaigns, where acronyms used to represent channel statistics of measurement campaigns are given in Table 2.2.

2.3 Empirical Channel Models from Measurement Campaigns

Channel parameters can change frequently with time and space due to the cruising capability of UAVs. Many measurement campaigns have been performed to corroborate connections between channel parameters and experimental setups. Despite of all these efforts, there are no unified answers, and conclusions still need to be established using reliable channel models. This section reviews the empirical models that characterize air-to-air and air-to-ground propagation channels.

2.3.1 Air-to-Air Channel Characterization

The air-to-air propagation channel is an important aspect of inter-UAV communications and can be exploited in applications, such as multi-UAV networks or UAV swarms [11], flying ad hoc networks [12], aerial wireless sensor networks [91], and wireless back-haul connections using emerging technologies [115], [116]. In all these applications, characteristics of the air-to-air propagation depend mostly on the environmental conditions, UAV flight direction, LOS alignment, relative velocities and ground reflections. Very few empirical studies have been conducted to characterize air-to-air channels. For instance,

Table 2.1: Summary of measurement campaigns.

Ref.	**Frequency**	**UAV**	**Scenario**	**Altitude (meters)**	**Channel Statistics**
[8]	PCS, AWS, 700 MHz	Quadcopter	Mixed suburban	122	PL, RSRP, RSRQ, HO, CDF
[75]	2 GHz	Airship	Urban	100-170	RSS, PDF, CDF, AFD, LCR, PSD, AF
[76]	2 GHz	Airship	Urban	150-300	PL
[77],[78]	2 GHz	Airship	Urban, wooded	100-170	RSS, CDF, DG, AFD, LCR
[79]	5.76 GHz, 1.817 GHz	Hexacopter	Suburban	0-50	PL, SF, K, PDP, RMS, CDF
[80]	2.585 GHz	Hexacopter	Suburban	0-300	PDP, K, RMS, CDF
[81]	4.3 GHz	Quadcopter	Open field, Suburban	4-16	PL, SF, μ, ξ, TOA, PDP, CDF, RMS, BC
[83]	5.8 GHz	Octocopter	Residential, mountainous	-	RMS, DS, CDF
[92]	2.4 GHz	Hexacopter	Laboratory, outdoor	10-40	PL, PAS, K, PDF
[93]	802.11a	Quadcopter	Open field, campus area	20-100	RSS, PL, UDP
[94]	802.11a	Quadcopter	Open field	15-110	RSS, PL, PAS, UDP, CDF
[95]	802.11a	Fixed-wing	Airfield	~46	Pr, RSS, UDP
[96]	802.11a/g, 900 MHz	Fixed-wing	Airfield, Rural	~46 , ~107-274	Pr
[97]	GSM, UMTS	Fixed-wing, captive balloon	Urban, rural	0-500	RSS, HO
[98]	GSM, UMTS, LTE	Weather balloon	Urban	18	Pr
[99]	LTE (800 MHz)	Hexacopter	Rural	15-100	PL, SF
[100]	LTE (850 MHz)	Quadcopter	Suburban	15-120	PL, SF
[101]	909 MHz	Quadcopter	Open field, mock village	40-60	PL, PES
[110]	802.11 b/g	Fixed-wing	Farmland	75	PAS, PLR, PRR, AF, DG
[113]	EDGE, HSPA+, LTE	Hexacopter	-	10-100	Pr, RTT, J

Table 2.2: Acronyms used to define channel statistics of measurement campaigns.

Acronym	**Text**	**Acronym**	**Text**
AF	Auto-correlation Function	PL	Path Loss
AFD	Average Fade Duration	RMS-DS	Root Mean Square-Delay Spread
BC	Coherence Bandwidth	PRR	Packet Reception Rate
CDF	Cumulative Distribution Function	Pr	Received Power
DG	Diversity Gain	PLR	Packet Loss Rate
DS	Doppler Spread	RSS	Received Signal Strength
HO	Handover	RSRP	Reference Signal Received Power
J	Jitters	RSRQ	Reference Signal Received Quality
K	Rician factor	RTT	Round Trip Time
LCR	Level Crossing Rate	SF	Shadow Fading
PAS	Power Azimuth Spectrum	TOA	Time of Arrival
PDF	Probability Density Function	μ	Mean of Nakagami-m Factor
PDP	Power Delay Profile	ξ	Standard Deviation of Nakagami-m Factor
PES	Power Elevation Spectrum	UDP	User Datagram Protocol Throughput

in [89–91], the air-to-air channel was shown to be better than the air-to-ground channel in terms of PLE. In [89], the authors found that the ground-to-ground channel performed poorly with a PLE of 3.57, while PLE for air-to-air and air-to-ground channels were estimated to be 1.92 and 2.13, respectively. Similarly, in [90], the PLE was estimated from the log-distance propagation model as 0.93 and 1.50 for air-to-air and air-to-ground propagation, respectively. On the other hand, the authors of [91] have observed that the received signal strength for air-to-ground, air-to-air and ground-to-air propagation improves with extended UAV altitude and deteriorates as UAV distance increases. They observed that the air-to-air channel followed two-ray propagation with a PLE of 2.05. Whereas, the presence of communication gray zones leads to asymmetry in air-to-ground and ground-to-air channels and PLEs of 2.32 and 2.51, respectively.

Aerial link characterization has been conducted in [92] and [94] using a IEEE 802.11 radio. In [92], the impact of the UAV altitude on air-to-air propagation was investigated for large-scale variations and small-scale fading distribution. In this study, path loss was determined by the Friis equation with a PLE of 2.6 and a fading channel distribution that fits with the height-dependent Rician factor K. In [94], a log-distance model was used to analyze the path loss for vertical and horizontal distances. In this work, the minimum mean squared error (MMSE) method was utilized to compute PLEs of 2.03 and 2.01 for the air-to-air and air-to-ground channels, respectively.

Although UAVs are placed in a 3D environment for real multi-UAV applications, the existing studies only considered the behavior of the air-to-air propagation in a 2D plane. Moreover, these campaigns were conducted for short-range communication in an interference-limited environment. The impact of the frequency variance due to Doppler shift on the capacity and reliability of air-to-air propagation is still unexplored. The air-to-air channel characterization highlights that the propagation conditions are highly time-varying due to variations in the communication distance, altitude and UAV mobility. Also, significant attenuation occurs outside the LOS condition and under this scenario it may be difficult to maintain continuous connectivity for long range communi-

cation. Therefore, these open research issues need to be addressed to improve scalability and adaptability of the air-to-air propagation channel in multi-UAV systems. Large-scale fading statistics of the air-to-air channel are summarized in Table 2.3.

Table 2.3: Large-scale fading statistics for air-to-air channel.

Ref.	**PL model**
[89]-[91]	PL(dB) = $10\alpha\log_{10}(d)$, α =1.922 [89], α =0.93 [90], α =2.05 [91]
[92]	RSS(dB) = $P_t + G_{\text{UAV}_1} + G_{\text{UAV}_2} + 10\log_{10}(\frac{\lambda}{4\pi d})^{\alpha}$, P_t =20 dBm, $G_{\text{UAV}_1} = G_{\text{UAV}_2}$ = 5 dBi, α = 2.6, f_c =2.4 GHz
[94]	PL(dB) = PL(d_0) + $10\alpha\log_{10}(\frac{d}{d_0})$, $d = \sqrt{d_h^2 + d_v^2}$, PL(d_0) = 46.4 dB, α =2.03, $d_h \in \{0, \cdots, 100 \text{ meters}\}$, d_v = 50 meters, d_0 = 1 meter
α: PLE, d: separation distance, d_0: reference distance, d_h: horizontal distance, d_v: vertical distance, G_{UAV}: UAV antenna gain	

2.3.2 Large-Scale Fading Statistics for Air-to-Ground Channel

Most of the air-to-ground channel measurements focus on large-scale statistics, such as path loss and shadowing. For instance, in [8], the analytical path loss model was used to evaluate the performance of LTE network with UAV platform, where most of the path loss samples computed by measurements were lumped between the reference PLE of 2.0 and 4.0. For the urban environment in [76], the measured results showed that the path loss follows a distance-independent trend and is significantly affected by a low elevation angle. For the suburban environment in [79], the impact of UAV altitude and distance on the path loss was analyzed. For a vertical UAV en-route, a simplified dual slope path loss model was considered and it was found that the PLE is negative below a break-point altitude because of a partially cleared first Fresnel zone. When the UAV altitude increased

above the break-point level the path loss was similar to free space propagation because the first Fresnel zone was cleared. In [81], the effect of UAV altitude and the optimal placement of the ground receiver for path loss was stochastically modeled for both static and mobile UAVs in both open field and suburban scenarios. Foliage losses and Doppler frequency shift were taken into account. In addition, shadow fading was modeled with a zero-mean Gaussian distribution and analyzed using a PDF. A further empirical study was conducted in [85], to evaluate the influence of distance on path loss attenuation, and found degraded performance of the air-to-ground channel due to detrimental effect of interference from the 802.11 devices operating in the surrounding test area. Moreover, in [86], received signal strength declined with the distance and followed the Friis channel model. In [87], the air-to-ground propagation channel in the single-hop UAV system followed the log-distance model, where higher throughput was attained over longer distance.

For an open field and a campus environment in [93], path loss was evaluated with the free space model. In [95] and [96], PLE was estimated using linear regression. In [97], distance and frequency independent empirical path loss model was proposed for urban and rural terrains, where the altitude of aerial mobile station was accounted as the key parameter. In contrast, the empirical propagation model in [98] suggested that the path loss model is dependent on the distance in 3D plane and the operating frequency. In this case, other modeling parameters, such as the UAV altitude and the tilt angle of BS sector antenna, were also considered. The altitude-dependent path loss model was proposed in [99], where path loss and shadow fading decreased as the UAV altitude increased from 15 to 120 meters and at about 100 meters the propagation condition matched with that of free space. Conversely, in [100], the angle-dependent air-to-ground propagation channel model was presented, which encompasses excess path loss attenuation and shadow fading model. In this work, the model parameters are dependent on the angle between cellular BS and airborne UAV. In [101], the combinational model was developed to determine the low coverage zones in the cellular-connected UAV network. This model iden-

tified causes, such as two-ray ground reflections, diffraction losses and nulls in antenna radiation pattern as the predominant factors for path loss.

Path loss and shadowing statistics for the air-to-ground propagation channel presented in this section demonstrated that the UAV flight dynamics, such as the altitude, distance and elevation angle, are the dominant contributors for the large-scale fading. Therefore, the development of realistic UAV propagation model requires these parameters be considered in 3D coordinates. Also, considerable attention is needed for characterizing antenna design and orientations, as this will further improve UAV communications. Table 2.4 summarizes the large-scale fading statistics for the air-to-ground channel.

Table 2.4: Large-scale fading statistics for air-to-ground channel.

Ref.	**PL model**
[8]	PL(dB) $= P_{tx} - 10\log_{10}(12.\text{BW}) - \text{RSRP} + G_{\text{UAV}} + G_{\text{BS}}$ P_{tx}: maximum transmit power, BW: transmission bandwidth, RSRP: measured reference signal received power, G_{UAV}: gain of UAV antenna, G_{BS}: gain of BS antenna
[76]	PL(dB) $= -10\log_{10}[\frac{0.05\lambda}{2h^2}(d_{2d} + r_b^2 d_{2r})] - 20\log_{10}(1-\exp\varrho)^2$, $\varrho = -0.6038 \times 0.109^{\upsilon}$, $\upsilon \approx h\sqrt{\frac{2}{\lambda d_2}}$, h: obstruction height, d_2: distance between receiver and obstruction, d_{2d}: direct-ray distance between receiver and obstruction, d_{2r}: reflected-ray distance between receiver and obstruction, r_b: reflection coefficient
[79]	Vertical: $\text{PL(dB)} = \begin{cases} \text{PL}(d_0) + 10\alpha_1\left(\log_{10}\frac{d}{d_0}\right) & \text{if } d < d_b, \\ \text{PL}(d_0) + 10\alpha_1\left(\log_{10}\frac{d}{d_0}\right) + 10\alpha_2\left(\log_{10}\left(\frac{d}{d_b}\right)\right) & \text{if } d \geq d_b, \end{cases}$ (α_1, σ_1) = (0.74, 1.23 dB), (α_2, σ_2) = (2.29, 2.15 dB), d_b = 9 meters

Continuation of Table 2.4	
	Horizontal: PL(dB) = PL(d_0) + 10$\alpha\left(\log_{10}\frac{d}{d_0}\right)$, for horizontal distance of 20 meters: $\left(\alpha,\sigma,\text{PL}(d_0)\right)$ = (0.93, 5.5 dB, 77.9 dB), for horizontal distance of 30 meters: $\left(\alpha,\sigma,\text{PL}(d_0)\right)$ = (1.01, 3.9 dB, 74.6 dB)
[81]	Static UAV: PL(dB) = PL(d_0) + 10$\alpha\left(\log_{10}\frac{d}{d_0}\right) - \log_{10}\frac{\triangle h}{h_{\text{opt}}} + C_p + \zeta$, $\triangle h = \lvert h_g - h_{\text{opt}}\rvert$, $\triangle f = \left(\frac{\triangle v}{c}\right)\cdot f_c$, $\zeta \sim N(0,\sigma^2)$, C_p = 0 dB, d = 5.6 meters to 16.5 meters, h_g = (1.5 meters, 7 centimeters), $\left(\alpha,\sigma,\text{PL}(d_0)\right)$ = (2.6471, 3.37 dB, 34.905 dB) for open environment, $\left(\alpha,\sigma,\text{PL}(d_0)\right)$ = (2.7601, 4.8739 dB, 30.4459 dB) for suburban environment, Mobile UAV: PL(dB) = PL(d_0) + 10$\alpha\left(\log_{10}\frac{d}{d_0}\right)$ − $\log_{10}\frac{\triangle h}{h_{\text{opt}}}$ + C_p + $10x\log_{10}\left(\frac{f_c+\triangle f}{f_c}\right)+\zeta$, $\left(\alpha,\sigma,\text{PL}(d_0)\right)$ = (2.6533, 4.02 dB, 34.906 dB for open environment at UAV speed of 32 kph), $\left(\alpha,\sigma,\text{PL}(d_0)\right)$ = (2.8350, 5.3 dB, 30.446 dB) for suburban environment at UAV speed of 32 kph, and x: frequency dependent path loss factor and negligible at small velocities
[85]	RSS(dBm) = $-95 + 10\log_{10}\left(K_0.d^{-\alpha}\right)$, α = 2.34, $K_0 = 3.6\times10^{-1}$
[86]	RSS(dB) = $P_t + G + 10\log_{10}\left(\frac{\lambda}{4\pi d}\right)^{\alpha}$, P_t = 20 dBm, G = 1dB, f_c = 2.4 GHz, α = 2.3
[87]	PL(dB) = 10$\alpha\log_{10}(d)$, $\alpha \approx$2 for beyond 100 meters distance
[89–91]	PL(dB) = 10$\alpha\log_{10}(d)$, α = 2.132 (air-to-ground), 3.57 (ground-to-ground) [89], 1.50 (air-to-ground) [90], 2.32 (air-to-ground), 2.51 (ground-to-air), 3.1 (ground-to-ground) [91]

Continuation of Table 2.4	
[94]	PL(dB) = PL(d_0) + $10\alpha \log_{10}\left(\frac{d}{d_0}\right)$, $d = \sqrt{d_h^2 + d_v^2}$, PL(d_0) = 46.4 dB, α = 2.01 (air-to-ground), $d_h \in \{0, \cdots, 100 \text{ meters}\}$, d_v = 50 meters, d_0 = 1 meter
[93]	RSS(dBm) = $P_{rx}(d_0) - 10\alpha \log_{10}\left(\frac{d}{d_0}\right)$, α = 2.2 (open), 2.5–2.6 (campus), P_{rx}: received power at d_0
[95, 96]	RSS(dBm) = $A - 10\alpha log_{10}(d)$, (α, A) = (1.80, -37.5) [95], (α, A) = (1.04, -55.12) [96]
[97]	Urban: PL(dBm) = $89.5357 + (\frac{h_U^3}{10000} + 0.0108h_U^2 + 0.8588h_U)$ Rural: PL(dBm) = $78.2186 - 0.0013h_U^2 - 0.0052h_U$, $h_U \in \{0, \cdots, 500 \text{ meters}\}$
[98]	PL(dB) = $20\log(\frac{4\pi d_0}{\lambda}) + X_{\text{dis}} + X_{\text{freq}} + X_{\text{hei}} + X_{\text{ang}}$, $X_{\text{dis}}, X_{\text{freq}}, X_{\text{hei}}, X_{\text{ang}}$: 3D distance, frequency, altitude and tilt angle-dependent parameters
[99]	PL(dB) = $\alpha(h_U)10\log_{10}(d) + \beta(h_U) + \zeta$, $\zeta \sim N(0, \sigma(h_U))$, for h_U = 15 - 100 meters: $\alpha(h_U)$ = 2.9 – 2.0, $\beta(h_U)$ -1.3 – 35.3 dB, $\sigma(h_U)$ = 7.7 – 3.4 dB
[100]	PL(dB) = $\alpha 10\log_{10}(d) + A(\phi - \phi_0)\exp\left(-\frac{\phi - \phi_0}{B}\right) + \eta_0 + \zeta$ $\zeta \sim N(0, a\phi + \sigma_0)$, α = 3.04, A = -23.29, B = 4.14, ϕ_0 = -3.61, η_0 = 20.70, a = -0.41, σ_0 = 5.86
[101]	PL(dB) = $-20\log_{10}\lvert v\rvert + 40\log_{10}(d) - 10\log_{10}\left(h_{\text{BS}}^2 h_U^2\right)$, v: Kirchoff diffraction parameter

d: separation distance, d_0: reference distance, d_b: break-point distance, C_P: foliage loss, σ, standard deviation, h_g: height from ground level, h_{opt}= optimal height from ground level, f_c: carrier frequency, h_U: UAV altitude, h_{BS}: BS altitude, $\triangle f$: Doppler shift, K_0: transmission gain, G: antenna gain, A: y-intercept, λ: wavelength

2.3.3 Small-Scale Fading Statistics for Air-to-Ground Channel

Fading amplitude statistics are important for the analysis of the small-scale variations in multipath propagation using the first order statistics, such as CDF and PDF, to study the random behavior of fading channels. Also, second order statistics, such as level crossing rate (LCR), average fade duration (AFD) and fade depth (FD), are useful to analyze the severity of fading due to the spatial-temporal variations. In this subsection, several commonly used models for UAV communication small-scale fading distributions are discussed.

The ***Loo Model*** is a composite channel model which accounts for Rician and Log-normal distributions. To this end, LOS component is modeled by the log-normal distribution and multipath components usually tends to follow the Rician model. In [75], the fading statistics were studied for the narrowband air-to-ground propagation channel in urban areas using the Loo model. In this case, the statistical analysis of CDF found that the empirical data fits with the simulated time series. The PDF for Loo model is

$$f(y) = \frac{y}{\sigma^2\sqrt{2\pi\Sigma_A^2}} \int_{a=0}^{\infty} \frac{1}{a} \exp \frac{-\left(20\log a - M_A\right)^2}{2\Sigma_A^2} \exp \frac{-\left(y^2+a^2\right)}{2\sigma^2} I_0\Big(\frac{ya}{\sigma^2}\Big) da, \tag{2.1}$$

where M_A and Σ are respectively, the mean and standard deviation of the Gaussian distribution for the magnitude of the LOS signal, a and σ, respectively, denote the magnitude of the LOS and the diffuse multipath components of Rician distribution and $I_0(.)$ is the zeroth-order modified Bessel function.

The ***Rayleigh Model*** is well known in scattering environment. The study in [73] found that the CDF of the air-to-ground propagation fading channel follows Rayleigh distribution for the field measurements with large elevation angles in a mixed-urban environment. Furthermore, the scattering environment was theoretically tested for co-operative relay based UAV systems in [117]. Also, an analytical study in [118] suggested that the multiple-access ground-to-air channel can be modeled with the Rayleigh distri-

bution for the UAV heading. The PDF for the Rayleigh fading distribution is

$$f(a) = \frac{a}{\sigma_2} \exp \frac{-a^2}{2\sigma^2}, \tag{2.2}$$

The ***Rician Model*** is used to approximate the fluctuations in the fading channel with LOS. In the literature, this case is appropriate for the HAP in [46–48], [60, 63, 73] and for the scattered multipath environments in the LAP in [79, 80, 92]. For the Rician channel, the Rician K factor is a quantitative parameter to measure the severity of the multipath fading. In [79], the variations in the received signal amplitude for the air-to-ground propagation was found as K=5.29 dB for ascending and descending directions of the UAV altitude and K up to 19.14 dB for horizontal flight trials in two different zones at the altitudes of 20 meters and 30 meters. On one hand, for the air-to-ground propagation, [80] proposed Rician K as a piece-wise function of the altitude with a break-point of 16 meters. On the other hand, the air-to-air channel characterization in [92], studied the influence of the altitude-dependent Rician K due to scattered ground reflections and found that, as UAV elevated from 10 meters to 40 meters, the value of K increases from 3.533 dB to 10.048 dB. This work indicated that the impact of the ground reflected multipath fading reduces with increasing UAV altitude. Theoretical implications of Rician fading channels were found in [50] to improve MIMO gain for air-to-ground propagation in a hilly rural scenario and in [119], when combined with two-state Markov model to capture channel non-stationarity. The PDF of the Rician distribution is given by

$$f(y|a,\sigma) = \frac{a}{\sigma_2} \exp \frac{-\left(a^2 + y^2\right)}{2\sigma^2} I_0\Big(\frac{ay}{\sigma^2}\Big), \tag{2.3}$$

where $y \geq 0$, a and σ denotes the magnitude of the LOS and the diffuse multipath components, respectively. Also, the Rician parameter K is defined as:

$$K = \frac{a^2}{2\sigma^2}. \tag{2.4}$$

The ***Nakagami-m and Weibull fading models*** are appropriate for characterizing the UAV fading channels intended for high altitude applications [117]. The Rayleigh channel distribution is a special case of Nakagami-m. In [81], magnitudes of individual multipath components were collected for different time delay bins and modeled by the Nakagami-m distribution. In this case, mean and standard deviation of the m parameter were empirically estimated. As a result, the mean was found to be small for both open and suburban areas under the influence of vegetation, and large variance was observed due to thick suburban scattering. Furthermore, in [94], the CDF analysis found that the Nakagami-m distribution fits the empirical data better compared with Rayleigh distribution. Both Nakagami-m and Weibull fading distributions can offer substantial flexibility to study the UAV fading channel characteristics in diverse environment. However, empirical studies have not yet been initiated for development of statistical channel model based on Weibull distribution, as for vehicle-to-vehicle channel modeling [120]. The PDF of Nakagami-m fading distribution is given by

$$f(y;m,\Omega) = \frac{2m^m}{\Gamma(m)\Omega^m}(y^{2m-1})\exp(\frac{-my^2}{\Omega}), \tag{2.5}$$

where $\Gamma(.)$ is the Gamma function, m and Ω are the Nakagami shape and spread controlling parameters, respectively, and given by

$$m = \frac{\mathrm{E}^2[X^2]}{\mathrm{Var}[X^2]} \tag{2.6}$$

$$\Omega = \mathrm{E}[X^2]. \tag{2.7}$$

The PDF of the Weibull distribution is given by

$$f(y) = \frac{\beta}{a^\beta} y^{(\beta-1)} \exp -(\frac{y}{a})^\beta, \tag{2.8}$$

where β is a shape parameter defining the severity of the fading, $a = \sqrt{\mathrm{E}(y^2)/\Gamma[(2/\beta)+1]}$ and $\Gamma(.)$ is the Gamma function. The Rayleigh distribution is a special case of the Weibull

distribution for a value of $\beta = 2$.

Doppler spread and delay dispersion, UAV channels tend to possess higher Doppler spread than the conventional radio channel because the relative velocities of UAVs are higher. In [79] and [80], delay spread resolution was in micro-seconds for a suburban environment. In [81], excess delay and RMS delay spread were of the order of nano-seconds for a foliage environment. In this case, channel impulse response was obtained by Clean algorithm[1]. However, frequency variance due to Doppler shift is not significant in [80, 81] due to the low velocity of UAVs. In [83], for the mountainous desert scenario, the median RMS delay spread and the Doppler frequency spread were roughly 0.06 μs and 28.96 Hz, respectively. For the residential area, the measured median RMS delay spread and the Doppler frequency spread were approximately 0.03 μs and 28.06 Hz, respectively. The RMS delay spread attained in the desert terrain was larger due to the rough mountainous scatters along the flight path than those in the residential area. In this case, RMS delay spread was modeled as a log-normal distribution. However, these works lack the second order statistics, such as AFD, LCR and FD, for the spatial-temporal variations in the air-to-ground propagation channel.

Fading channel statistics for most low altitude air-to-ground propagation cases reported in the literature are analyzed with the Nakagami-m and Rician distributions. The Weibull distribution is still unexplored. Also, estimation of the fading channel characteristics for the air-to-air propagation with regards to altitude and surface scattering is an open research issue. Table 2.5 provides the empirical fading distributions for small-scale variations with both manned aircrafts and UAVs.

[1] Clean algorithm is a de-convolution algorithm which was first used in radio astronomy to enhance images of the sky and in microwave communication [121]. In [81], this algorithm was used in UWB propagation to eliminate noise in the air-to-ground channel.

Table 2.5: Small-scale fading distributions.

Ref.	Scenario	Frequency band	UAV channel	Fading distribution
[46]-[48]	Over water [46], hilly [47] and suburban [48]	Wideband	air-to-ground	Rician
[60]	Urban	Wideband	air-to-ground	Rician
[63]	hilly	Wideband	air-to-ground	Rician
[73]	Mixed urban	Wideband	air-to-ground	Rician (for small elevation angles), angle-dependent Rayleigh (for large elevation angles)
[75]	Urban	Narrowband	air-to-ground	Loo model (Rician & Log-normal)
[79]	Suburban	Narrowband	air-to-ground	Rician
[80]	Suburban	Narrowband	air-to-ground	Rician
[81]	Open field and suburban	Ultra-Wideband	air-to-ground	Nakagami-m
[92]	Outdoor	IEEE 802.11	air-to-air	Rician
[94]	Open field	IEEE 802.11	air-to-ground	Nakagami-m

2.4 Analytical Channel Models

Analytical channel models are useful for characterizing the propagation behavior under certain assumptions and parameters. They can predict the performance of communication systems. For example, the channel behavior of land mobile satellite systems can be analyzed using the multi-state Markov chain model [38, 39]. Generally there are three major modeling approaches: deterministic, stochastic and geometry-based stochastic.

2.4.1 Deterministic Channel Model

In deterministic models, environmental clutter is placed in certain layouts. This approach assumes large dimensions of the environmental objects in comparison with the wavelength, it does not compensate for diffuse scattering. The accuracy of these channel models depends on the environment-specific database which consists of the information related to the terrain topography, the electrical parameters of buildings and other obstruction materials. Deterministic models can be realized by ray-tracing software, which can depict the realistic behavior of the electromagnetic wave propagation and simulate path loss and shadowing effects.

In [40], 3D ray-tracing was performed to characterize the altitude-dependent attenuation in the air-to-ground propagation for the suburban environment. In [41] and [42], analytical propagation models have been studied for the air-to-ground channel characterization in an urban environment for frequencies ranging from 200 MHz to 5 GHz and altitudes from 100 to 2000 meters. In [41], the path loss and shadowing statistics were examined as a function of elevation angle and the aerial altitude through 3D ray-tracing. The authors have provided analytical path loss expressions. Also, the shadowing was fitted using the log-normal distribution with the standard deviation dependent on the elevation angle. The work in [42] utilized knife-edge diffraction theory to model the LOS probability, which considered the statistical parameters to account for height, size and coverage area of buildings in the simulation.

In [19, 43, 44], environmental topography was realized with the statistical parameters recommended by the ITU. In [19], a closed-form expression was formulated for determining the coverage performance in terms of the maximum cell radius and the optimal altitude. In that study, the free space path loss model was extended using the excessive attenuation factor for different LOS and NLOS propagation conditions. In [43], a generic path loss model for a low altitude platform was proposed, where the channel model parameters were estimated by 3D ray-tracing at 700 MHz, 2000 MHz and 5800

MHz. In that work, the air-to-ground channel conditions favoring LOS and NLOS propagations were grouped distinctly and analyzed with the group occurrence probability as the conditional PDF. Simulation results demonstrated that the impact of elevation angle was significant on the excess path loss. This work was extended in [44] to provide the analytical framework for optimization of the average radio coverage probability and the maximum transmission rate to achieve the required QoS. However, in these works, propagation conditions depend upon the altitude and coverage radius of the UAV. As the altitude increases with respect to radius, the LOS probability tends to increase for all ground positions. Therefore, such channel models can only be appropriate for the high-rise urban environment with an average building height of 60 meters. In contrast, the channel model in [122] was recommended for the modern metropolitan areas with densely located skyscrapers. However, this model requires more environmental data, such as shape of buildings with surrounding geometry.

The path loss model in [19] addressed the technical challenges in UAV communication, such as optimum deployment of the UAV in [44, 45], outage and BER analysis in [123], energy efficiency of UAV networks in [124–126], interference management in a multi-UAV scenario in [127], latency in UAV-enabled cellular networks in [128] and UAV flight endurance time in [129]. Furthermore, this model complements the optimum deployment of UAVs to ensure maximum reliability in terms of the outage capacity and the BER using static and mobile aerial relays in [130]. It increases the number of users in a cellular-assisted UAV network in [131] and UAV for data caching purposes in [132]. In these applications, the UAV channel model incorporates both LOS and NLOS propagation conditions for a certain set of environmental parameters. Also, the appropriate placement of the UAV is of paramount importance.

These studies have suggested that deterministic UAV channel models account for the reciprocity ascertained in the propagation channel to the UAV placement and the propagation conditions in different environments. However, in [40–42], channel models were confined to the urban and the suburban environments and did not capture gener-

ality for other environments. Channel models in [19, 43] are applicable for environmental statistics based on ITU recommendations. These studies have characterized propagation channels for a static UAV and ignored the fading effects due to the small-scale variations. In contrast, studies in [79, 81, 92, 94] have empirically analyzed the variations in the received signal strength and provided large-scale and small-scale statistical properties of UAV channels. However, these works have largely overlooked the impact of environment on the propagation conditions and consequently the UAV coverage analysis. Furthermore, experimental work has not yet been conducted for UAV channel modeling in metropolitan areas with skyscrapers. In contrast, reference [122] provided the analytical approach and ray-tracing simulations for the air-to-ground propagation characteristics in a metropolitan scenario emulated by the Manhattan grid. Therefore, more empirical and analytical studies are required to provide ubiquitous coverage using UAV networks in versatile environments and specifically for metropolitan areas, considering that UAVs have been envisaged as a potential candidate to support 5G mobile communication systems [133]. Some of the deterministic UAV channel models are reported in Table 2.6.

2.4.2 Stochastic Channel Model

For UAV communication, stochastic channel models can be designed using the TDL system with different numbers of taps, each of which can accommodate fading statistics of the multipath components derived from the channel impulse response. In this case, fading statistics of individual taps can be analyzed empirically from measurements and numerically by computer simulation. However, the accuracy of these model depends on the estimation of stationary intervals in the non-stationary UAV channel.

In [46–48], wideband stochastic channel models were proposed from the data collected in different environments, using the estimated stationary interval of 15 meters in the C band. For over water settings in [46], the air-to-ground channel employed the TDL model to characterize the two-ray propagation with an additional multipath com-

Table 2.6: Deterministic models.

Ref.	Analytical Model	Parameters
[19]	$\text{PL(dB)} = \frac{\varepsilon_{\text{LOS}}-\varepsilon_{\text{NLOS}}}{1+a\times\exp\left(-b\left[\arctan\left(\frac{h_{\text{U}}}{r}\right)-a\right]\right)} + 10\log d + 20\log\left(\frac{4\pi f_c}{c}\right)+\varepsilon_{\text{NLOS}},$	$d = \left(h_{\text{U}}^2 + r^2\right)$, r: coverage radius, c: speed of light, For f_c = 2000 MHz: suburban$(\varepsilon_{\text{LOS}},\varepsilon_{\text{NLOS}},a,b)$ = (0.1, 21, 4.88, 0.43), urban$(\varepsilon_{\text{LOS}},\varepsilon_{\text{NLOS}},a,b)$ = (1, 20, 9.61, 0.16), dense urban$(\varepsilon_{\text{LOS}},\varepsilon_{\text{NLOS}},a,b)$ = (1.6, 23, 12.08, 0.11), high-rise urban$(\varepsilon_{\text{LOS}},\varepsilon_{\text{NLOS}},a,b)$ = (2.3, 34, 27.23, 0.08)
[41]	$\text{PL(dB)} = \begin{cases} -0.58+0.549\exp\left(\frac{(90-\phi)}{24}\right), & \text{LOS} \\ \eta_0-\eta_1\exp\left(-\frac{(90-\phi)}{\nu}\right), & \text{NLOS} \\ \iota_0-\iota_1\exp\left(\frac{(90-\phi)}{\omega}\right), & \text{OLOS} \end{cases}$ Shadow fading: $\sigma\text{(dB)}=\rho(90-\theta)^{\gamma}$,	ϕ: elevation angle, for 200 MHz: (η_0,η_1,ν)= (9.08, 6.40, 12.01), (ι_0,ι_1,ω)= (2.11, 0.41, 22.07), for 5000 MHz: (η_0,η_1,ν)= (20.43, 14.60, 10.50), (ι_0,ι_1,ω)= (6.23, 0.4787, 22.65), LOS channel at 200 MHz and 100 m altitude: (ρ,γ)= (0.0143, 0.9941), NLOS channel at 200 MHz and 5000 MHz: (ρ,γ)= (0.7489, 0.4638) & (2.7940, 0.2259), obstructed-LOS (OLOS) channel at 200 MHz and 5000 MHz: (ρ,γ)= (0.3334, 0.3967) and (0.8937, 0.3713)
[42]	LOS probability at a street level: $\text{P}_{\text{LOS}} = \begin{cases} 1-\frac{S_c\sin\vartheta}{W_s}, & 0<S_c<W_s/\sin\vartheta \\ 0, & S_c>W_s/\sin\vartheta \end{cases}$ LOS probability of an area: $\text{P}_{\text{LOS}} = \frac{2}{\pi}\left[\vartheta_c - \frac{S_c(1-\cos\vartheta_c)}{W_e}\right]$,	ϑ: street angle, ϑ_c: critical street angle, W_s: street width, S_c: critical distance between ground station to adjacent buildings, H: building height, h_g: ground station height, W_e: estimated street width, λ: wavelength, W_s = 15 meters, ϑ = 90°, $\Delta H = H - h_g$, H = 11.71 meters, h_g = 15 meters, W_e = 44.2 meters, $S_c > \Delta H\cot\phi + \frac{0.16\lambda\cos\phi+\sqrt{(0.16\lambda\cos\phi)^2+0.32\lambda\Delta H\sin\phi}}{\sin^2\phi}$, $\sin\vartheta_c = \begin{cases} \frac{W_e}{S_c}, & W_e \le S_c \\ 0, & \text{otherwise} \end{cases}$
[43]	$\text{PL(dB)} = 20\log\left(\frac{\triangle h}{\sin\phi}\right)+20\log\left(f_{\text{MHz}}\right)-27.55,$ LOS probability: $\text{P}_{\text{LOS}} = a\left(\phi-\phi_0\right)^b$	$\triangle h = h_{\text{U}} - h_g$, h_{U} = 200 meters, h_g = 1.5 meters, f_{MHz} = 700, 2000, 5800, ϕ_0 = 15°, for 700 MHz: suburban$(a=0.77, b=0.05)$, urban$(a=0.63, b=0.09)$, dense urban$(a=0.37, b=0.21)$, high-rise urban$(a=0.06, b=0.58)$

ponent as the intermittent ray. In this work, the authors have argued that the statistics for LOS and reflected components can be analyzed either as the curved earth two-ray (CE2R) model or the flat earth two-ray (FE2R) model [134]. The probability of the existence of the intermittent multipath component was estimated by the exponential distribution as a function of link distance. The TDL model with nine taps has been proposed for mountainous terrain [47] and for the suburban environment [48].

In [135] and [136], a stochastic model was developed with the narrowband assumption to characterize the aeronautical air-to-ground channel. In [135], the stochastic model was designed for characterizing the air-to-ground propagation in terms of transmission coefficients assuming that the quadrature components reflected from the ground surface can be modeled as a zero-mean Gaussian process. Also, Doppler spectrum analysis was performed for the diffuse multipath components. In [136], the proposed model was developed with the TDL system having both LOS and NLOS taps, where the amplitude attenuation and the multipath delay of NLOS components were assumed to be Rayleigh distributed and Gaussian random processes, respectively, while the phase shift was uniformly distributed. In addition, the Doppler frequency shift was characterized as a random process. However, the channel stationarity interval was not computed and fading statistics were assumed to be constant for the random time duration.

Stochastic models provide useful analysis of the time-varying characteristics of the UAV channel. For instance, reference [137] proposed the TDL model to capture the small-scale characteristics of multipath components. Furthermore, the stochastic model accommodates multi-antenna systems to boost the reliability of MIMO channel in terms of BER in [138] and capacity in [139]. In these works, the stochastic model only provides numerical analysis and lacks validation by measurement results. On the one hand, empirical data have been collected from the measurement campaigns in [79, 81, 83] to study the impact of UAV flight dynamics and environment on the small-scale fading. However, these studies did not consolidate the fading statistics using the TDL model. Also, estimation of the stationary interval in the UAV channel was ignored in

these works. On the other hand, [46–48] did estimate the stationary interval in stochastic TDL models for different operating environments. However, these campaigns were conducted using manned aircraft at high altitude. Therefore, the effective stochastic framework has to be developed for UAV channels in low altitude which also accommodates channel non-stationarity. Table 2.7 summerizes the channel response from the TDL models reported in this chapter.

Table 2.7: TDL models.

Ref.	**TDL model**
[46]	$h(\tau,t) = h_{2-ray}(\tau,t) + w_3(t)A_3(t)\exp(-j\varphi_3(t))\delta(\tau-\tau_3(t))$, h_{2-ray} denotes FE2R or CE2R model, $w_3(t) \in \{1,0\}$ represents presence/absence of the intermittent ray and modeled as $p(d) = a\exp(bd)$, A_3 is the amplitude of the intermittent ray and modeled by the Gaussian distribution, $\varphi_3 \in \{0,2\pi\}$ is the uniformly distributed phase of the intermittent ray, τ_3 is the excess delay of the intermittent ray and modeled as $p(\tau_3) = \frac{1}{\mu}\exp-(\tau_3 - 100/\mu)$, (a,b) = (0.17,-0.25) over sea water and (0.03,-0.15) over freshwater, μ= 17 ns, 6 ns $\leq \tau_3 \leq$ 7 ns, d: link distance
[47], [48]	$h(\tau,t) = A_1(t)\delta(\tau-\tau_1(t)) + A_2(t)\exp(-j\varphi_2(t))\delta(\tau-\tau_2(t)) + \sum_{L=3}^{9} w_L(t)A_L(t)\exp(-j\varphi_L(t))\delta(\tau-\tau_L(t))$, A, φ and τ denotes amplitude, phase and excess delay, respectively, subscripts 1, 2 and L represents LOS, reflected and L^{th} intermittent multipath components, respectively, variations of w_L and τ_L are modeled as a linear function of link range, $\varphi_L \in \{0,2\pi\}$ is the uniformly distributed phase, $10\log\left(\frac{A_L^2}{A_1^2}\right)$ represents relative power of intermittent components and follows a Gaussian distribution
[136]	$y(t) = A_1(t)\cos[2\pi\{f_c+\triangle f\}(t-\tau_1(t))] + \sum_{L=2}^{N} A_L(t)\cos[2\pi\{f_c+\triangle f\}(t-\tau_L(t)) + \varphi_L(t)] + n(t)$, A_1 is the amplitude of LOS path, A_L represents amplitude of NLOS paths and assumed as Rayleigh random process, $\varphi_L \in \{-\pi,\pi\}$ is the phase shift of NLOS paths and modeled as the uniform random process, $\triangle f$ denotes Doppler frequency shift and modeled as time-variant random process, $\tau_1 = 25$ μs, τ_L is excess delay of NLOS components and modeled as the Gaussian random process with mean and standard deviation of 30 μs and 5 μs, respectively, $n(t)$ is white Gaussian noise

2.4.3 Geometry-based Stochastic Channel Model

Geometry-based stochastic modeling approach obtains the spatial-temporal channel characteristics with the stochastic output in a 3D geometric simulated environment. The accuracy of this model is dependent on the simulation of the virtual environment confined in some geometrical shapes, such as cylindrical or elliptical where communication nodes within scattering region follow a certain probability distribution. The geometric based channel model for the analysis and simulation of the air-to-ground radio communication was proposed in [49]. It characterized the multipath propagation in a cluttered environment around the ground station confined within a virtual 3D ellipsoidal geometry to analytically evaluate delay, gain, phase and angle of arrival (AOA) of individual multipath components. In addition, the path loss model may be determined using the log-distance model between the airborne platform and the clutters. Therefore, the proposed model is equally applicable to determine both narrowband and wideband channel statistics and well suited for designing antenna diversity system and antenna arrays. This work was extended in [50] for theoretical estimation of the MIMO performance for the low altitude air-to-ground propagation and also characterized the propagation loss for LOS and multipath components using the log-distance path loss model with log-normal shadowing. In this model, the small-scale fading due to spatial variations was modeled by the Rician distribution to analyze the severity of the fading due to the scattering phenomenon. Furthermore, the probability of error was simulated for a single-input single-output (SISO) system and compared with a 2×2 space-time block coding and a 2×2 spatial multiplexing gain using maximum likelihood detection. In [51], a 3D air-to-ground propagation model was proposed for the dense scattering environment considering LAP. The model was derived for a direction of arrival and the delay dependent Doppler spectrum with the approximation of linear distribution of the scattering point. In this work, the analytical results were compared with the simulation results by using the terrain based digital elevation model and found that the terrain morphology

affects the Doppler-delay spread spectrum.

In [52], a realistic 3D geometric-based stochastic model has been developed for the air-to-ground communication between an airborne platform and the BS as an elevated plane. The proposed model considered scattering points as uniformly distributed around the BS. In this study, the spatial characteristics were analyzed with the closed-form analytical expressions. In [53], the geometric-based stochastic approach has been utilized for UAV channel modeling to analytically characterize a 2×2 MIMO enabled air-to-ground propagation in a 3D plane. In this case, the model was developed with the assumption that the ground scatters were distributed on the cylindrical surface and scatter free airborne environment. Based on the proposed model, analytical expressions were used to study the impact of the elevation angle and the direction of the UAV movement on the space-time correlation function in a non-isotropic environment.

While deterministic and stochastic models can provide useful understanding of the propagation characteristics in the UAV communication, these models are usually not feasible with a large number of simulation parameters. The Geometry-based stochastic channel model emerged as a preferable method to derive analytical expressions for the predominant performance metrics. The practicability of such model is to predict coverage and capacity performance. For instance, downlink coverage analysis has been performed in [54] for the multiple UAVs modeled as a uniform binomial point process at the fixed altitude and a single ground user. Also, in [140], the network planning approach has been developed based on the stochastic geometry. In these studies, ground users were spatially positioned with a uniform distribution. Furthermore, in [141], extended coverage and enhanced capacity has been achieved by concurrency between a single UAV and device-to-device users distributed as a Poisson point process (PPP). However, a more realistic UAV channel model based on the stochastic geometry framework can accommodate non-uniform distribution for both UAVs and ground users and therefore, can be considered as the future research direction in this domain. The Implication of the geometric-based stochastic approach is to model the channel non-stationarity, to

get insights of the angular information for multipath components in scattering regions [49, 52, 53], and for joint Doppler-delay spectrum [51]. However, these studies are largely simulation based. Therefore, the empirical framework has to be developed to characterize propagation with regard to spatial-temporal variations in the non-stationary UAV channels. Some analytical expressions to determine AOA using geometry-based model are given in Table 2.8. Finally, the pros and cons of different UAV channel modeling approaches are listed in Table 2.9.

Table 2.8: Geometry-based stochastic model.

Ref.	Geometry-based stochastic model
[49]	The PDF of AOA as a function of elevation angle (ϕ) around the ground receiver: $f(\phi) = \frac{\frac{x_a^2}{x_a^2-x_b^2}-1}{2\pi\gamma\left(\frac{x_a}{\sqrt{x_a^2-x_b^2}}-\cos\phi\right)^2}$, where x_a and x_b are subsequently the major and minor axis of the planar elliptical scattering surface, $\gamma = \frac{x_a}{\sqrt{x_a^2-x_b^2}}\left(\frac{x_a^2}{x_a^2-x_b^2}-1\right)^{\frac{1}{2}}$
[52]	The PDF of AOA with respect to airborne platform: $f(\Psi_{ap},\phi_{ap}) = \frac{\left(l_{ap,max}^3-l_{ap,min}^3\right)\cos\phi_{ap}}{3V}$, where Ψ_{ap} and ϕ_{ap} are, respectively, the azimuth and the elevation angle observed from the airborne platform, $l_{ap,max}$ and $l_{ap,min}$ are the distance between the UAV and, respectively, the farthest and the nearest scatter point The PDF of AOA with respect to the elevated ground plane: $f(\Psi_{bs},\phi_{bs}) = \frac{\left(l_{bs,max}^3-l_{bs,min}^3\right)\cos\phi_{bs}}{3V}$, where Ψ_{bs} and ϕ_{bs} are, respectively, the azimuth and the elevation angle observed from the BS, $l_{bs,max}$ and $l_{bs,min}$ are the distance between the BS and, respectively, the farthest and the nearest scatterer point, and V is the volume of the scattering region
[53]	The von Mises PDF of AOA as a function of azimuth angle: $f(\Psi) = \frac{\exp k\cos(\Psi-\Psi_\mu)}{2\pi I_0(k)}, -\pi < \Psi \leq \pi$, where k is a spreading control parameter, $\Psi_\mu \in [-\pi,\pi]$ is the mean angle of the distribution of scatterers in a 2D plane, $I_0(.)$ is the zeroth-order modified Bessel function, k=3, Ψ_μ=π, The cosine PDF of AOA as the function of elevation angle: $f(\phi) = \frac{\pi}{4\phi_m}\cos(\frac{\pi}{2}\frac{\phi-\phi_\mu}{\phi_m})$, with mean angle ϕ_μ= $\frac{\pi}{6}$ and variance ϕ_m=$\frac{\pi}{4}$

Table 2.9: Pros and cons of channel modeling approaches.

Pros	**Cons**
Empirical Channel Model	
• Large-scale fading can be analyzed by linear regression technique [95, 96] and curve fitting [97] applied on the received signal strength	• Tedious and expensive measurement campaigns
• Path loss model presented as closed-form expressions with correction factors based on environment conditions [81], UAV altitude [97, 99] and elevation angle [100]	• Channel characterization depends upon the multipath resolution of the channel sounder, antenna design and propagation environment
• Small-scale fading can be characterized by the superposition of all multipath components in the form of channel impulse response [79–83]	• Size and payload constraints of different UAV types
• Channel characterization is possible for the air-to-air propagation [89–92, 94] with different UAV flight dynamics and velocities	• Restrictions on UAV flight altitude by national civil aviation regulatory authorities [56–58]
Deterministic Channel Model	
• Reliable characterization of the air-to-ground propagation for large-scale fading statistics [19, 40–44]	• Environment specific modeling approach

Continuation of Table 2.9	
Pros	**Cons**
• Effective optimization for coverage [44, 45], reliability [123, 130] and capacity performance in UAV communications • Often presented as closed-form expressions [19, 40–44]	• Require large databases of environment geometries such as shape, size and position of all obstacles [40]
Stochastic Channel Model	
• Low computational complexity to emulate complete UAV propagation characteristics in versatile environment [136] • Characterization of multipath components can be done with both empirical analysis [46–48] and numerical analysis [135, 136]	• Estimation of fading statistics are dependent on the stationary interval of the dynamic UAV channel
Geometry–based Stochastic Channel Model	
• 3D channel characterization is possible with less environmental parameters to study the channel state information in UAV propagation for e.g. angular information due to spatial-temporal variations without considering non-stationarity in the UAV channel [49, 51]	• Accuracy is dependent on the distribution of scatters confined in a target area of specific shapes

Continuation of Table 2.9	
Pros	**Cons**
• Suitable for the analytical realization of UAV-MIMO channel in LAP [50, 53]	• High computational complexity

2.5 Important Issues for Channel Modeling

2.5.1 Airframe Shadowing

In UAV communication, the radio path between aircraft and ground control station may be blocked by aircraft structure, such as wings, fuselage or engine. Also, during flight maneuvering or banking turns, the direct LOS path may be severed and thus induce shadowing. In the case of small size UAVs, airframe shadowing may occur due to different types of UAVs, such as multi-rotors, sharp transitions in flight dynamics, aerodynamics due to structural design, type and placement of on-board antenna and material. In the context of UAV channel characterization, airframe shadowing is still unexplored, as most of the measurement campaigns pertinent to this phenomena are initiated with manned aircrafts in high altitude. Therefore, the characterization of airframe shadowing with multi-rotor UAVs in low altitude is an interesting topic. For manned aircraft, in [60], channel measurements were extracted for the communication link between aircraft and satellite. Characterization of the air-to-ground channel in the C band was performed in [61]. Reference [62] analyzed the CDF of the received signal power during the circular flight track. In [63], airframe shadowing was reported due to wings and engine of the commercial A320 aircraft. Empirical airframe shadowing model was proposed in [64].

2.5.2 Stationary Intervals

One of the most important characteristics that distinguish UAV communication from conventional communication is the non-stationarity in UAV channels, where the WSSUS assumption is violated. Therefore, wideband frequency-dispersive channel statistics are important within the stationary interval of the non-stationary UAV channel. No comprehensive study is available in the literature that addresses non-stationarity for the UAV propagation channel in LAP. Therefore, estimation of the stationary interval is a contemporary research topic. Efforts to characterize the air-to-ground channel with stationarity interval were made in [112]. In this study, the stationary interval was computed for wideband measurements using temporal PDP correlation coefficient method, whereas, spatial correlation collinearity was considered for narrowband measurements. The estimated stationary interval from both of these methods was approximately 15 meters or 250λ in the C band with the bandwidth of 50 MHz, where λ is the wavelength.

2.5.3 Diversity Gain

Diversity is beneficial to enhance the reliability of communication systems, particularly when deep fades dominate. Terrestrial MIMO has been widely recognized to offer superior diversity gain and high spectral efficiency in rich multipath environments. However, its applicability in UAV communication is still restrained by several factors. First, the spatial multiplexing gain in the airborne MIMO is often hindered by the lack of scattering environment near UAVs, which could only provide minimal throughput improvement in comparison with single antenna UAV systems. Second, it might be difficult for small size UAVs to accommodate multiple antennas or antenna arrays with large inter-element distance to improve spatial multiplexing gain. However, smaller carrier wavelengths can make it feasible to mount a small antenna array, but at the expense of higher path loss. Furthermore, power consumption by the multiple antenna system places a major constraint on battery operated UAVs. Moreover, UAV-MIMO gain can be further

curtailed due to difficulty in acquiring accurate channel state information for a highly time-variant air-to-ground channel. Despite these challenges, some studies have exploited MIMO technology in the airborne environment. For example, in [65], a 4×4 MIMO-enabled OFDM system was used to increase the average throughput by 2 times and the range extension by 1.6 times in comparison to a SISO system. In [66], multiple helicopter mounted antennas were utilized to achieve the SNR gain of approximately 13 dB. In [68], the spatial multiplexing gain was achieved with a 2×2 MIMO configuration and consequently enhanced the throughput gain up to 8 times for most of the flight route. However, these studies were conducted with manned aircrafts in the HAP. For UAV communications, there are very few measurement campaigns on the effect of multiple antenna systems. In [77] and [78], the air-to-ground channel characterization was initiated with a 1×4 antenna configuration. In this work, carrier-to-noise ratio (CNR) gain was compared for the common combining strategies such as selection, equal-gain and maximal ratio combining (MRC). In [110], the performance of multiple receiver and transmitter nodes was evaluated by the correlation coefficient. In this case, the packet delivery rate was boosted by 25 % on average due to the poor correlation at the multiple receiver nodes in a 1×4 configuration and by 37 % with the selection diversity using three transmitters in a 3×4 setup. Measurement of a 4×4 MIMO channel in [111] revealed that despite of the sparse multipath environment, poor spatial correlation provides significant capacity gain due to the planar wavefronts generated by near-field reflections at the ground receiver side.

In these studies, multiple antenna systems were used to combat fading in multipath propagation and to attain higher throughput. To achieve these objectives, the value of correlation coefficient due to fading at antenna elements provides insights about the achievable MIMO gain. In this case, large performance improvement can be achieved with low correlation coefficient. However, available literature is scarce for empirical evaluation of the correlation coefficient. Therefore, more measurement campaigns are required to study UAV-MIMO systems from the channel characterization viewpoint.

2.6 Open Research Problems

UAV propagation channels have significant importance in optimizing the coverage, reliability and capacity performance of UAV communication. Despite of all these advancements, many research issues remain open. This section will discuss some research challenges and potential opportunities for characterizing UAV channels for future measurement campaigns and the development of realistic UAV channel model.

2.6.1 UAV Measurement Campaigns

Measurement campaigns are beneficial for the formulation of effective UAV channel models, evaluating the performance of UAV communication systems and network planning. However, propagation aspects of UAV communication change regionally due to UAV environment. In the literature, most of the UAV campaigns are launched in urban, suburban and open fields with mostly clear LOS conditions, whereas, measurement efforts are still missing for the dense urban scenario, metropolitan areas with skyscrapers and over water bodies. Therefore, more extensive measurement campaigns are required. Moreover, the use of channel sounding equipment is important with regard to on-board space limitations, payload weight, bandwidth requirements and multipath resolution. To this end, channel characterization with USRP hardware, such as N-210 [79, 80, 108], B-210 [83], X-310 [142, 143] and B-200 mini can provide flexible platforms due to lighter weight, low power consumption, wideband frequencies and capable of testing different wireless communication protocols, such as multi-carrier and MIMO system in a UAV communication framework. Other possible choices for channel measurement hardware used by different researchers are the P410 UWB radio [81], autonomous mobile network scanner by Rohde & Schwarz [99] and third generation (3G), and fourth generation (4G) enabled smart-phones [100, 113]. In addition, the effects of antenna placement on UAVs and the gain from UAV-MIMO systems for both the air-to-air and air-to-ground propagation are not well studied. Furthermore, the choice of aerial altitude platforms and dif-

ferent types of UAVs are also important aspects for both the UAV applications and channel characterization. In this case, multi-rotor and fixed-wing UAVs may be preferred for static and mobile UAV applications, respectively. However, for both types, the impact of UAV space and take-off weight (UAV weight with payload) can put constraints on the flight endurance time. Therefore, heavy-duty UAVs are more desirable to carry enough wireless equipment, for instance, DJI S-1000 and Agras MG-1 can accommodate a payload of around 7 kg and 10 kg, respectively. Also, UAVs should generate enough thrust to combat the atmospheric turbulence which may be detrimental in some UAV applications demanding stability for critical and continuous connectivity.

2.6.2 UAV Propagation Channel Models

Communication in UAV networks takes place over air-to-air and air-to-ground channels. In this case, the air-to-air channel is intended for inter-UAV communication for coordination and collaboration in UAV swarms, while the air-to-ground channel is used for relaying data between UAVs and ground stations. Most of the UAV propagation models are proposed with the approximation of time-invariant channels when non-stationarity is ignored in the estimation of the small-scale statistics, this may lead to erroneous conclusions. Therefore, it would be interesting to analyze the UAV propagation channel with the estimation of the stationary interval using temporal PDP correlation coefficient [112], correlation matrix distance [112], spectral divergence [144] and evolutionary spectrum [145] methods. Furthermore, the channel non-stationarity can be modeled by the flexibility of the geometric-based stochastic approach by considering time-variant parameters. The research on multidimensional UAV channel modeling is still in its preliminary stages as most of the empirical models reported large-scale statistical properties of the UAV channel with regard to flight dynamics, altitude and communication distance. Furthermore, airframe shadowing by small size rotary UAVs has not received commensurate level of attention and more empirical studies are required to study this phenomenon for both the air-to-ground channel in single-hop networks and air-to-air

propagation in multi-hop networks. In addition, ray-tracing can be used to probe the airframe shadowing, as computer-aided design (CAD) tools are capable of incorporating UAV shape, metallic properties and different maneuvering positions.

In this chapter, various channel models have been reported from the existing literature on UAV communications. However, free space and probabilistic LOS channel models were predominantly used for theoretical analysis of air-to-ground propagation in UAV communications. The probabilistic LOS channel model is used in chapter 3, 4, and 5 of this thesis due to two main reasons. First, to imitate application scenarios of different urban environments in different system models considered in these chapters. Second, to evaluate the impact of environmental parameters on the overall performance of the considered UAV systems. However, in some cases the average path loss expression of the probabilistic LOS model [19] in Table 2.6 may not provide enough degree of freedom for analytical tractability. Therefore, in chapter 4, the probabilistic LOS model is curve-fitted with a three-variable power function to derive closed-form expressions. Moreover, distance-dependent LOS model with PLE of 2 (propagation in free space) and 4 (propagation in urban environment) is used for comparison with the approximation of the probabilistic LOS model under the same system model settings. Furthermore, in chapter 3 and 5, the probabilistic LOS model is useful to evaluate the impact of the optimal UAV altitude on the overall network performance.

2.7 Conclusion

This chapter has provided a comprehensive review of the UAV channel characterization with measurement campaigns and statistical channel models. It has categorized the UAV channel measurement campaigns in LAP based on the narrowband or wideband channel sounder, low-cost and low-power channel sounding solution, and widely deployed ground infrastructure. This chapter also reviewed empirical models for air-to-ground and air-to-air propagation channels. Then the UAV channel modeling approaches were

classified as deterministic, stochastic and geometric-stochastic models. Furthermore, challenging issues were discussed in the practicability of UAV communications related to airframe shadowing, channel non-stationarity, and diversity techniques. Finally, the future research challenges were presented which will be helpful to provide further insight of the UAV channel characterization for launching future measurement campaigns and proposing a pragmatic framework for effective UAV channel models.

Chapter 3

Optimum Deployment Strategy of Multiple UAVs

3.1 Introduction

UAVs equipped with radio transceivers can satisfy the requirements for an aerial communication platform by serving either as a mobile BS or as an airborne relay. Due to their flexible deployment, UAVs can be used in multi-tier UAV-assisted cellular networks to provide on-demand communication services in disaster areas and to enhance coverage, capacity and reliability performances of existing terrestrial cellular networks [133]. However, several challenges, such as optimal 3D placement, flight endurance time, energy constraints and interference management, may impede the widespread applicability of UAV communications.

In UAV communications, aerial BSs are mostly used as LAPs to provide ground coverage as UAV-based small cells (USCs). The size of USCs varies according to the altitude, position, transmit power, and type of UAVs and characteristics of the environment. In this regard, the optimum placement of UAVs to analyze the coverage performance of USCs has attracted great research interest. For instance, in [19] and [100], the UAV deployment issue has been considered for the coverage enhancement of a single USC. In

[124], the authors presented the UAV placement method in a 3D space to enlarge the coverage area. References [130] and [146] analyzed the optimal UAV altitude to maximize the coverage area with minimum outage probability for a given SNR threshold. In [147], the authors analyzed the optimization problem for UAV placement to increase the number of covered users with various QoS demands. However, these works were conducted for networks with a single UAV. When multiple UAVs are available, references [114] and [148] exploited the deployment of multiple UAVs to expand coverage for the ground users with the minimum number of aerial BSs. Furthermore, most of the works either optimize the horizontal coordinates of UAVs for a constant UAV altitude above the ground [149] or optimize the UAV altitude while keeping a constant horizontal position [150, 151]. These studies analyzed the UAV placement problem using optimization framework in an interference-free environment. However, in the multi-UAV scenario, interference may be inevitable, as spectrum scarcity may necessitate frequency reuse over the spatial domain [152], causing interference in UAV-assisted cellular networks. Therefore, effective interference mitigation framework is required to maximize the coverage performance and guarantee reliable communications.

From the perspective of UAV communications, several works have been carried out to characterize the interference generated by UAVs and the impact of interference from terrestrial BSs on the UAV connectivity. For example, reference [45] proposed a deployment method for multiple UAVs using circle packing theory to maximize the coverage performance and to compensate interference with the adjustment in UAV's altitude and the gain of directional antenna. In [129], the authors analyzed the coverage performance of USCs with and without interference for two UAVs. References [142] and [153] used empirical measurements to characterize the impact of UAV altitude on interference incurred by terrestrial LTE networks. The authors in [154] presented an interference-aware placement strategy for UAV relays to overcome traffic congestion and to compensate outage in LTE networks. In [155], simulation was carried out using commercial software to study the effect of UAV altitude on coverage area and inter-cell interference. In

[156], the interference alignment principle was exploited to manage the interference in small-cell networks. In [157], a circle placement problem was formulated without considering coverage overlapping to avoid interference and to achieve maximum user coverage and power efficiency. Most of these studies have relaxed the overlapping coverage constraints to avoid the co-channel interference. Also, the separation distance between UAVs is an important parameter that determines the trade-off between coverage and interference generated by UAVs, but no comprehensive results are available in the literature to study this parameter in the multi-UAV network.

In UAV communications, co-channel interference primarily occurs when multiple UAVs share the same frequency resources at the same time in spatially separated locations. Therefore, some research efforts have been devoted to consider the effect of co-channel interference in the performance analysis of UAV communications. For example, reference [118] took into account the effect of co-channel interference between different data user streams in ground-to-air uplink transmission. Reference [158] considered the impact of co-channel interference in the problem formulation of the UAV trajectory optimization. In [159], the authors derived a closed-form expression of the ground user coverage probability to characterize the influence of co-channel interference while capturing the effect of density of UAV deployment, UAV antenna beam-width and the optimum altitude. On the other hand, interference management techniques have been proposed in the existing literature. For example, in [160], the multi-antenna UAV scheme was proposed as the co-channel interference cancellation technique. Furthermore, references [161] and [162] demonstrated that caching can be used for interference management in UAV communications. In reference [163], the coordinated multipoint (CoMP)[1] architecture was exploited for multi-UAV system to mitigate interference and offer high UAV mobility. In [165], a path-planning algorithm was proposed to achieve a trade-off between the maximization of energy efficiency and minimization of both the interference and latency. In [166], cooperative non-orthogonal multiple access (NOMA) was proposed to

[1] Coordinated multipoint (CoMP) architecture support cooperative communications over multiple transmission and reception points [164].

mitigate the uplink interference in cellular-connected UAV communication. However, these techniques may require excessive power for signal processing which can increase the power expenditure of battery-operated UAVs.

Motivated by the above observations, this chapter studies the effect of co-channel interference generated by multiple UAVs on the coverage area performance, which is defined as the ratio of the sum of effective coverage area of USCs to the target area as a function of the separation distance between UAVs. The multi-UAV network consists of a primary UAV surrounded by secondary UAVs operating in a coordinated framework in two scenarios. First, this work assumes the symmetric deployment of UAVs that have the same optimal altitude and transmit power. Second, in the asymmetric deployment of UAVs, a primary UAV is placed at an optimal altitude and secondary UAVs are located above and below the optimal altitude with different transmit power. In both cases, the worst-case scenario of the co-channel interference generated by UAVs is considered. The optimal separation distance for a given target area with predefined SINR is studied. Numerical results show that the coverage area performance depends on the SINR threshold, the separation distance between UAVs, and the number of UAVs and their formations.

The main contributions of this chapter are summarized as follows:

- Different from [114] and [148], which not include the effects of co-channel interference between multiple UAVs in the placement optimization problem, this chapter proposes a coordinated multi-UAV framework to study the coverage area performance in the presence of co-channel interference. Specifically, multiple UAVs are deployed at predefined coordinates in a 2D Cartesian plane by exploiting a hexagonal layout. These coordinates are specified for a minimum UAV separation distance to avoid collision in a given target area and utilize SNR measures to find the optimal altitude of UAVs.

- After the initial deployment of UAVs at the specific coordinates and the optimal altitude, this chapter characterizes the impact of the UAV separation distance on the

coverage area optimization in the presence of co-channel interference with the help of SINR metrics to meet the threshold requirement for the worst-case scenario. Compared with [129], this work studies the coverage area performance for multiple UAVs that can be deployed in one-dimensional (1D) or 2D formations in a single snapshot, while [129] only considered two UAVs deployed in 1D formations. Also, compared with the circle packing approach in [127] and the circle placement approach in [157], this work considers the realistic overlapping scenario of USCs which results in the reduction of the effective coverage area due to the interference and consequently the shape of USCs varies according to the separation distance between UAVs. The results then provides the useful insights for enabling an harmonious integration of multiple USCs in UAV communications.

- Using the proposed UAV deployment framework, this chapter analyzes the system-level performance in terms of the coverage probability of the ground user located at the boundary of the USC with the maximum coverage distance. The results are then used to determine the minimum number of UAVs needed to achieve a target coverage probability at different UAV separation distances.

The rest of this chapter is organized as follows. The system model is introduced in Section 3.2, including the use of the practical channel model. Section 3.3 presents the framework for the deployment of multi-UAV network and assesses the coverage area performance and the coverage probability in presence of interference. Section 3.4 presents numerical results. Section 3.5 summarizes the main conclusions of this chapter.

3.2 System Model

Coordinated multi-UAV networks can be used to alleviate the co-channel interference in UAV communications. As a general multiple UAV model for M aerial BSs, this work assumes that the primary UAV is static and fixed on top of the center of a specified target area to serve as a reference node to adjust the separation distance, while secondary UAVs

are placed at predefined deployment coordinates. The secondary UAVs in this work are static after optimization so that the coverage is also static on the ground. The static coverage assumption is made to ensure that the coverage performance is satisfactory inside the USCs while meeting the stringent SINR requirement and also considering that UAVs and ground users are static. Fig. 3.1 depicts a downlink UAV transmission system that consists of the primary UAV and secondary UAVs positioned at an altitude of h_p and h_s meters, respectively. Without loss of generality, a 2D Cartesian system is considered in which seven UAVs are used in the Euclidean plane of the square target area with a side length of l meters and assume hexagonal layout for UAV deployment. It should be noted that the use of seven UAVs in Fig. 3.1 is only for illustration purpose. The model is applicable to any number of UAVs but in practice, large numbers are highly unlikely due to the exponentially increasing complexity for UAV control, such as collision avoidance and ground coordination. In this case, P_0 is the projection center of the primary UAV and $S_{1,\cdots,M-1}$ are the coordinates of secondary UAVs located at the vertices, where $M = 7$ in Fig. 3.1. As a result, spatial isolation between interfering UAVs is possible with the same separation distance D. Moreover, coordinated multi-UAV networks can be deployed based on the layout of regular convex polygons to meet the coverage requirement inside the specific target area with the required number of UAVs. The advantage of such coordinated scheme is that it can react to failure of any UAVs quickly by reformation of the deployment strategy to the nearest regular polygon layout. The considered multi-UAV network offers resilience in case of malfunctioning BSs and providing coverage in post-disaster areas.

In the absence of interference, r_a is the maximum coverage distance at the boundary points A_1 and A_2 in the primary and secondary USC, respectively. In the presence of interference, r_p and r_s are coverage distances that attain a minimum performance, respectively, for boundary points A_3 and A_4 in the primary and secondary USC. $r_{i\in\{1,\cdots,M-1\}}$ are distances to represent the worst-case scenario of the co-channel interference generated at the boundary of the primary USC from the projection of $M-1$ secondary UAVs.

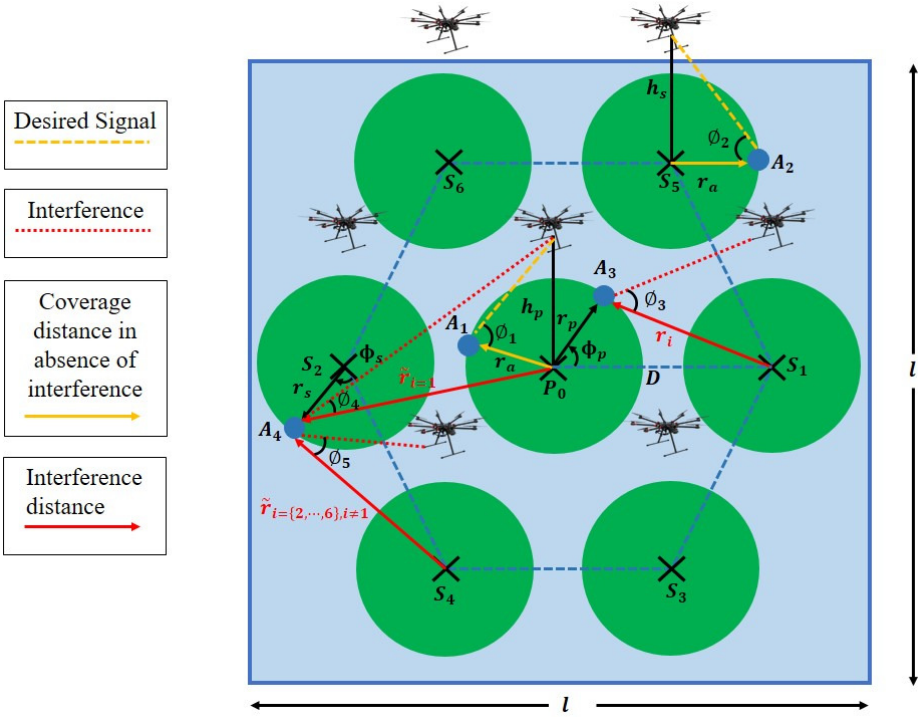

Figure 3.1: Diagram of the multiple interfering UAVs scenario.

Also, $\widetilde{r}_{i\in\{1,\cdots,M-1\}}$ denote the interference distances from the boundary point of the serving secondary USC to the coordinates of all remaining UAVs in the network. The coverage performances of both the primary and secondary UAVs are dependent on r_p and r_s as a function of D for a specific range of coverage angles, respectively, Φ_p and Φ_s.

3.2.1 Channel Model

In this chapter, a realistic channel model is used in which air-to-ground path loss is modeled with both LOS and NLOS components. To this end, one of the most suitable channel models was proposed in [19], which is predominantly utilized in the literature to facilitate the optimization of UAV placement in [44, 114, 124, 127, 129, 130, 147, 157, 167]. This model considers the effect of the environment with parameters a and b to characterize

the air-to-ground propagation with the probability of LOS as

$$\mathrm{P}_x = \frac{1}{1 + a \times \exp\left(ab - b\phi_x\right)}, \tag{3.1}$$

where $x \in \{1,2,3,4,5\}$ represents elevation angles $\phi_1, \phi_2, \phi_3, \phi_4$, and ϕ_5 at boundary points in five scenarios shown in Fig. 3.1. In the case of non-interfering link, the elevation angle for the primary UAV at point A_1 is $\phi_1 = \frac{180}{\pi} \arctan\left(\frac{h_p}{r_a}\right)$ and the mean path loss is given as [167]

$$\overline{\mathrm{PL}}_p(\mathrm{dB}) = A \times \mathrm{P}_1 + 10\log_{10}(h_p^2 + r_a^2) + B. \tag{3.2}$$

The elevation angle for secondary UAV at point A_2 is $\phi_2 = \frac{180}{\pi} \arctan\left(\frac{h_s}{r_a}\right)$ and the mean path loss is given as

$$\overline{\mathrm{PL}}_s(\mathrm{dB}) = A \times \mathrm{P}_2 + 10\log_{10}(h_s^2 + r_a^2) + B. \tag{3.3}$$

For the interference received in the primary USC at the boundary point A_3 from secondary UAVs, $\phi_3 = \frac{180}{\pi} \arctan\left(\frac{h_s}{r_i}\right)$ for $i = \{1,2,\cdots,M-1\}$ and the mean path loss is given as

$$\overline{\mathrm{PL}}_i(\mathrm{dB}) = A \times \mathrm{P}_3 + 10\log_{10}(h_s^2 + r_i^2) + B. \tag{3.4}$$

For the interference incurred in the serving secondary USC at point A_4 by the primary UAV, the interference distance between projection coordinate P_0 and boundary point A_4 is $\widetilde{r}_{i=1}$. Therefore, $\phi_4 = \frac{180}{\pi} \arctan\left(\frac{h_p}{\widetilde{r}_{i=1}}\right)$ and the mean path loss is given as

$$\widetilde{\mathrm{PL}}_{i=1}(\mathrm{dB}) = A \times \mathrm{P}_4 + 10\log_{10}(h_p^2 + \widetilde{r}_{i=1}^2) + B. \tag{3.5}$$

For the interference received in the same secondary USC at point A_4 from the remaining secondary UAVs, $\phi_5 = \frac{180}{\pi} \arctan\left(\frac{h_s}{\widetilde{r}_i}\right)$ for $i = \{2,\cdots,M-1\}$ and the mean path

loss is given as

$$\widetilde{\mathrm{PL}}_i(\mathrm{dB}) = A \times \mathrm{P}_5 + 10\log_{10}(h_s^2 + \tilde{r}_i^2) + B. \tag{3.6}$$

where $A = \varepsilon_{\mathrm{LOS}} - \varepsilon_{\mathrm{NLOS}}$, $B = 20\log(\frac{4\pi f}{c}) + \varepsilon_{\mathrm{NLOS}}$, $\varepsilon_{\mathrm{LOS}}$ and $\varepsilon_{\mathrm{NLOS}}$ denote the excessive path loss factors which rely on the propagation environment as well as on the LOS and NLOS conditions, respectively. Also, f is the carrier frequency and c is the speed of light.

The above channel model is considered due to its predominant usage in the formulation of the optimization problem for UAV placement. With such a model, a trade-off of the UAV altitude can be exploited for the UAV deployment at the optimal altitude where the minimum path loss will be attained by a single UAV while transmitting at the minimum power and covering the maximum coverage area on the ground under the SNR threshold requirement. In addition, the system parameters and channel characteristics are the same for all UAVs. Next, $\overline{\mathrm{PL}}_s$ and $\overline{\mathrm{PL}}_p$ will be used to present SNR measures. Also, $\overline{\mathrm{PL}}_i$, $\widetilde{\mathrm{PL}}_{i=1}$, and $\widetilde{\mathrm{PL}}_i$ will be used for SINR metrics.

3.3 Coverage area performance of coordinated multi-UAV network

Interference control is one of the major challenges in radio resource management of UAV communications. Intuitively, it is evident from the considered system model that in the absence of coordination between UAVs, a large value of D would deteriorate the coverage performance by moving the coverage areas of multiple UAVs outside the boundary of the target area but leave a big gap between them for protection. Conversely, a small value of D leads to the overlap of USC areas to provide more coverage but cause strong co-channel interference when all participating UAVs use the same frequency resources at the same time. Therefore, an optimal separation distance between UAVs exists and provides a trade-off between interference avoidance and maximum coverage. This section

defines the deployment strategy for the considered multi-UAV system and then employs it to present the coverage area performance and the coverage probability as a function of the UAV separation distance.

3.3.1 Optimal UAV Altitude

Fig. 3.2 illustrates the cases of symmetric and asymmetric deployments based on UAV altitude. In the symmetric case, the altitudes and transmit powers of all UAVs are identical. However, for the asymmetric case, the primary UAV is placed at an optimal altitude and secondary UAVs can be located above or below this altitude. Therefore, the first goal of this work is to place the primary UAV at the optimal altitude h_P to achieve the maximum ground coverage in a specific target area for a given r_a. In this regard, the boundary point A_1 on the ground is covered when its SNR is above a certain threshold Ψ_{th} for a minimum transmit power, $P_{t,p}$, i.e.

$$\mathrm{SNR}(r_a, h_p) = \frac{P_{r,p}}{N_0} \geq \Psi_{th}, \tag{3.7}$$

where $P_{r,p} = P_{t,p} \times 10^{\frac{-\overline{\mathrm{PL}}_p}{10}}$ is the received power in the absence of interference, $\overline{\mathrm{PL}}_p$ is given in (3.2), and N_0 is the noise power.

The SNR for the secondary UAV is given as

$$\mathrm{SNR}(r_a, h_s) = \frac{P_{r,s}}{N_0} \geq \Psi_{th}, \tag{3.8}$$

where $P_{r,s} = P_{t,s} \times 10^{\frac{-\overline{\mathrm{PL}}_s}{10}}$ is the received power in the absence of interference, $P_{t,s}$ is the corresponding transmit power of secondary UAVs at altitude h_s, and $\overline{\mathrm{PL}}_s$ is given in (3.3).

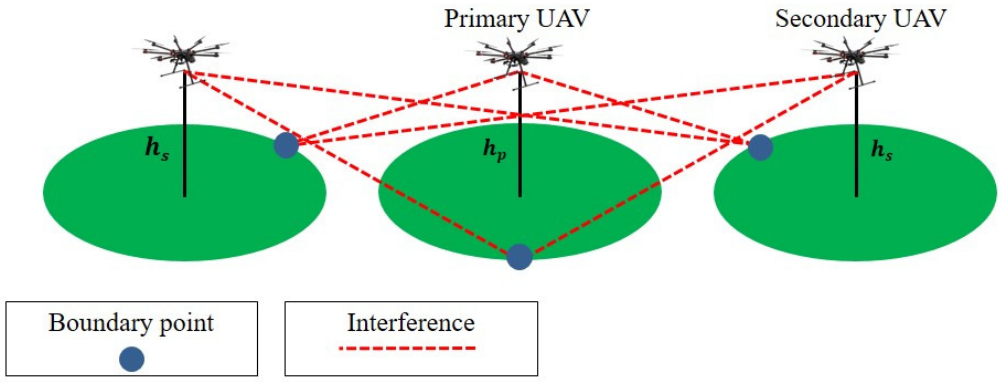

(a) $h_p = h_s$

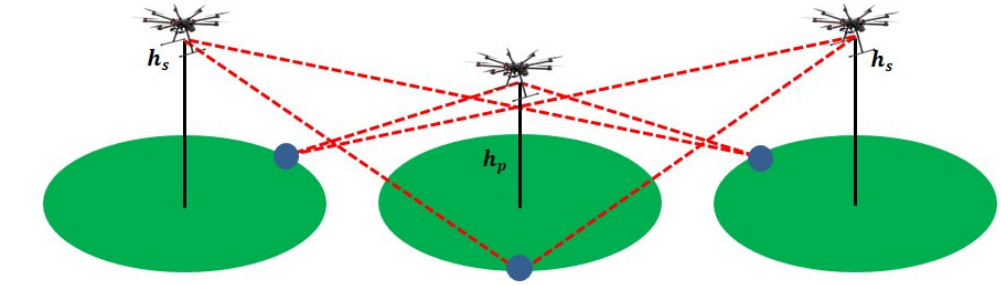

(b) $h_p < h_s$

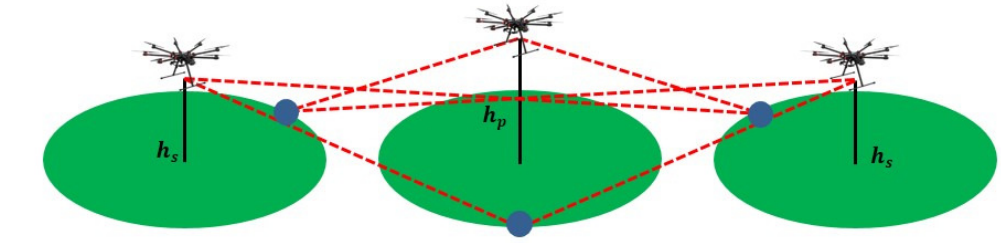

(c) $h_p > h_s$

Figure 3.2: Illustration of symmetric and asymmetric UAV deployment scenarios.

3.3.2 UAV Projection Coordinates

This chapter focuses on the use of quasi-stationary UAVs, where their positions remain unchanged for a specific duration of time. For such setup, it is important to determine the placement coordinates of UAVs to avoid collision between them and to provide spatial isolation between UAVs to control the interference. Therefore, the deployment strategy assumes that the primary UAV is fixed at $P_0 = \{0,0\}$. When $M = 7$, the coordinates of secondary UAVs in the hexagonal layout are given as

$$S_{1,\cdots,M-1} = \begin{cases} S_1\big(D_{min}+D,0\big) \\ S_2\big(-(D_{min}+D),0\big) \\ S_3\big(\frac{1}{2}(D_{min}+D),-\frac{\sqrt{3}}{2}(D_{min}+D)\big) \\ S_4\big(-\frac{1}{2}(D_{min}+D),-\frac{\sqrt{3}}{2}(D_{min}+D)\big) \\ S_5\big(\frac{1}{2}(D_{min}+D),\frac{\sqrt{3}}{2}(D_{min}+D)\big) \\ S_6\big(-\frac{1}{2}(D_{min}+D),\frac{\sqrt{3}}{2}(D_{min}+D)\big), \end{cases} \tag{3.9}$$

where $D_{min} = \frac{\overline{\mathrm{PL}_s}}{4} - r_a$ is the minimum separation distance to avoid collision between UAVs and to ensure minimum coverage performance for all participating UAVs in the presence of interference. In this case, D is the only variable which controls the coverage area performance within a target area.

3.3.3 Signal-to-Interference-plus-Noise Ratio (SINR) Analysis

SINR is a commonly used metric for wireless communication systems to characterize the impact of interference generated by adjacent BSs. This affects the received signal strength at a ground user and consequently defines the coverage area of the cell. This chapter assumes that the participating UAVs in the considered system interfere with each other during the downlink transmission. In this case, a boundary user at point A_3 is served by the primary UAV in the presence of interfering secondary UAVs when its

SINR satisfies the threshold requirement Ψ_{th}. As a result, SINR can be defined as

$$\mathrm{SINR}\big(r_p(D),\Phi_p\big)=\frac{P_{r,p}}{I+N_0}\geq\Psi_{th}, \tag{3.10}$$

where r_p is related to the interference distance r_i as

$$r_i=\sqrt{r_p^2+D^2+2r_pD\cos(\pi-\Phi_p)}, \tag{3.11}$$

and $I=P_{t,s}\sum_{i=1}^{M-1}10^{\frac{-\overline{\mathrm{PL}}_i}{10}}$ is the co-channel interference generated by secondary UAVs, and $\overline{\mathrm{PL}}_i$ is given in (3.4).

For the boundary point A_4 in the secondary USC, the SINR is given as

$$\mathrm{SINR}\big(r_s(D),\Phi_s\big)=\frac{P_{r,s}}{\widetilde{I}+N_0}\geq\Psi_{th}, \tag{3.12}$$

where r_s is dependent on the interference distance $\widetilde{r}_i$ as

$$\widetilde{r}_i=\sqrt{r_s^2+D^2+2r_sD\cos(\pi-\Phi_s)}, \tag{3.13}$$

and

$$\widetilde{I}=P_{t,p}\times10^{\frac{-\widetilde{\mathrm{PL}}_{i=1}}{10}}+P_{t,s}\sum_{i=2}^{M-1}10^{\frac{-\widetilde{\mathrm{PL}}_i}{10}}, \tag{3.14}$$

$\widetilde{\mathrm{PL}}_{i=1}$ is given in (3.5), and $\widetilde{\mathrm{PL}}_i$ is given in (3.6).

3.3.4 Coverage Area Performance as a Function of Optimal Separation Distance

The coverage area ratio determines the overall coverage area performance of the considered multi-UAV system. Particularly, it is defined as the ratio of the total effective area

covered by both the primary and secondary USCs to the target area as

$$A_c(D) = \frac{2}{l^2}\Big[\int_0^{r_p(D)} \int_{\Phi_p=0}^{\Phi_p=\pi} R\,dR\,d\Phi + (M-1) \times \int_0^{r_s(D)} \int_{\Phi_s=0}^{\Phi_s=\Phi_{max}} R\,dR\,d\Phi \Big], \Phi_{max} \leq \pi, \tag{3.15}$$

where l^2 is the area of the square target area considered in the system model. Note that this work considers SINR measure which is dependent on the position of the ground user. Therefore, an analytical expression for the coverage area ratio is too complicated to be derived. Following (3.15), the minimum coverage area ratio can be obtained at $D = D_{min}$. Also, Φ_{max} limits the coverage of secondary UAVs that might project outside the target area and is given as

$$\Phi_{max} = \pi - \arccos\Big\{\frac{D_{min} + D}{r_s}\Big\}. \tag{3.16}$$

Finally, the optimal separation distance can be computed by searching (3.15) numerically as

$$D_{opt} = \arg\max_D A_c(D). \tag{3.17}$$

Analytical expressions for D_{opt} is difficult to obtain, if not impossible. Therefore, this work will use simulation to study the effect of D on $A_c(D)$ and to determine D_{opt} for maximum coverage area ratio.

3.3.5 Coverage Probability of the Worst-Case Scenario

The coverage probability is defined as

$$\mathbb{P}_c = \mathscr{P}[\text{SINR} \geq \Psi_{th}], \tag{3.18}$$

which can be written as $\mathbb{P}_c = \mathscr{P}[\text{SINR}(D) \geq \Psi_{th}]$ as the SINR depends on the separation distance between UAVs and the threshold Ψ_{th} determined by the requirement of

the ground user. This performance metric quantifies the reliability of the air-to-ground channel in presence of co-channel interference by satisfying the threshold requirement. In addition, this metric is useful to evaluate the performance of the air-to-ground channel for command and control (CnC) in multi-UAV network [168]. A reliable CnC is crucial for safe UAV deployment and better traffic management in UAV communications.

For the proposed coordinated multi-UAV network, the shape of the coverage regions of the primary and secondary UAVs may not be completely circular in the presence of the co-channel interference. As a result, the coverage distances r_p and r_s varies non-uniformly for the primary and secondary USCs, respectively, as the value of D changes. In this case, severe interference can be observed at the boundary points of USCs. The coverage probability for a boundary user located at the maximum distance r_p from the projection of the primary UAV by considering the aggregate interference from all secondary UAVs is given as

$$\mathbb{P}_c = \mathscr{P}\Big[\frac{P_{r,p}}{I+N_0} \geq \Psi_{th}\Big] = \mathscr{P}\Big[P_{r,p}(\text{dB}) \geq P_{min}\Big]. \tag{3.19}$$

where $\mathscr{P}[.]$ denotes probability, $P_{r,p}$ is the received power in the absence of interference, $P_{min} = 10\log_{10}(\Psi_{th}I + \Psi_{th}N_0)$ is the minimum received power (in dB) for successful detection in presence of interference, and I can be extracted from (3.10). Similarly, the coverage probability can be determined for a ground user located at the maximum coverage distance r_s from the projection of the serving secondary UAV by considering aggregate interference from remaining UAVs by using (3.12).

3.4 Numerical Results and Discussion

In this section, numerical results are presented. Simulation parameters for suburban and urban environments are listed in Table 3.1.

Fig. 3.3 shows the optimal altitude for the primary UAV using (3.7) to have the minimum transmit power in order to attain the coverage at the maximum radial dis-

Table 3.1: Simulation parameters.

Parameter	Value
l	2000 meters
f	2 GHz
N_0	-120 dBm
Ψ_{th}	10 dB
suburban (ε_{LOS}, $\varepsilon_{\text{NLOS}}$, a, b)	0.1 dB, 21 dB, 4.88, 0.43
urban (ε_{LOS}, $\varepsilon_{\text{NLOS}}$, a, b)	1 dB, 20 dB, 9.6, 0.28

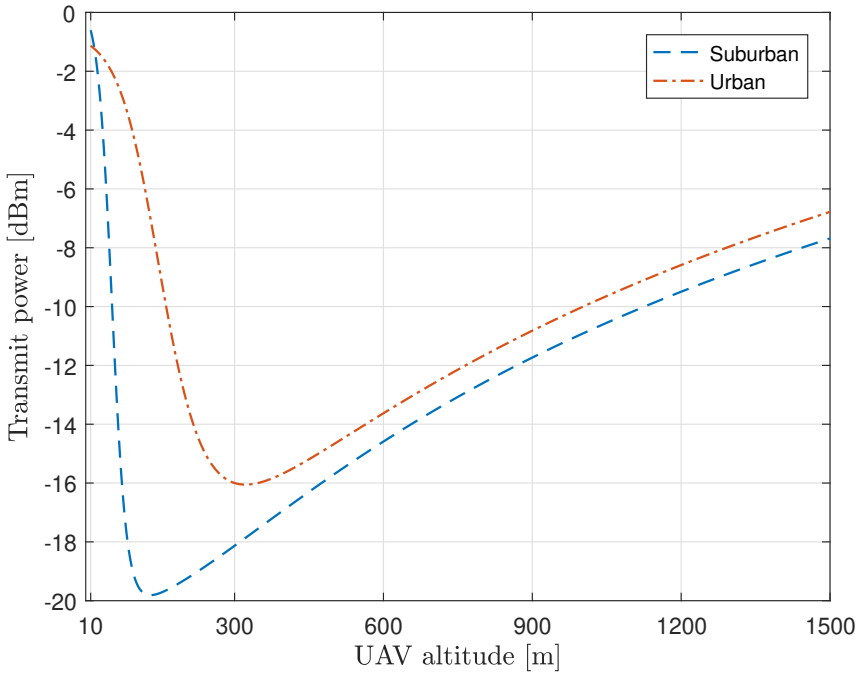

Figure 3.3: UAV altitude versus transmit power for urban and suburban environment with r_a=350 meters.

tance of 350 meters and satisfy the threshold requirement of Ψ_{th}=10 dB. Actually, the optimal altitude is the minimum possible altitude which offers the lowest path loss between the UAV and the ground user with the minimum transmit power. This leads to the best communication performance in the absence of interference. Fig. 3.3 also shows that the optimal altitude and minimum transmit power depends on the propagation environment. For instance, the optimal altitude is 131 meters and 314 meters in suburban and urban scenarios, respectively. This result is important for the power minimization

in planning multi-UAV networks.

Fig. 3.4 and Fig. 3.5 shows the ground coverage pattern in a specific target area with different numbers of UAVs for the minimum and the maximum coverage, respectively, in suburban environment with the threshold of Ψ_{th} = 10 dB and the optimal altitude of 131 meters for all UAVs. The projection coordinates of UAVs are marked by black '×'. Particularly, Fig. 3.4a and Fig. 3.5a present the coverage of three UAVs placed along a single axis in 1D formation with the separation distance of 247 meters and 747 meters, respectively. Fig. 3.4b and Fig. 3.5b depicts the coverage region of five UAVs deployed in 2D formation with the separation distance of 247 meters and 847 meters, respectively. Fig. 3.4c and Fig. 3.5c shows the coverage area of seven UAVs deployed in 2D formation with the separation distance of 247 meters and 847 meters, respectively. Expressions (3.10) and (3.12) are used to achieve the SINR requirements at the ground points for the coverage of different UAVs deployed at coordinates specified by (3.9). These results, use 10^3 sample points for individual UAVs to test ground coverage requirement and the green patches represent the coverage area of USCs that achieve the threshold requirement in the presence of interference. In this case, the separation distance of 747 meters in 1D formation and 847 meters in 2D formation compensates the strong co-channel interference because the maximum coverage area of the primary UAV is optimally confined within the target area, while a small portion of the coverage region of secondary UAVs falls outside the target area. Furthermore, as the gap between USCs increases beyond these separation distance, the coverage area of secondary UAVs further moves outside the target area which results in undesirable coverage leakage. On the other hand, the separation distance of 247 meters in both 1D and 2D formations can cause detrimental interference effect on the coverage performance as the effective coverage area shrinks because of overlapping. However, one of the major limitation of the proposed multi-UAV system is that for the given SINR threshold it may not be possible to cover the entire target area and thus there are coverage holes in the network where the ground users may not receive the communication services directly from the UAV system. To this end, two

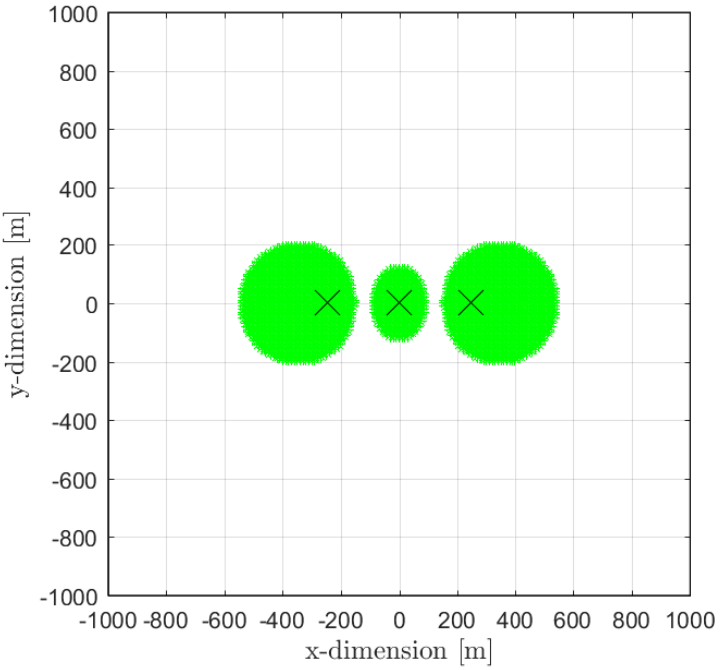

(a) Three interfering UAVs.

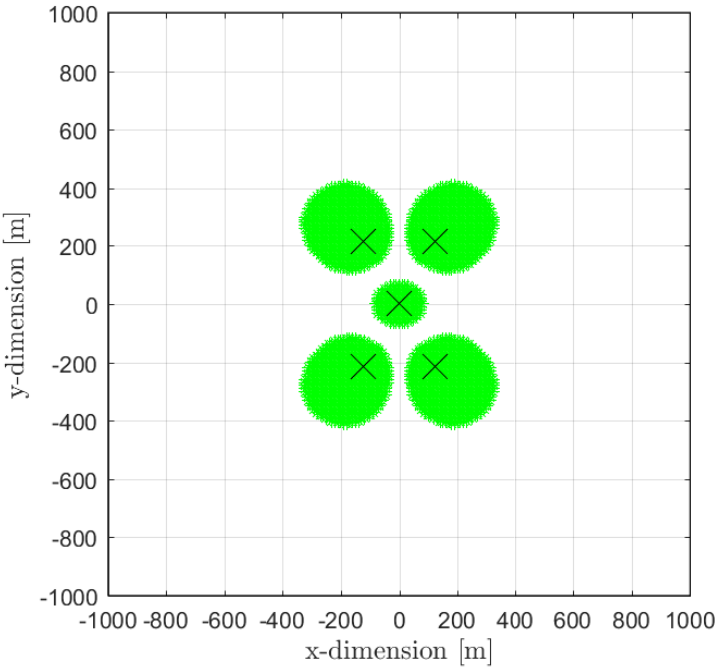

(b) Five interfering UAVs.

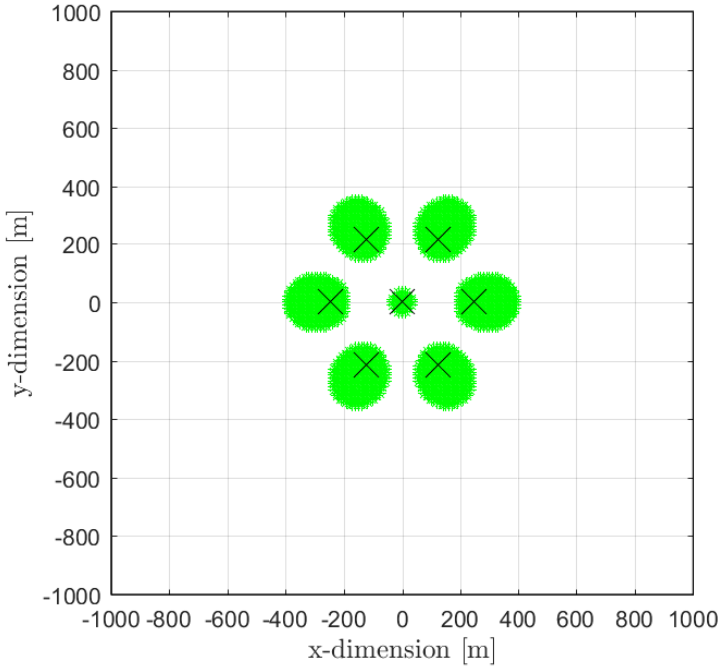

(c) Seven interfering UAVs.

Figure 3.4: Coverage map for coordinated multi-UAV deployment for different numbers of UAVs in suburban environments to attain minimum coverage.

possible solutions exists to overcome this limitation. First, to deploy the proposed multi-UAV communication system as a component of the heterogeneous network where the coverage holes will be filled either by the legacy systems (GSM or UMTS) or by the modern radio access technologies of 4G and 5G. Second, to reuse the frequency spectrum in the form of multi-layer multi-UAV system where multiple UAVs will utilize different transmission frequencies at different altitudes.

Fig. 3.6 shows the coverage performance as the ratio of the effective coverage area of USCs to the target area. In the simulation, 'fsolve' in MATLAB was used to find coverage distances r_p in (3.11) and r_s in (3.13) for the considered multi-UAV network and then apply them in (3.15)-(3.17) to observe the effect of the UAV separation distance on the coverage area performance in suburban and urban environments. Clearly, to mitigate the interference and to improve the coverage performance with a higher number of

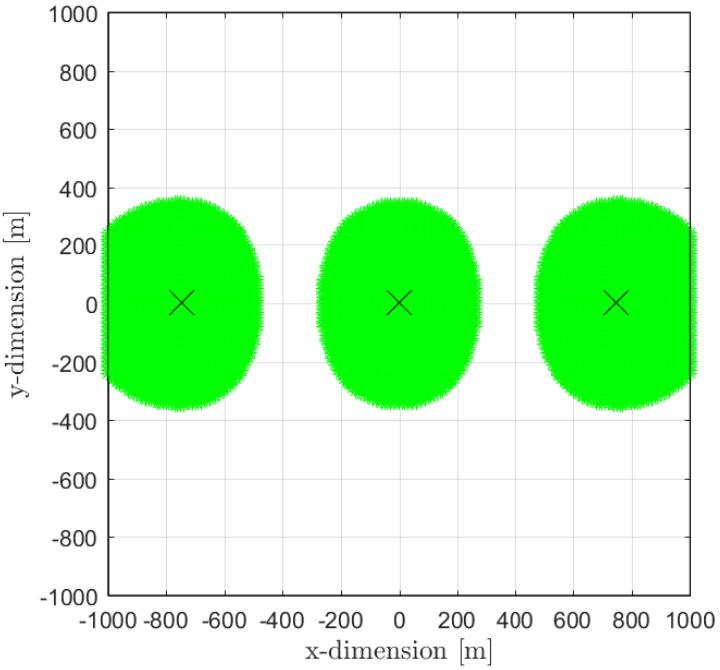

(a) Three interfering UAVs

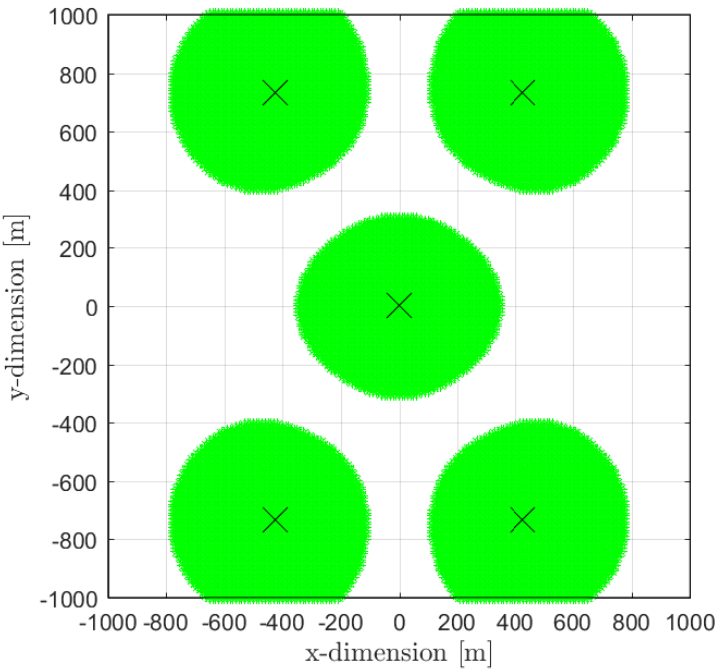

(b) Five interfering UAVs

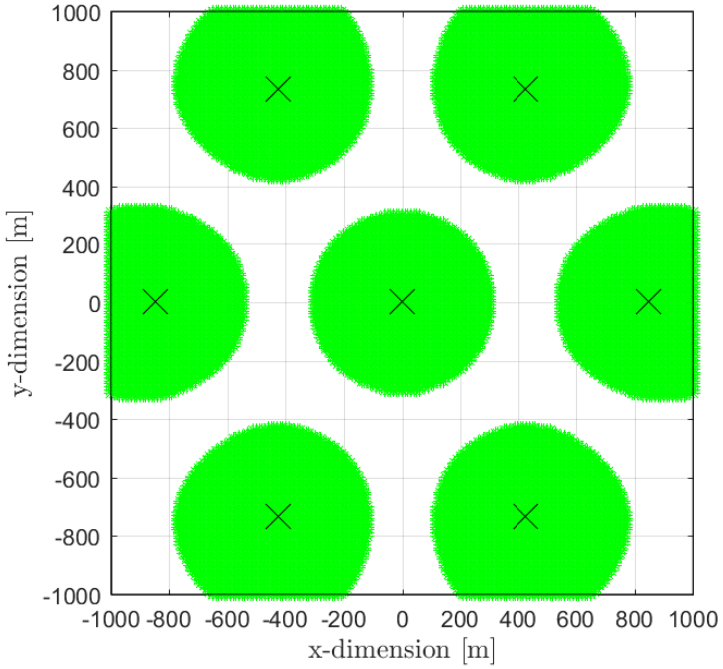

(c) Seven interfering UAVs

Figure 3.5: Coverage map for coordinated multi-UAV deployment for different numbers of UAVs in suburban environments to attain maximum coverage.

UAVs, the coverage regions of UAVs must be isolated with proper adjustment in the separation distance. One notices that the coverage ratio changes with the number of UAVs and the environmental conditions.

In Fig. 3.6a, when using the optimal altitude i.e. $h_p = h_s$, better coverage performance is observed with three UAVs for $D < 350$ meters in comparison with five and seven UAVs due to lessen co-channel interference. In contrast, for the case of $h_p < h_s$ in Fig. 3.6b, the coverage performance degrades as the altitude of secondary UAVs increased from the optimal value because of higher path loss. For the case of $h_p > h_s$ in Fig. 3.6c, best coverage area ratio is observed for $D < 500$ meters. However, as the separation distance increases from 500 meters the coverage performance becomes sub-optimal in urban environment. In these results, the minimum coverage area ratio is consistent with $D = 1250$ meters and $D = 1500$ meters for 1D and 2D formations, respectively, when the

maximum coverage of primary USC is attained and secondary UAVs moved out of the target area. Furthermore, it is observed that to achieve the maximum coverage area ratio, the optimal separation distance is dependent on the deployment formation of the UAVs rather on the number of UAVs or the environment. For instance, with three UAVs deployed in the 1D formation, the optimal separation distance is 747 meters. Whereas, for five and seven UAVs deployed in 2D formation, the optimal separation distance is 847 meters.

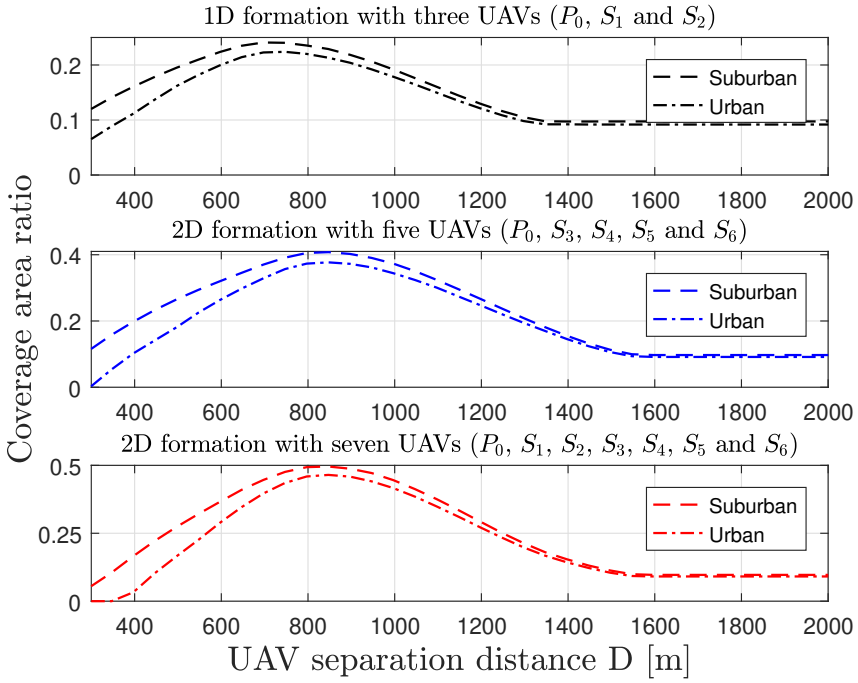

(a) $h_p = h_s$

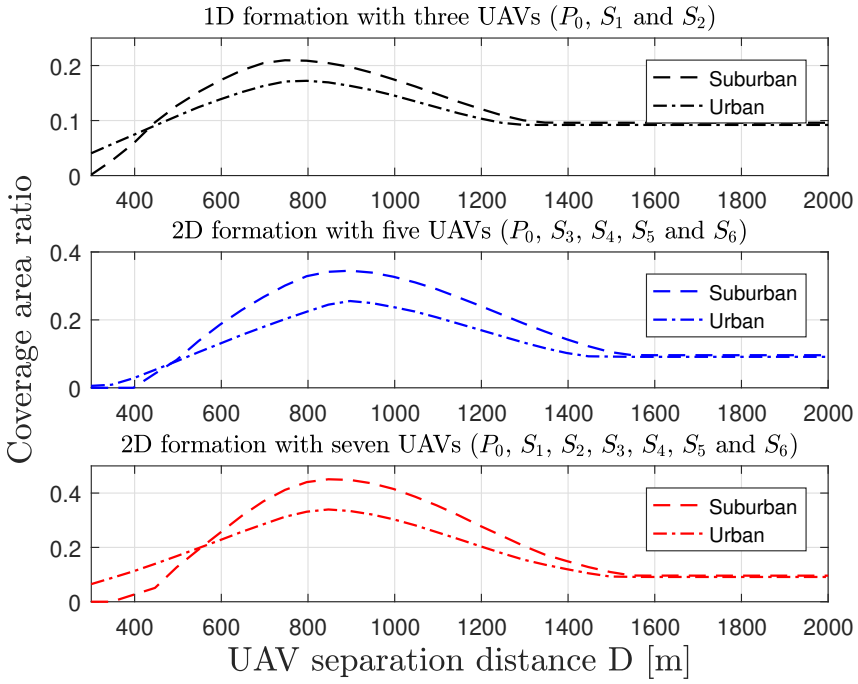

(b) $h_p < h_s$

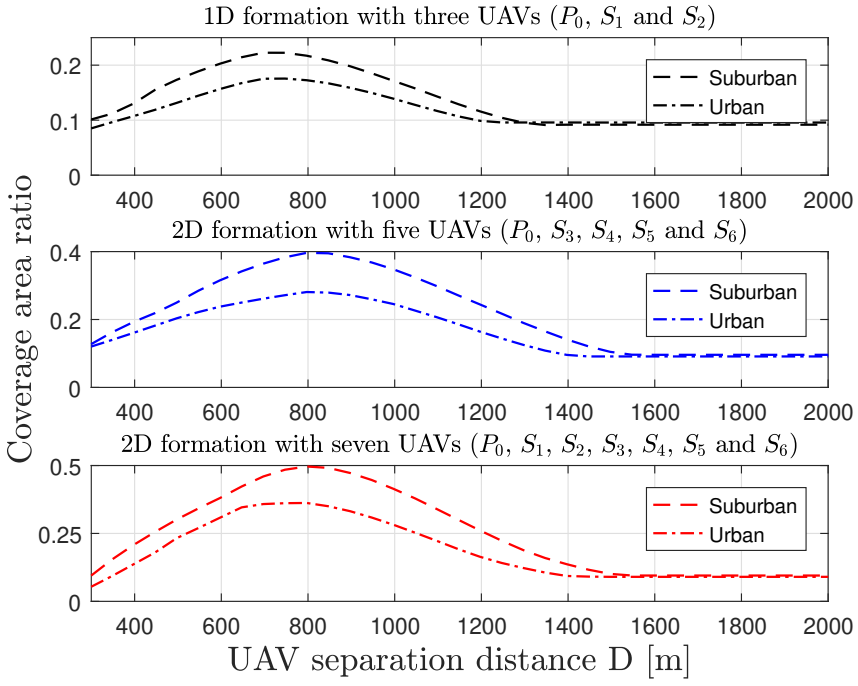

(c) $h_p > h_s$

Figure 3.6: Coverage area ratio versus separation distance for different numbers of UAVs in suburban and urban environments.

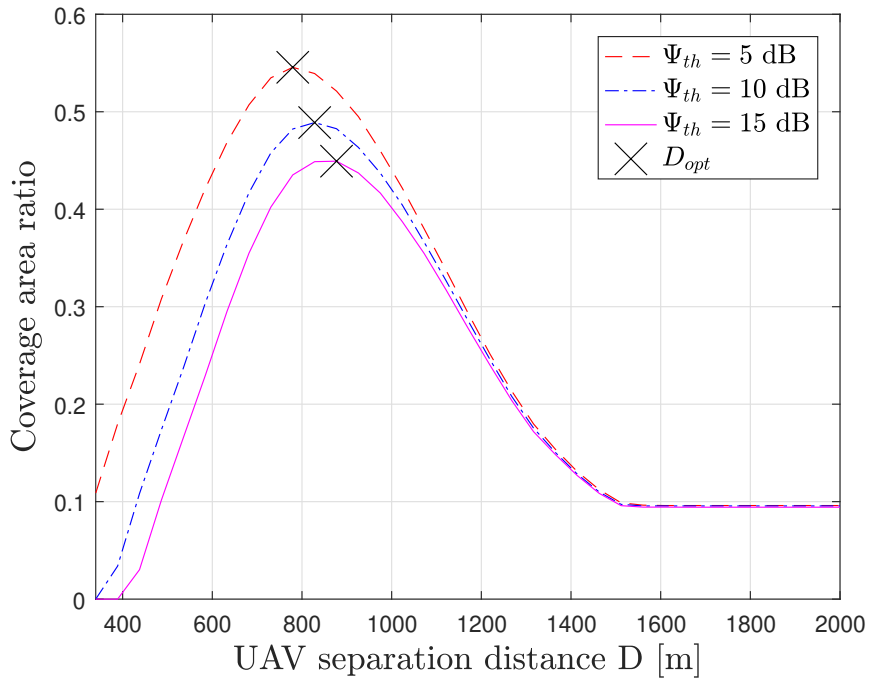

Figure 3.7: Coverage area ratio versus separation distance for seven UAVs deployed in urban environment with different SINR threshold.

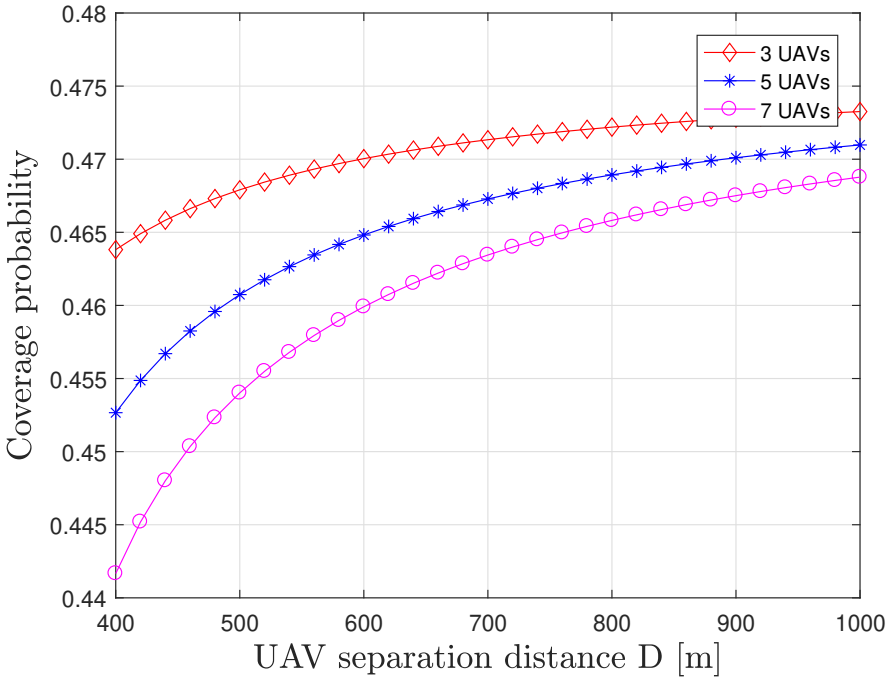

Figure 3.8: Boundary user coverage probability in the primary USC for the severe interference generated from secondary UAVs for different number of UAVs in urban environment with the threshold of $\Psi_{th} = 10$ dB.

Fig. 3.7 illustrate the impact of the SINR threshold on the coverage ratio and the optimal UAV separation distance in the urban environment for seven interfering UAVs. According to Fig. 3.7, the optimal UAV separation distance increases with the SINR threshold. For example D_{opt} = 780 meters for Ψ_{th} = 5 dB, D_{opt} = 847 meters for Ψ_{th} = 10 dB, and D_{opt} = 897 meters for Ψ_{th} = 15 dB. On the other hand, the maximum coverage area ratio decreases as the SINR threshold increases. For example, the maximum coverage area ratio is 0.54 for Ψ_{th} = 5 dB, 0.49 for Ψ_{th} = 10 dB, and 0.45 for Ψ_{th} = 15 dB.

Fig. 3.8 shows that the coverage probability of the boundary user in the primary UAV cell in (3.19) with the threshold of Ψ_{th} = 10 dB. Fig. 3.8. depicts that the user coverage probability improves as the separation distance increases. In this case, the better user performance is possible in the worst-case scenario of the co-channel interference with the minimum required number of UAVs.

These results show that the aerial BSs can work similarly as the ground BSs with defined coverage patterns following principles of CoMP systems for interference management [169]. This is important for the development of UAV BSs as a supplementary but flexible infrastructure to be compatible with existing fixed infrastructure.

3.5 Conclusion

The optimal separation distance between UAVs to mitigate co-channel interference and maximize the overall coverage performance has been studied in suburban and urban environments. For this, the coordinated multi-UAV network was designed that allowed to provide the useful insights on the integration of multiple USCs in UAV communications. Results in this chapter showed that the coverage area performance is dependent on the number of UAVs, operational environment, deployment coordinates or network formation, and separation distance between UAVs. In fact, a proper adjustment of the UAV separation distance can balance the co-channel interference to avoid coverage leakage outside the target area. This work could be extended for UAVs with different mobility

laws and a multiple-tier UAV deployment to study the consequences of cross-tier interference in UAV communications. In this case, coverage performance by multiple UAVs can be determined by multi-dimensional search for the optimal UAV altitudes and the separation distances.

Chapter 4

Effect of User Mobility and Channel Fading on UAV Communications

4.1 Introduction

UAVs can be used as aerial access points to extend the coverage of wireless networks [133]. Such networks can provide practical significance in a mobile environment due to the maneuverability of UAVs. On the other hand, in mobile networks, the presence of mobility can induce time-varying characteristics into the received signal [170]. The variation caused by the user mobility together with the fluctuation in the channel gain generated by multipath fading can degrade the performance [29].

Most existing works on the performance analysis of UAV communication systems consider fixed ground users. For example, reference [117] analyzed the performance of the individual air-to-ground links in a cooperative UAV network with a fixed ground user in various fading scenarios. Reference [130] derived the performance measures for the air-to-ground communication link in a relaying system with a UAV, a remote BS, and a user at the edge of the coverage cell. The system-level performance for multiple spatially distributed ground users has also been analyzed. For example, reference [26] derived the altitude-dependent outage probability to maximize the coverage performance where

ground nodes follow a PPP. In all these works, the placement strategies of UAVs have been studied but the effect of ground user mobility on the communication performance has been ignored.

To capture the essential performance of UAV communications, it is necessary to consider the effect of ground user mobility. Various models have been reported in the literature for user mobility in mobile and ad hoc networks [171]. One such model is the random waypoint (RWP) model [172] that has been predominantly adopted in various communication systems. For example, reference [31] studied the impact of the receiver mobility on the SNR in an indoor scenario using a VLC system. For physical layer security, reference [173] provided general expressions for the outage and capacity performance for a ground user that moves according to the RWP model. This result was compared with the random distance model and the border mobility model. Another study in [174] analyzed the secrecy outage performance in the presence of moving interferers in a RWP network. For UAV communications, the authors in [27] and [175] derived statistics for the SIR, in which multiple UAVs move according to the RWP model in the vertical direction. However, none of these works has provided a comprehensive analysis on the effect of ground user mobility in the UAV communications.

Motivated by the above observations, this chapter presents an analytical framework to investigate how ground user mobility and the fading channel affect UAV communications. Specifically, this work derives closed-form expressions for the PDF, the CDF, the outage probability, and the average BER of the UAV system where the ground user follows the RWP model for user mobility and the small-scale channel fading follows the Nakagami-m model. Numerical results are presented for the ground-to-air LOS channel and the elevation angle-dependent probabilistic channel [19] to show how different performance metrics change with the system parameters as design guidelines.

The main contributions of this chapter are summarized as follows:

- Compared to [27] and [175] that derived statistics for mobile UAVs for the fixed ground user at the center of the UAV cell, this work provides mathematical frame-

work that studies the impact of UAV channel models, ground user mobility using the RWP model, and small-scale fading channel on the outage performance in noise-only and interference-limited scenarios.

- Performance analysis is provided for the uplink UAV communication system, where the closed-form expressions are derived for the statistics of SNR i.e PDF and CDF, and accordingly outage probability can be determined.
- Closed-form expressions for the average BER are derived for the noise-only scenario.
- Statistics of SIR are derived in the form of tractable analytical expressions where multiple interfering users moves according to the RWP mobility model and outage performance is compared with the case of static interfering users.

The rest of this chapter is organized as follows. The system model is introduced in Section 4.2, including the use of channel models and mobility model. Section 4.3 presents the statistics of SNR. Section 4.4 presents the analytical framework to derive performance metrics, including outage probability and average BER in noise-only scenario. Section 4.5 derives the expressions for PDF and CDF to study the impact of uplink interference generated from the mobile interfering users. Section 4.6 presents numerical results and simulation parameters. Section 4.7 summarizes the main conclusions of this chapter.

4.2 System Model

Fig. 4.1a depicts the uplink of a UAV communication system that initially consists of an aerial BS positioned at an altitude of h meters communicating with a single mobile ground user in the noise-only scenario. Later, the intrusion of multiple interfering mobile users in Fig. 4.1b generates the strong jamming signal at the UAV that can be detrimental for uplink UAV communications. Thus, in absence of an appropriate multiple

access technique, the system model in Fig. 4.1b is undesirable for practical applications and considered here for analyzing the combined effect of user mobility, propagation environment, and fading channel in the interference-limited environment. In order to save battery and to simplify the system, this work considers the use of a static multi-rotor UAV[1]. For a 2D Cartesian coordinate system, O_c is assumed as the projection coordinate of the UAV at the center of the circular area. During the communication in Fig. 4.1b, the desired and interfering ground users are randomly moving inside the circular region, such that their spatial positions are determined by the distance r_U and r_I from the center within a range of $0 \leq r_U \leq D_U$ and $0 \leq r_I \leq D_I$, respectively. In this case, r_U and r_I are random variables and D_U and D_I are the maximum radial distances. Next, this section will specify the channel models and the mobility model for the considered system.

4.2.1 Channel Model

This chapter takes into account both the LOS and the probabilistic LOS channel models to extend the analysis for variety of propagation environments. First, this work assume that the air-to-ground channel is dominated mainly by LOS conditions and that the power loss depends on the propagation distance. Therefore, the received power at the UAV can be given as

$$P_U^A = \frac{P_t \delta |g|^2}{d_U^\alpha} = \frac{P_t \delta |g|^2}{(r_U^2 + h^2)^{\frac{\alpha}{2}}}, \tag{4.1}$$

where d_U denotes the air-to-ground propagation distance between UAV and the desired user, δ represents the channel power at the reference distance of 1 meter, $|g|^2$ is the fading power, P_t is the transmission power of the desired ground user, and α is the PLE which usually satisfies $2 \leq \alpha \leq 4$ between free space and obstructed propagation environments [177]. Thus, $\alpha = 2$ and $\alpha = 4$ can be considered as upper and lower limits of the performance, respectively. This model is useful in certain scenarios, where it is non-

[1] In some cases, UAVs consume less energy in mobility than in hovering [176].

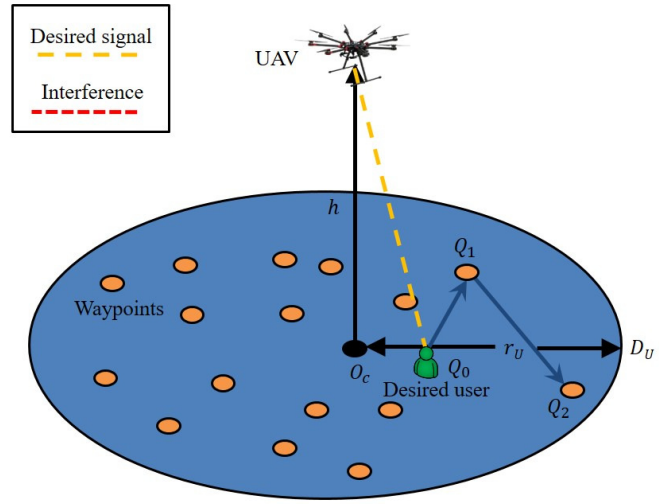

(a) Noise-only scenario.

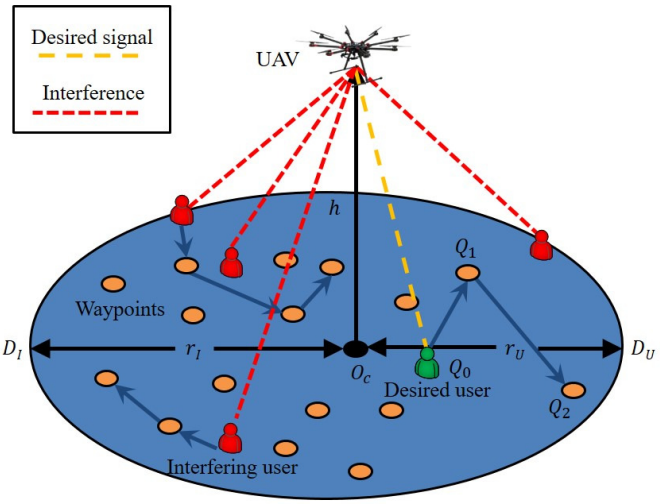

(b) Interference-limited scenario.

Figure 4.1: System model.

trivial to classify the environment (urban, dense urban, etc.), and the parameters of the probabilistic model may not be available, For instance, in post-disaster and mountainous areas.

Second, this work uses the probabilistic LOS model where the air-to-ground propagation is dependent on the environmental parameters and the elevation angle between

the UAV and the ground user. In this case, the received power at the UAV can be expressed as

$$P_U^B = \frac{P_t |g|^2}{Q_U}, \tag{4.2}$$

where $Q_U = 10^{\frac{\mathrm{PL}_U}{10}}$ is the absolute power loss and PL_U is the air-to-ground propagation path loss given by

$$\mathrm{PL}_U(\mathrm{dB}) = \frac{\left(\varepsilon_{\mathrm{LOS}} - \varepsilon_{\mathrm{NLOS}}\right)}{1 + a \times \exp\left(-b\left(\phi - a\right)\right)} + 20\log_{10}\left(\frac{4\pi f}{c}\right) + 20\log_{10}\left(\sqrt{r_U^2 + h^2}\right) + \varepsilon_{\mathrm{NLOS}}, \tag{4.3}$$

and $\phi = \arctan\left(\frac{h}{r_U}\right)$ is the elevation angle, a, b, $\varepsilon_{\mathrm{LOS}}$, and $\varepsilon_{\mathrm{NLOS}}$ are the constants related to the propagation environments, f is the carrier frequency, and c is the speed of light. However, (4.3) is too complicated to analytically characterize the effect of the ground user mobility because this expression is in implicit form, such that neither r_U nor h can be written explicitly. Thus, the curve fitting approach is used to fit the probabilistic LOS channel for simplification. To this end, the curve fitting method yields a three-variable power function for Q_U as

$$Q_U = a_2 r_U^{b_2} + c_2, \tag{4.4}$$

where a_2, b_2, and c_2 are the curve fitting parameters dependent on the environment and the elevation angle between UAV and the ground user.

To model the fading channel, the Nakagami-m model is considered due to its analytical tractability. This model is also reported in several measurement campaigns reported in Table 2.5. The analysis of this work consider normalized average fading power. Therefore, the PDF of the channel power follows a Gamma distribution as

$$f_{|g|^2}(x) = \frac{m^m x^{m-1}}{\Gamma(m)} \exp(-mx), \quad x \geq 0, \tag{4.5}$$

where m is the Nakagami-m parameter that defines the severity of the fading channel and assumed an integer in this work for simplicity and $\Gamma(.)$ is the Gamma function.

4.2.2 Mobility Model

According to reference [171], the classification of the mobility models is illustrated in Fig. 4.2. In this work, the RWP model is adopted because it presents the statistical properties of randomness in the form of well defined analytical expressions. Also, it gives non-uniform spatial distribution of the ground user distance. On the other hand, the random distance model may not be suitable for the considered system model because it gives the uniform spatial distribution of the ground user distance. Other practical models such as, the Manhattan mobility model simulates the mobility pattern of the ground user at the street level and the Freeway mobility model emulates the movement pattern of the highly mobile ground users on highways. However, these models and other models listed above do not have well defined analytical expressions to derive the statistics for SNR and SIR. Mostly the adaptability of such models in ad hoc networks is possible with the commercial simulation software which may not lead to any closed-form expressions of performance metrics

This work assumes that the user mobility follows the RWP model. In this model, as shown in Fig. 4.1, the ground user (marked with green colour) initially starts from point Q_0. Then, a destination point (know as waypoint) Q_1 is chosen from a uniform distribution inside the circular area and the ground user moves along a straight path from Q_0 to Q_1 at a constant speed. After reaching waypoint Q_1, a new destination point Q_2 is selected and this process continues. Following the RWP model, the PDF of the desired user and interfering user distance is given in a polynomial form in [170, Table 1] and is summarized in [29] in an equivalent form of

$$f_{r_U}(r_U) = \sum_{i=1}^{n} \beta_i \frac{r_U^{\alpha_i}}{D_U^{\alpha_i+1}}, \quad 0 \le r_U \le D_U, \tag{4.6}$$

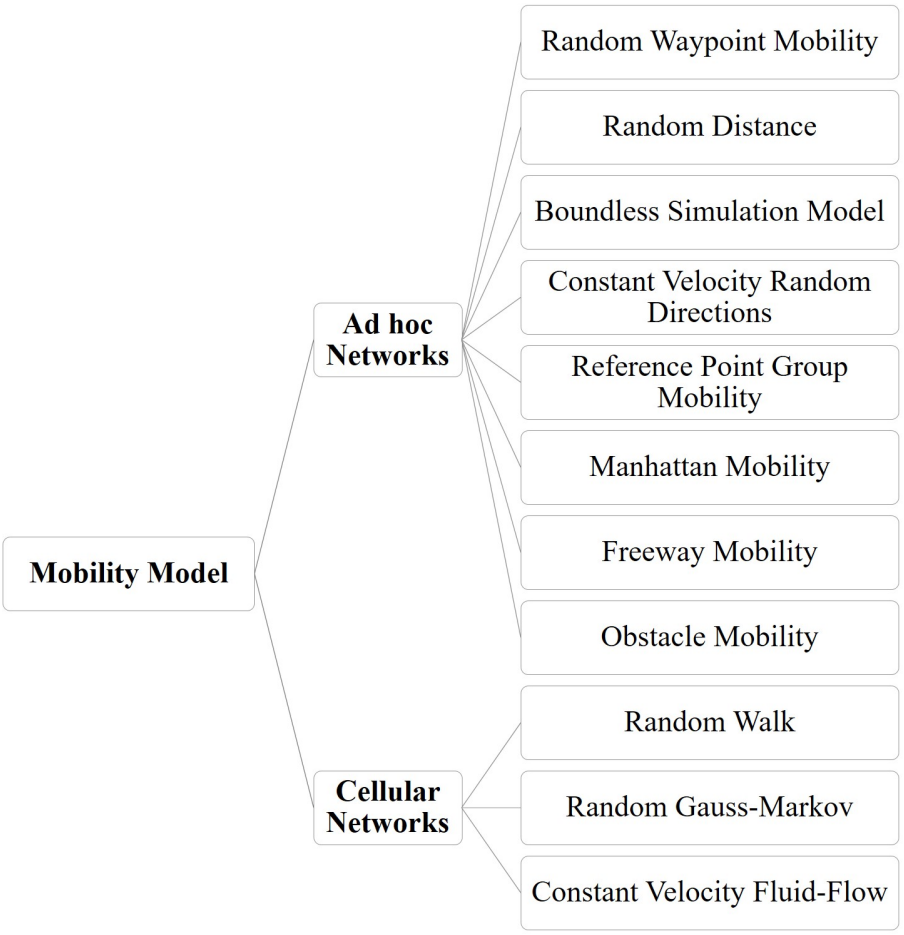

Figure 4.2: The classification of the mobility models.

and

$$f_{r_I}(r_I) = \sum_{i=1}^{n} \beta_i \frac{r_I^{\alpha_i}}{D_I^{\alpha_i+1}}, \quad 0 \le r_I \le D_I, \tag{4.7}$$

respectively, where n is determined by the dimension of space (1D, 2D, and 3D) considered, β_i and α_i are constants determined by the user mobility in specific dimension. Moreover, all ground users are assumed to be placed on a 2D surface, as shown in Fig. 4.1. In this work, $n = 3$ for the 2D case, $\beta_i = \left[\frac{324}{73}, \frac{-420}{73}, \frac{96}{73}\right]$, and $\alpha_i = [1,3,5]$ [170, Table 1]. It can be verified that integrals of (4.6) and (4.7) give 1.

4.3 Statistics of Signal-to-Noise Ratio (SNR)

This section presents the statistics of the received SNR at the UAV for LOS model using (4.1) and for probabilistic LOS model using (4.2) and (4.4) as $\lambda_r^A = \frac{E_U^A|g|^2}{\sqrt{1+\frac{r_U^2}{h^2}}^{\alpha}}$ and $\lambda_r^B = \frac{E_U^B|g|^2}{\left(1+\frac{a_2}{c_2}r_U^{b_2}\right)}$, respectively, where $E_U^A = \frac{P_t\delta}{N_0}h^{-\alpha}$, $E_U^B = \frac{P_t}{N_0 c_2}$, and N_0 is the noise power.

4.3.1 Probability Density Function (PDF)

For the LOS model, denote $X = E_U^A|g|^2$ and $Y = \left(1+\frac{r_U^2}{h^2}\right)^{\frac{\alpha}{2}}$. Let $Z = \frac{X}{Y}$, where X and Y are independent random variables. Hence, the general expression for the PDF of Z is given by

$$f_Z(z) = \int_1^{\sqrt{1+\left(D_U/h\right)^2}^{\alpha}} y f_X(zy) f_Y(y) dy. \tag{4.8}$$

Substituting $\alpha = 2$ in (4.8), the PDF of Z can be derived using binomial expansion $(1+q)^m$ [178, eq.(1.110)] and the lower incomplete Gamma function $\gamma(.,.)$ [178, eq.(3.381.1)], as

$$f_Z(z) = \frac{z^{m-1}\exp\left(-\frac{z}{E_U^A/m}\right)}{2\Gamma(m)\left(E_U^A/m\right)^m}\sum_{i=1}^{n}\sum_{j=0}^{m}\frac{\beta_i}{\left(D_U^2/h^2\right)^{\alpha_i+1}}\binom{j}{m}\frac{\gamma\left(\frac{\alpha_i+1}{2}+j, \frac{(D_U/h)^2}{E_U^A/m}z\right)}{\left(\frac{z}{E_U^A/m}\right)^{\frac{\alpha_i+1}{2}+j}}. \tag{4.9}$$

For $\alpha = 4$, the PDF can be derived from (4.8) as

$$f_Z(z) = \frac{z^{m-1}}{4\Gamma(m)\left(E_U^A/m\right)^m}\sum_{i=1}^{3}\frac{\beta_i}{\left(D_U/h\right)^{\alpha_i+1}}U_i, \tag{4.10}$$

where

$$G(\mu,\rho,\psi) = \frac{\gamma\left(m+\mu, \frac{\chi^{\rho}}{E_U^A/m}z\right) - \gamma\left(m+\mu, \frac{\chi^{\psi}}{E_U^A/m}z\right)}{\left(\frac{z}{E_U^A/m}\right)^{m+\mu}}, \tag{4.11}$$

and $U_1 = G(\frac{1}{2},2,0)$, $U_2 = G(1,0,2)$, $U_3 = G(\frac{3}{2},2,0)$, and $\chi = \frac{D^2+h^2}{h^2}$. This work is not able to derive the results for an arbitrary value of α, but $\alpha = 2$ and $\alpha = 4$ can provide useful performance benchmarks.

Similarly, for the probabilistic LOS model, let $X = E_U^B|g|^2$, $Y = 1 + \frac{a_2}{c_2} r_U^{b_2}$, and $Z = \frac{X}{Y}$. Thus, the PDF of Z can be derived as

$$f_Z(z) = \frac{z^{m-1}\exp\left(-\frac{z}{E_U^B/m}\right)}{b_2\Gamma(m)\left(E_U^B/m\right)^m} \sum_{i=1}^{n}\sum_{j=0}^{m} \frac{\beta_i (a_2/c_2)^{-\frac{\alpha_i+1}{b_2}}}{D_U^{\alpha_i+1}} \binom{j}{m} \frac{\gamma\left(\frac{\alpha_i+1}{b_2}+j, \frac{(a_2/c_2)D_U^{b_2}}{E_U^B/m} z\right)}{\left(\frac{z}{E_U^B/m}\right)^{\frac{\alpha_i+1}{b_2}+j}}. \quad (4.12)$$

4.3.2 Cumulative Distribution Function (CDF)

For LOS model, the CDF for the received SNR at the UAV can be given as

$$F_Z(z) = \int_1^{\sqrt{1+\left(D_U/h\right)^2}^{\alpha}} \int_0^{zy} f_X(x) f_Y(y) dx dy. \quad (4.13)$$

Substituting $\alpha = 2$ in (4.13), the CDF can be derived as

$$F_Z(z) = \sum_{i=1}^{n} \frac{\beta_i}{\alpha_i+1} - \frac{\exp\left(-\frac{z}{E_U^A/m}\right)}{2} \sum_{i=1}^{n}\sum_{j=0}^{m-1}\sum_{k=0}^{j} \frac{\beta_i}{(D_U/h)^{\alpha_i+1}} \frac{\binom{k}{j}}{j!} \frac{\gamma\left(\frac{\alpha_i+1}{2}+k, \frac{(D_U/h)^2}{E_U^A/m} z\right)}{\left(\frac{z}{E_U^A/m}\right)^{k+\frac{\alpha_i+1}{2}-j}}. \quad (4.14)$$

Substituting $\alpha = 4$ in (4.13), the CDF can be derived as

$$F_Z(z) = \sum_{i=1}^{n} \frac{\beta_i}{\alpha_i+1} - \sum_{i=1}^{n}\sum_{s=1}^{4} \frac{\left(\frac{z}{E_U^A/m}\right)^{m-1}}{4\left(D_U/h\right)^{\alpha_i+1}} S_s, \quad (4.15)$$

where $S_1 = G(-\frac{1}{2},2,0)$, $S_2 = 2\cdot G(1,0,2)$, $S_3 = G(\frac{1}{2},2,0)$, and $S_4 = G(0,0,2)$.

For the probabilistic LOS model, the CDF can be derived as

$$F_Z(z) = \sum_{i=1}^{n} \frac{\beta_i}{\alpha_i + 1} - \frac{\exp\left(-\frac{z}{E_U^B/m}\right)}{b_2} \sum_{i=1}^{n} \sum_{j=0}^{m-1} \sum_{k=0}^{j} \frac{\beta_i (a_2/c_2)^{-\frac{\alpha_i+1}{b_2}}}{D_U^{\alpha_i+1}} \frac{\binom{k}{j}}{j!} \frac{\gamma\left(\frac{\alpha_i+1}{b_2} + k, \frac{(a_2/c_2)D_U^{b_2}}{E_U^B/m} z\right)}{\left(\frac{z}{E_U^A/m}\right)^{k+\frac{\alpha_i+1}{b_2}-j}}. \tag{4.16}$$

4.4 Performance Analysis

This section provides expressions for the outage probability and the average BER of UAV communication system.

4.4.1 Outage Probability

Outage probability is defined as the probability when the received SNR or SIR falls below a predefined threshold λ as

$$P_{out} = Pr(Z < \lambda) = F_Z(\lambda). \tag{4.17}$$

where the CDF of $F_Z(z)$ is given in Section 4.3.

4.4.2 Average Bit Error Rate (BER)

The average BER for the digital binary modulation scheme in terms of the upper incomplete Gamma function $\Gamma(.,.)$ [178, eq.(8.350.2)], is given as [179]

$$P_e = \frac{1}{2\Gamma(\theta)} \int_0^\infty \Gamma(\theta, z\Phi) f_Z(z) dz = \frac{\Phi^\theta}{2\Gamma(\theta)} \int_0^\infty z^{\theta-1} \exp(-z\Phi) F_Z(z) dz, \tag{4.18}$$

where parameters Φ and θ depend on the type of modulation. For example, $\Phi = \{1, 1/2\}$ for binary phase-shift keying (BPSK) and binary frequency-shift keying (BFSK), respectively, and $\theta = \{1, 1/2\}$ for differential BPSK/non-coherent BFSK and coherent BPSK/BFSK, respectively.

For $\alpha = 2$, substituting (4.14) in (4.18), the average BER in terms of the Gauss hypergeometric function ${}_2F_1(\cdot,\cdot;\cdot;\cdot)$ using [178, eq.(6.455.2)] and [178, eq.(6.381.4)] is derived as

$$P_e = \frac{1}{2}\Big[\sum_{i=1}^{n}\frac{\beta_i}{\alpha_i+1} - \frac{\Phi^\theta}{\Gamma(\theta)}\sum_{i=1}^{n}\sum_{j=0}^{m-1}\sum_{k=0}^{j}\frac{\beta_i\binom{k}{j}}{j!}\frac{(E_U^A/m)^\theta (D_U/h)^{2k}\Gamma(\theta+j)}{(\alpha_i+1+2k)\big[1+(D_U/h)^2+(E_U^A/m)\Phi\big]^{\theta+j}} \times {}_2F_1\Big(1,\theta+j;\frac{\alpha_i+1}{2}+k+1;\frac{(D_U/h)^2}{1+(D_U/h)^2+(E_U^A/m)\Phi}\Big)\Big]. \tag{4.19}$$

For $\alpha = 4$, substituting (4.15) in (4.18), the average BER is derived as

$$P_e = \frac{1}{2}\Big[\sum_{i=1}^{n}\frac{\beta_i}{\alpha_i+1} - \sum_{i=1}^{n}\sum_{s=1}^{4}\frac{\Big(\frac{1}{E_U^A/m}\Big)^{m-1}}{4\big(D_U/h\big)^{\alpha_i+1}} I_s\Big], \tag{4.20}$$

where $H(\tau,\upsilon) = \frac{1}{m+\tau}\Big[\frac{\chi^\upsilon}{R}\times{}_2F_1(1,m+b-1;m+\tau+1;T) - \frac{1}{U}\times{}_2F_1(1,m+b-1;m+\tau+1;W)\Big]$, $I_1 = H(-\frac{1}{2},2m-1)$, $I_2 = -2\times H(1,2m+2)$, $I_3 = H(\frac{1}{2},2m+1)$, $I_4 = -H(0,2m)$, $R = \Big(\frac{\chi^2}{E_U^A/m}+\Phi\Big)^{\theta+m-1}$, $T = \frac{\chi^2}{\chi^2+(E_U^A/m)\Phi}$, $U = \Big(\frac{1}{E_U^A/m}+\Phi\Big)^{\theta+m-1}$ and $V = \frac{1}{1+(E_U^A/m)\Phi}$.

For probabilistic LOS model, substituting (4.16) in (4.18), the average BER is derived as

$$P_e = \frac{1}{2}\Big[\sum_{i=1}^{n}\frac{\beta_i}{\alpha_i+1} - \frac{\Phi^\theta}{\Gamma(\theta)}\sum_{i=1}^{n}\sum_{j=0}^{m-1}\sum_{k=0}^{j}\frac{\beta_i\binom{k}{j}}{j!}\frac{\big(E_U^B/m\big)^\theta\Big(\frac{a_2 D_U^{b_2}}{c_2}\Big)^k\Gamma(\theta+j)}{(\alpha_i+1+kb_2)\Big[1+\frac{a_2 D_U^{b_2}}{c_2}+\big(E_U^B/m\big)\Phi\Big]^{\theta+j}} \times {}_2F_1\Big(1,\theta+j;\frac{\alpha_i+1}{b_2}+k+1;\frac{\frac{a_2 D_U^{b_2}}{c_2}}{1+\frac{a_2 D_U^{b_2}}{c_2}+(E_U^B/m)\Phi}\Big)\Big]. \tag{4.21}$$

4.5 Impact of Interference on Outage Performance

This section consider the scenario when the desired ground user is surrounded by L Nakagami-m interfering users (marked with red colour) in two cases. The first case as-

sume independent and identically distributed static interfering users at approximately the same distance from the desired user. The second case consider the randomly moving interfering users according to the RWP model. In both cases, the co-channel interference is incurred when the interfering users send signals to degrade the received signal at the UAV in the uplink transmission.

4.5.1 Statistics of Signal-to-Interference Ratio (SIR)

The aggregate interference[2] at the UAV for LOS and probabilistic LOS channels is given as $V^A = \sum_{l=1}^{L} \frac{E_I^A |g_l|^2}{\sqrt{1+\frac{r_{I_l}^2}{h^2}}^{\alpha}}$ and $V^B = \sum_{l=1}^{L} \frac{E_I^B |g_l|^2}{\left(1+\frac{a_2}{c_2} r_{I_l}^{b_2}\right)}$, respectively, where $E_I^A = P_t \delta h^{-\alpha}$ and $E_I^B = \frac{P_t}{c_2}$. This work assumes that the aggregate interference can be approximated by a Gamma-distributed random variable, which is a reasonable assumption as validated by findings of the numerical test in Fig. 4.3. Therefore, the PDF of a Gamma distribution can be expressed as

$$f_V(v) = \frac{v^{\kappa-1}}{\Gamma(\kappa)\gamma^{\kappa}} \exp\left(-\frac{v}{\gamma}\right), \quad v \geq 0 \tag{4.22}$$

where κ and γ are the shape and scale parameters, respectively. For static interfering users, these parameters are defined in Table 4.1. On the other hand, for mobile interfering users, these parameters are determined by the method of moment-matching. Using (4.7) and [178, eq. (3.194.1)],

$$M_A = \mathrm{E}\{\frac{1}{\sqrt{1+(r_I/h)^2}^{\alpha}}\} = \sum_{i=1}^{n} \frac{\beta_i}{\alpha_i+1} {}_2F_1\left(\frac{\alpha}{2}, \frac{\alpha_i+1}{\alpha}; \frac{\alpha_i+1}{\alpha}+1; \left(D_I/h\right)^2\right), \tag{4.23}$$

$$M_B = \mathrm{E}\{\frac{1}{1+(a_2/c_2) r_I^{b_2}}\} = \sum_{i=1}^{n} \frac{\beta_i}{\alpha_i+1} {}_2F_1\left(1, \frac{\alpha_i+1}{b_2}; \frac{\alpha_i+1}{b_2}+1; -(a_2/c_2) D_I^{b_2}\right). \tag{4.24}$$

[2] For a tractable analysis, this work assumes that the interference power is dominant as compared to the noise power [54].

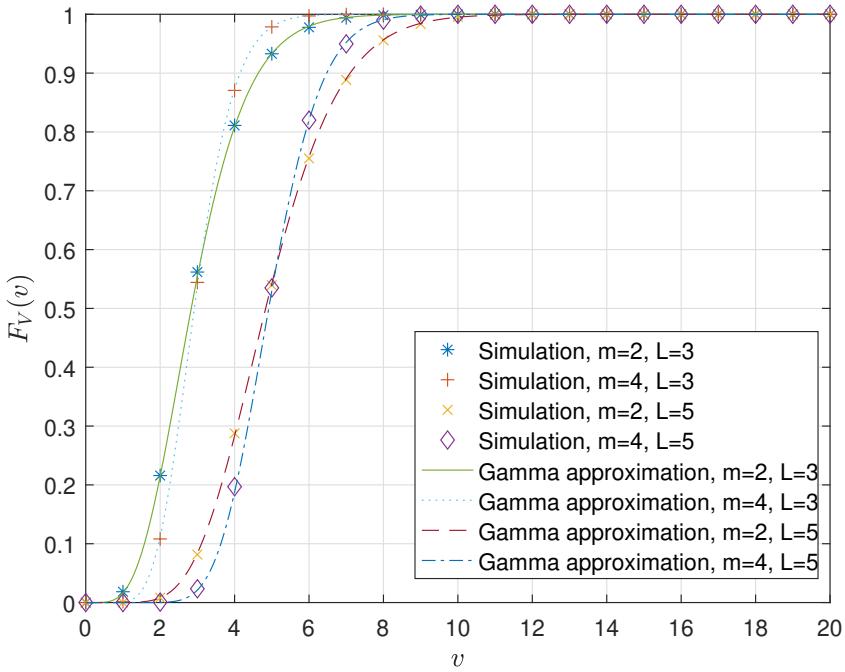

Figure 4.3: Comparison of simulated CDF and Gamma-distributed CDF.

Similarly,

$$N_A = \mathrm{E}\{\frac{1}{\left(\sqrt{1+(r_I/h)^{2^\alpha}}\right)^2}\} = \sum_{i=1}^{n} \frac{\beta_i}{\alpha_i+1} {}_2F_1\Big(\alpha, \frac{\alpha_i+1}{\alpha}; \frac{\alpha_i+1}{\alpha}+1; -\big(D_I/h\big)^2\Big), \tag{4.25}$$

$$N_B = \mathrm{E}\{\frac{1}{\left(1+(a_2/c_2)r_I^{b_2}\right)^2}\} = \sum_{i=1}^{n} \frac{\beta_i}{\alpha_i+1} {}_2F_1\Big(2, \frac{\alpha_i+1}{b_2}; \frac{\alpha_i+1}{b_2}+1; -(a_2/c_2)D_I^{b_2}\Big). \tag{4.26}$$

$E\{|g|^2\} = 1$, and using [178, eq.(3.381.4)], $E\{|g|^4\} = 1+\frac{1}{m}$. Thus, for a LOS channel, one has $E\{V\} = LE_I^A M_A$ and $E\{V^2\} = L(E_I^A)^2(L-1)M_A^2 + L(E_I^A)^2(1+\frac{1}{m})N_A$. Finally, since $E\{V\} = \kappa\gamma$ and $E\{V^2\} = \kappa\gamma^2 - \kappa^2\gamma^2$ from moment-matching, the κ and γ parameters for the LOS and probabilistic LOS models are given in Table 4.2.

Next, for the LOS model, denote $Z_I = \frac{P_U^A}{V^A}$ as the received SIR. For $\alpha = 2$, the CDF of P_U^A i.e., $F_{P_U^A}(z_I)$ can be determined by replacing E_U^A with E_I^A in (4.14). Also, the PDF of

Table 4.1: κ and γ parameters for static interfering users.

Channel model	$\boldsymbol{\kappa}$	$\boldsymbol{\gamma}$
LOS	mL	$\frac{P_t\delta}{m\sqrt{D_I^2+h^2}^{\alpha}}$
Probabilistic LOS	mL	$\frac{P_t}{m(a_2 D_I^{b_2}+c_2)}$

Table 4.2: κ and γ parameters for mobile interfering users.

Channel model	$\boldsymbol{\kappa}$	$\boldsymbol{\gamma}$
LOS	$\frac{LM_A^2}{(1+\frac{1}{m})N_A-M_A^2}$	$E_I^A\left[\frac{N_A}{M_A}(1+\frac{1}{m})-M_A\right]$
Probabilistic LOS	$\frac{LM_B^2}{(1+\frac{1}{m})N_B-M_B^2}$	$E_I^B\left[\frac{N_B}{M_B}(1+\frac{1}{m})-M_B\right]$

V_A can be obtained from (4.22). Since P_U^A and V_A are independent, the CDF of Z_I is

$$F_{Z_I}(z_I)=\int_0^{\infty} F_{P_U^A}(vz_I)f_V(v)dv \tag{4.27}$$

Thus, using [178, eq.(6.381.4)] and [178, eq.(6.455.2)], the CDF of Z_I can be derived as

$$F_{Z_I}(z_I)=$$
$$\sum_{i=1}^{n}\frac{\beta_i}{\alpha_i+1}-\frac{1}{\Gamma(\vartheta)\gamma^{\vartheta}}\sum_{i=1}^{n}\sum_{j=0}^{m-1}\sum_{k=0}^{j}\frac{\beta_i\binom{k}{j}}{j!}\frac{\left(E_I^A/m\right)^{\vartheta}z_I^j\left(D_U/h\right)^{2k}\Gamma(\vartheta+j)}{(\alpha_i+1+2k)\left[\left(1+(D_U/h)^2\right)z_I+\frac{E_I^A}{m\gamma}\right]^{\vartheta+j}}\times$$
$$ {}_2F_1\left(1,\vartheta+j;\frac{\alpha_i+1}{2}+k+1;\frac{z_I\left(D_U/h\right)^2}{\left(1+(D_U/h)^2\right)z_I+\frac{E_I^A}{m\gamma}}\right). \tag{4.28}$$

Similarly, for probabilistic LOS model, denote $Z_I=\frac{P_U^B}{V^B}$ as the received SIR, the CDF of P_U^B i.e., $F_{P_U^B}(z_I)$ can be determined by replacing E_U^B with E_I^B in (4.16). Thus, the

CDF of Z_I can be derived as

$$F_{Z_I}(z_I) = \sum_{i=1}^{n} \frac{\beta_i}{\alpha_i+1} - \frac{1}{\Gamma(\vartheta)\gamma^{\vartheta}} \sum_{i=1}^{n} \sum_{j=0}^{m-1} \sum_{k=0}^{j} \frac{\beta_i \binom{k}{j}}{j!} \frac{(E_I^B/m)^{\vartheta} z_I^j \left((a_2/c_2) D_U^{b_2}\right)^k \Gamma(\vartheta+j)}{(\alpha_i+1+kb_2)\left[\left(1+(a_2/c_2)D_U^{b_2}\right) z_I + \frac{E_I^B}{m\gamma}\right]^{\vartheta+j}} \times {}_2F_1\left(1, \vartheta+j; \frac{\alpha_i+1}{b_2}+k+1; \frac{z_I(a_2/c_2)D_U^{b_2}}{\left(1+(a_2/c_2)D_U^{b_2}\right) z_I + \frac{E_I^B}{m\gamma}}\right). \quad (4.29)$$

Thus, the outage performance in presence of uplink co-channel interference can be computed as

$$P_{out} = Pr(Z_I < \lambda) = F_{Z_I}(\lambda). \quad (4.30)$$

where the CDF of $F_{Z_I}(z_I)$ are given in (4.28) and (4.29).

The derived analytical expressions (4.14)-(4.16) for the CDF of SNR, (4.19)-(4.21) for average BER, and (4.28)-(4.29) for the CDF of SIR are complex and unwieldy in their current form due to the use of nonlinear and special functions, such as Gauss hypergeometric function. This is preliminary work to study the impact of ground user mobility on UAV communications and the more manageable expressions are desired in the future. In this regard, one must focus on approximating the nonlinear functions with linear expressions or providing an asymptotic analysis. However, they are beyond the scope of this chapter.

4.6 Numerical Results and Discussion

This section analyzes the performance for different channel conditions and mobility. As an illustrative example, let $h = 100$ meters, $P_t = 30$ dBm, and $N_0 = -57$ dBm. Also, for $f = 2$ GHz, $c = 3 \times 10^8$ m/s, and $0 < r_u < 100$ m, the curve fitting parameters for $45° \leq$

$\theta_U \leq 90^\circ$ are $(a_2, b_2, c_2) = (7180, 2, 7.182 \times 10^7)$ in a suburban environment, $(a_2, b_2, c_2) = (8584, 2, 8.838 \times 10^7)$ in an urban environment, and $(a_2, b_2, c_2) = (4.73, 4.033, 1.125 \times 10^8)$ in a dense urban environment, respectively. The accuracy of the approximated probabilistic LOS function obtained via (4.4) is verified through adjusted R-square, which is the statistical value between 0 and 1 to determine the goodness-of-fit. Hence, for the parameters used in this section, the adjusted R-square values are 1, 1, and 0.9981, for suburban, urban, and dense urban environments, respectively. In the simulation, the RWP model is adopted by directly generating random distances in (4.6) and (4.7), and not the random waypoints. Then, these were used in (4.1)-(4.3) for the simulation of the received power. The solid lines represent the analytical results using (4.14)-(4.17) for outage performance in the absence of interference in Fig. 4.4, (4.19)-(4.21) for average BER in noise-only case in Fig. 4.5, and (4.28)-(4.30) for outage performance in presence of co-channel in Fig. 4.6, while the markers represent the simulation results. This work averaged simulation results using 10^5 runs.

Fig. 4.4 and Fig. 4.5 depicts the impact of PLE and different propagation environments on the outage and error performances in a noise-only case where a mobility scenario with a maximum distance of $D_U = 100$ meters and $D_U = 50$ meters are considered, compared with a static system where the ground user is deployed at half of the maximum distance. In the RWP model, the waypoints are uniformly chosen around the center but its probability density decreases towards the boundary of the circle [172, Fig. 5]. Consequently, the mobile user most likely locates near the mean distance $\bar{r}$ which can be approximated as $\bar{r} = \frac{D_U}{2}$ in the steady-state. This property is confirmed by results, as shown in Fig. 4.4. The outage performances of a mobile user randomly moving within $D_U = 100$ meters are approximately the same as those of a static user fixed at 50 meters for the same PLE. In addition, this work observes better outage performance for $\alpha = 2$ because the received power in (4.1) is higher compared with $\alpha = 4$. Also, for the probabilistic LOS model, the outage performance deteriorates as the power loss increases accordingly with dense urban, urban and suburban environments. It is also interesting

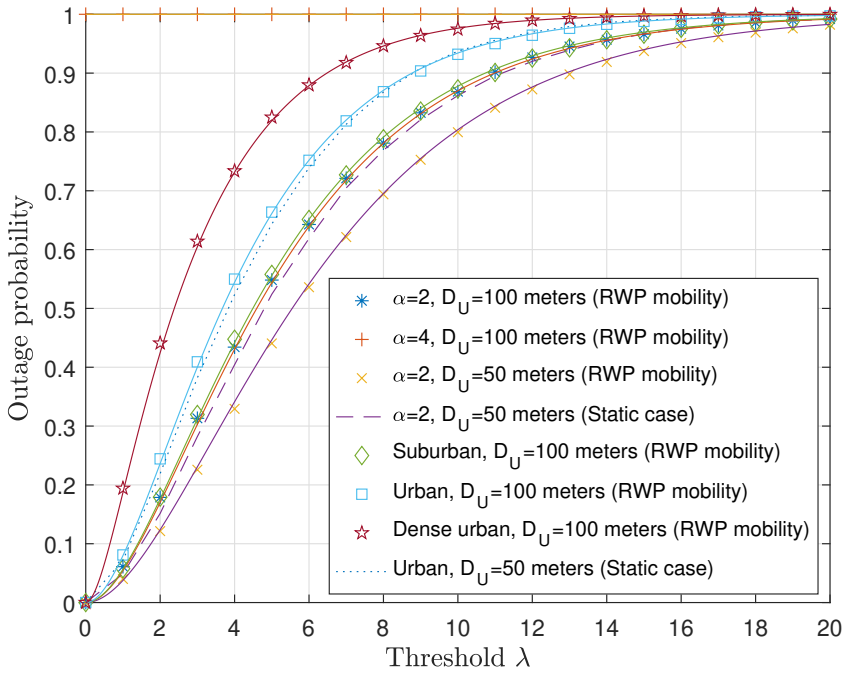

Figure 4.4: The outage probability versus threshold (λ) for $\alpha = \{2,4\}$ and different propagation environments for $m = 2$ in noise-only scenario.

to note that the outage performance of the probabilistic channel model is between those of the model in (4.1) with $\alpha = 2$ and $\alpha = 4$. This shows the usefulness of the LOS model as bounds. This is due to the fact that the probabilistic model combines the free space path loss with the excessive loss incurred by shadowing. In Fig. 4.5, better BER performance is observed for α=2 because the average received power is higher at $D_U = 50$ meters than at $D_U = 100$ meters. Also, the RWP mobility property holds for the average BER results to approximate the performance of a ground user randomly moving between O_c and D_U.

Fig. 4.6 examines the effect of Nakagami-m fading parameters and the amount of interference generated by both the stationary and the mobile interfering users on the outage performance. For the same D_I, the outage performance improves with the static interfering users because the separation distance between desired and interfering user increases. Also, as m increases, the fading severity decreases for the interfering user links and in turn, the outage probability increases due to the dominance of the interference in

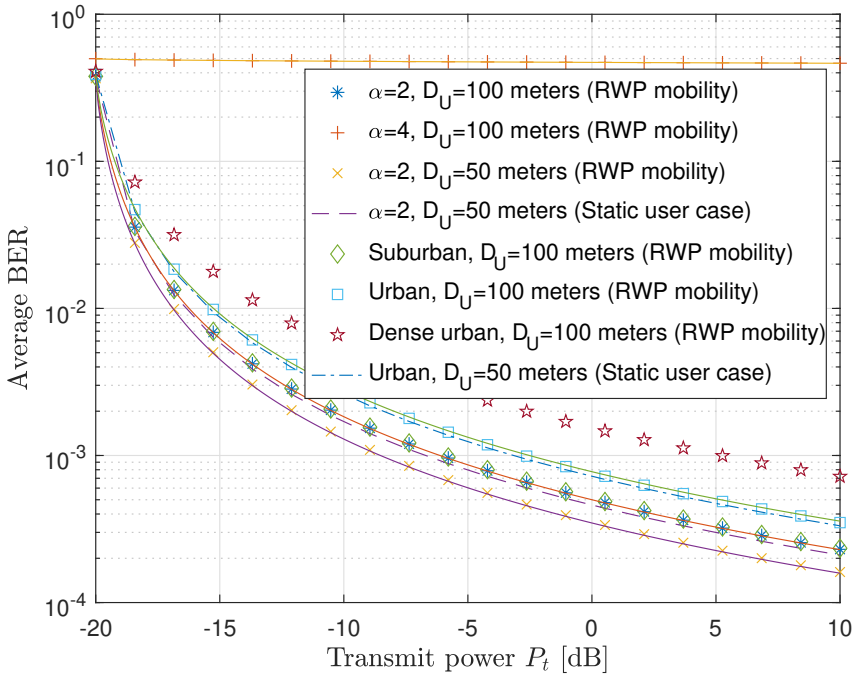

Figure 4.5: Average BER for BPSK versus transmit power (P_t) with m=2, α={2,4}, and with different propagation environments.

the system. These results provide the useful insights to the system designer to quantify the effects of the number of mobile interfering users, performance threshold, PLE, propagation environments, and Nakagami-m fading parameter on the outage performance of the considered UAV communication system.

4.7 Conclusion

This chapter has derived closed-form expressions for the CDF and analyzed the outage and BER performances for the uplink of UAV communication systems by using the RWP mobility model and the Nakagami-m channel fading model. This work has been extended for the outage analysis to the interference-limited scenario by using the Gamma approximation. Thus, this chapter provides useful design guidelines to quantify the effect of the user mobility, propagation environment, channel fading, and co-channel in-

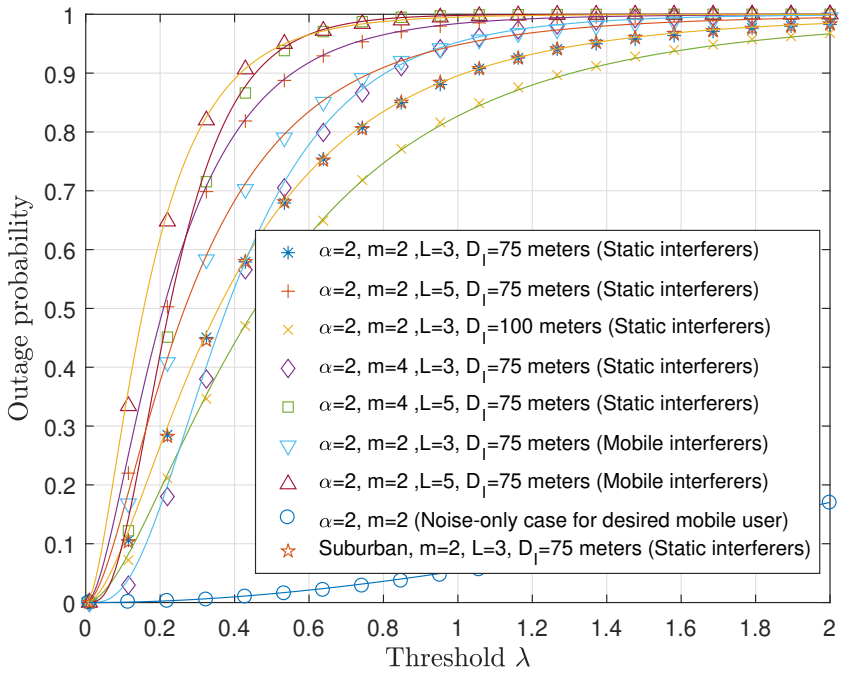

Figure 4.6: The outage probability versus threshold (λ) for D_U = 100 m, $m = \{2,4\}$ and $L = \{3,5\}$ with static and mobile interfering users.

terference on the UAV communications performance. Future extension includes the unpacking of parameters to simplify analytical expressions.

Chapter 5

Performance Analysis of Hybrid UAV Networks for Wireless Caching

5.1 Introduction

To meet the ever-increasing demand for high data rate and support the diversified traffic demand for future mobile networks, there have been rapid increases in the deployment of small-cell base stations (SBSs) that coexist with macro-cell cellular networks. However, the major challenge to accomplish these tasks is the congestion in the back-haul link due to the transmission of a large amount of data, resulting in high latency and low data rate [180]. On the other hand, the recent advances and the decreasing costs in the data storage technology make it more convenient to store a large amount of data at the edges of the wireless network at low cost. Furthermore, it has been observed that the majority of the data traffic comprises of the streaming and downloading of popular contents, such as high-definition videos on YouTube, podcasts, weather forecast, news bulletins, and maps. To this end, wireless edge caching is one of the most promising solutions. In the wireless local caching, the popular contents are stored in caches at the network edges, such as small cells and hand-held devices during off-peak time [181, 182]. Consequently, contents can be directly requested and accessed locally by users

during peak times to reduce the burden on back-haul networks as well as the transmission latency. Besides meeting the issues of overwhelming traffic demands by the dense deployment of BSs in the form of cache-enabled multi-tier hybrid networks, the energy efficiency of such networks is imperative from the network planning viewpoint [183]. Thus, the characterization of the energy efficiency performance will be compelling for understanding the impact of the design parameters of the network such as, BSs density, power consumption, and the QoS requirement. This chapter evaluates the energy efficiency performance of a hybrid caching network to successfully deliver the cached contents to the ground user for a given transmission requirement and then compare its efficacy with the separate UAV and ground networks. Furthermore, this work employs network-level performance metrics for the analysis of the successful content delivery.

UAVs can provide flexible access due to their maneuverability and hence, can be exploited as an aerial BS to facilitate high-speed transmission[133]. In UAV-enabled small cell networks, UAVs can be used as SBSs to support existing macro-cell BSs by off-loading the traffic congestion from the back-haul networks, particularly during big public events such as the Olympics games and music festivals, where the demand on the communication services increases. In contrast to the network caching with a fixed ground infrastructure, UAV-enabled caching can increase the likelihood of successful content transmission because the mobility of UAV can take caching content closer to the typical user. However, the deployment of UAVs can encounter many challenges, such as limited flying duration, energy consumption, and interference management. In the literature of UAV communications, the deployment of multiple UAVs is based either on the deterministic approach, such as the circle packing method in [45] and hexagonal placement in [184], or on the random distribution using tools of stochastic geometry.

Recently, research on the coexistence of the UAV-enabled network with the terrestrial network was presented in [168] and [185–187]. For these works, the spatial distribution of BSs is defined by a PPP. For instance, in [168] and [185–187], UAVs were distributed according to a 3D PPP and the terrestrial network was modeled by a 2D PPP.

However, most of these studies ignore the caching aspect in UAVs. In [188], the authors provided an analytical framework using independent PPPs for UAV and ground BSs to evaluate the performance of UAV assisted cellular networks in terms of SINR coverage probability. In [189], the authors modeled a multi-layer aerial network with PPP using air-to-ground and air-to-air channel models to evaluate the transmission probability and area spectral efficiency. In [190], probabilistic caching placement was investigated in a heterogeneous UAV network modeled with an independent homogeneous PPP without considering co-channel interference and in the absence of a terrestrial network. In [191], the authors presented a framework for the uplink transmission of cached contents from the ground SBSs distributed according to a homogeneous PPP to a single aerial UE over the ground-to-air channel. In [156], the UAV-assisted secure transmission was studied via caching, where UAVs offload the video traffic and deliver to mobile users in small cells. On the other hand, the authors in [33] presented the architecture of caching in a UAV-enabled small-cell network. However, an analytical framework for the performance analysis has not been provided for an aerial network that coexists with the ground network consisting of cache-enabled SBSs. The works in [132, 192, 193] utilized cache-enabled UAVs in a radio access network. However, these works does not model their system as a multi-tier caching network that consists of ground SBSs to supplement UAVs.

Content placement is the key challenge due to the limited caching capacity in SBSs, because spontaneous caching in nearby SBSs will incur more interference. Extensive research has been conducted to analyze the joint content placement and transmission performance as well as designing relevant caching strategies. For instance, [194] studied the optimal content placement of the cache-enabled heterogeneous cellular network. [195] proposed a caching strategy for the cluster-centric small-cell network that combines the most popular content and the large content diversity. This strategy was extended in [196] to a distributed relay network for improvements in outage performance. In [197], a heuristic solution was proposed to significantly improve the video

delivery performance in the cache-enabled wireless heterogeneous networks. In [198], the authors proposed a heuristic algorithm to maximize the transmission performance of cache-enabled multi-antenna and mmWave small-cell networks. Reference [199] analyzed and optimized the performance of content placement in terrestrial BSs and in mobile users that coexist in a heterogeneous wireless network. In [200], the cache-enabled nodes were grouped in disjoint clusters by the Matern hard core point process[1]. In [203], spatial caching strategy was proposed to improve content delivery probability and to avoid caching redundancy in a heterogeneous network. In [204], the authors studied the techniques to enhance the caching capacity in the mobile ad hoc networks. However, these works did not consider the content placement scheme in UAV-enabled networks using the realistic air-to-ground channel features in urban environments.

Small-cell networks are expected to provide significant improvement in the content delivery for higher transmission rates and to reduce the back-haul congestion of a network. In the previous works [194–200, 203, 204], cache-enabled networks were designed mostly for the ground BSs and therefore, the content caching and transmission schemes were developed mainly to maximize the performance of a small-cell network. On the other hand, UAV small-cell networks are very suitable to deploy aerial BSs as back-haul entities to connect users to the core network. However, the coexistence of the UAVs and the ground SBSs in a multi-tier caching network has been widely ignored.

The existing studies mentioned above have neither considered the modeling of a hybrid caching network which consists of the UAVs and ground SBSs that are randomly located according to the PPP in [205], nor analyze its content delivery and energy efficiency performances. Therefore, motivated by these observations, this chapter presents the guidelines to model the hybrid caching network and analyze the performance of the proposed content caching scheme which exploit the content diversity based on its popularity measures. The main contributions of this chapter are summarized as follows:

[1]Matern point process can be used to model positions of the simultaneous transmitting nodes since it conditions on having a minimum distance separating the points of the process [201, 202].

1. User association probability for the UAVs and the ground SBSs are derived using the tool of the stochastic geometry. Both UAVs and ground SBSs coexist in a network which adopts the density sharing scheme for the adequate deployment of UAVs and ground SBSs. Their locations are determined by the homogeneous PPPs. The typical user request for a particular file is highly likely to be associated with the cache-enabled UAV and ground SBS in a hybrid network based on the maximum received power criteria.

2. Successful content delivery probability is used to analyze the network performance, which represents the probability that a particular file requested by a typical user is not only cached at the UAV and SBS but also successfully delivered over the wireless channel. Furthermore, inter-tier and intra-tier interferences are taken into account and modeled by the Laplace transforms. The results reveal that the successful content delivery performance is dependent on the network parameters, such as the UAV and SBS density to control the interference and the UAV altitude, and also on the content-related parameters, such as the size of the content in the database, caching capacity of UAVs and SBSs, skewness in content popularity, and the target data rate.

3. Energy efficiency is a performance metric which is defined as the ratio of the area spectral efficiency for the successful content delivery to the average power consumption of the UAV for a given QoS threshold. The energy efficiency of the cache-enabled hybrid network is then compared with the separate UAV and ground networks to assess the effectiveness of the hybrid approach.

4. A wireless content caching scheme is proposed in which a portion of the caching capacity in each UAV and SBS is designated to cache the most popular content with the higher popularity probability. Thereafter, the contents with the moderate popularity are stored in the remaining portion of the caching capacity. Furthermore, the content delivery performance of the proposed caching scheme is com-

pared with the widely used popular content placement method in [194–198] as a baseline scheme which only cache most popular content.

The rest of the chapter is organized as follows. Section 5.2 presents the system model. The SINR analysis is given in Section 5.3. Section 5.4 defines the criteria for user association with the UAVs and ground SBSs, and hence, derive user association probability. The successful content delivery performance is analyzed in Section 5.5. The energy efficiency of the network design is formulated in Section 5.6. Then the proposed content caching scheme is given in Section 5.7. The numerical and simulations results are discussed in Section 5.8, and conclusions are drawn in Section 5.9.

5.2 System Model

This section describes the network topology, the channel model, and the content placement scheme for the cache-enabled hybrid network illustrated in Fig. 5.1. The commonly used symbols in this chapter and their meanings are listed in Table 5.1.

Table 5.1: Summary of symbols.

Symbols	**Meaning**
$\Phi_{\mathrm{U}}, \Phi_{\mathrm{G}}$	Location of UAVs in tier U, SBSs in tier G
$\lambda_{\mathrm{U}}, \lambda_{\mathrm{G}}$	Density of UAVs in tier U, SBSs in tier G
h	UAV altitude
η	Density control factor
K	Size of database
J	Caching capacity of each UAV and SBS
z	State of UAV being in LOS (z = L) and NLOS (z = N) conditions
f_k	The k-th file
b_k	Placement probability of file f_k in UAV and SBS cache
m_k	Popularity measure for the requested file f_k
g_o	Rayleigh fading gain with unit mean for desired link
g_i, g_j, g_l	Rayleigh fading gain with unit mean for interference link

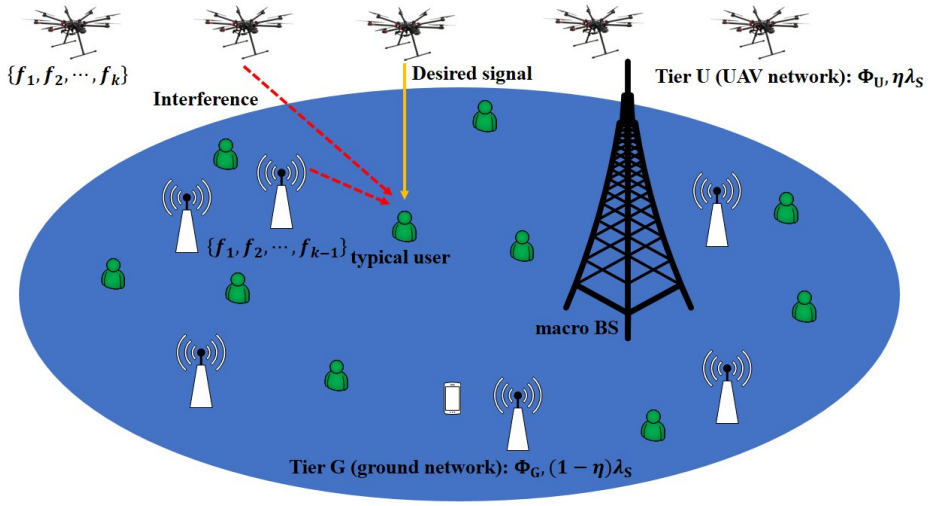

Figure 5.1: System model for cache-enabled hybrid network with UAVs and ground SBSs deployed according to PPP.

5.2.1 Network Topology

This chapter considers a three-tier time division multiplexing heterogeneous network with UAVs in tier U, ground SBSs in tier G, and one macro BS for back-haul connectivity. Specifically, UAVs are deployed as a cache-enabled aerial BSs in tier U in the presence of the already existing ground SBSs, where UAVs are fixed at an altitude of h meters and transmit with power P_U. In this case, the random deployment of UAVs follow the PPP in [205] due to three main reasons. First, the projection distribution is similar to the classic PPP when all UAVs hover at the same altitude. Second, the non-overlapping distribution points will avoid collision of UAVs. Third, to provide analytical tractability to model the uncertainty with the cache-enabled UAVs in the worst-case scenario [168, 185–187]. In tier G, SBSs are on the ground and transmit with power P_G. Furthermore, each UAV and SBS is assumed to be equipped with a single antenna. This chapter consider a density sharing scheme to determine an appropriate participation of the cache-enabled UAVs and ground SBSs in a hybrid network. The overall distribution of the cache-enabled nodes in a hybrid network is modeled by a homogeneous PPP Φ_S with density λ_S. The

UAVs and the ground SBSs in tier U and tier G follow two independent homogeneous PPPs Φ_U and Φ_G with densities $\lambda_U = \eta\lambda_S$ and $\lambda_G = (1-\eta)\lambda_S$, respectively. In this case, $0 \leq \eta \leq 1$ and the factor $1-\eta$ defines the percent of the active SBSs in a hybrid network with the condition that $\lambda_S \geq \lambda_U$ and $\lambda_S \geq \lambda_G$. Also, the ground users are spatially distributed according to an independent homogeneous PPP Φ_T with density λ_T. The user density is assumed to be much larger than the UAVs and SBSs densities ($\lambda_T \gg \lambda_U$ and $\lambda_T \gg \lambda_G$). Based on Slivnyak's theorem[2] of PPP in [205], the typical user is set as a ground reference point which is served by each UAV and SBS at each time slot.

5.2.2 Channel Model

For the downlink communication, air-to-ground channel is used between UAV and the typical ground user. In such channel, the path loss is dependent on the propagation environment and the UAV altitude. In this case, the LOS and NLOS links can be considered as separate components of the air-to-ground channel. Thus, the path loss for LOS and NLOS links can be given as [43]

$$L_{U,z}(X) = \beta_o X^{\alpha_z}; \qquad z \in \{L, N\}, \tag{5.1}$$

where $\beta_o = \left(\frac{4\pi f}{c}\right)^2$ is the frequency-dependent channel power at the reference distance of 1 meters, f is the carrier frequency, c is the speed of light, $z \in \{L, N\}$ denotes the condition of being LOS (z = L) or NLOS (z = N) links, $X = \sqrt{d^2 + h^2}$ is the propagation distance, d is the user distance from the projection of the UAV, α_L and α_N are the PLEs for the LOS and NLOS links, respectively. Also, the probability of having a LOS link is given as [19]

$$p_L(X) = \frac{1}{1 + a \times \exp\left(-b\left[\arcsin\left(\frac{h}{X}\right) - a\right]\right)}, \tag{5.2}$$

[2] Slivnyak's theorem states that for a PPP Φ, because of the independence between all of the points, conditioning on a point at x does not change the distribution of the rest of the process. Therefore, this theorem is sufficient to consider the network-performance analysis for a typical user located at the origin, without changing its statistical properties, which yields the expected experience for all users.

and the probability of having a NLOS link is given by $p_{\mathrm{N}}(X) = 1 - p_{\mathrm{L}}(X)$, where a and b are constants related to the environment.

In order to have tractable analysis, this work considers that the LOS probabilities for different communication links are independent [168]. As a result, one can break down the PPP Φ_{U} of UAVs into two independent in-homogeneous sub processes. In this case, PPPs $\Phi_{\mathrm{U}}^{\mathrm{L}}$ and $\Phi_{\mathrm{U}}^{\mathrm{N}}$ of UAVs that are in LOS and NLOS conditions with regards to ground user having non-constant densities $\lambda_{\mathrm{U}} p_{\mathrm{L}}(X)$ and $\lambda_{\mathrm{U}} p_{\mathrm{N}}(X)$, respectively. Hence, $\Phi_{\mathrm{U}} = \Phi_{\mathrm{U}}^{\mathrm{L}} \cup \Phi_{\mathrm{U}}^{\mathrm{N}}$.

In the ground network, the channel between tier G SBS and the typical user has path loss given by

$$L_{\mathrm{G}}(Y) = \beta_{\mathrm{o}} Y^{\alpha_{\mathrm{G}}} \tag{5.3}$$

where Y is the user distance from the ground SBS to typical user and α_{G} is the PLE of tier G.

5.2.3 Probabilistic Content Placement Method

This work assumes that the particular contents (such as popular multimedia files) are placed in the cache at both the UAVs and ground SBSs. A typical user randomly requests the contents from the finite content database $\mathscr{C} := \{f_1, \cdots, f_k, \cdots, f_K\}$, where the database size is K and the k-th file is requested with a probability of m_k. The contents are assumed to differ in popularity for all k and the files are requested in decreasing popularity, so that $m_k > m_{k+1} > \cdots > m_K$ and $\sum_{k=1}^{K} m_k = 1$. All content files are assumed to have the same normalized size equal to 1 [206]. Furthermore, each SBS can only store up to J contents, where $J \leqslant K$. Such an assumption is practical because all SBSs may not have enough capacity to store the entire database contents.

This chapter adopts the probabilistic content placement scheme used in [190, 194, 198] to select contents for caching at UAVs and ground SBSs while considering their

storage capacity. In this scheme, the caching probability b_k needs to meet the following condition

$$\sum_{k=1}^{K} b_k \leq J, \qquad 0 \leq b_k \leq 1, \forall k. \tag{5.4}$$

The condition in (5.4) allows each UAV and SBS to cache the maximum amount of the total content up to their caching capacity J. Note that, using the probabilistic content placement strategy, $\Phi_{\mathrm{G},k}$ and $\Phi_{\mathrm{U},k}$ are independent PPPs with densities $\lambda_{\mathrm{G},k} = b_k\lambda_{\mathrm{G}}$ and $\lambda_{\mathrm{U},k} = b_k\lambda_{\mathrm{U}}$ of the cache-enabled ground SBSs and UAVs, respectively. These SBSs and UAVs can support the typical user when the k-th content is requested, and $\Phi_{\mathrm{G}} = \cup_{k\in K}\Phi_{\mathrm{G},k}$, and $\Phi_{\mathrm{U}} = \cup_{k\in K}\Phi_{\mathrm{U},k}$, respectively. All the remaining un-cached contents having least popularity are served by the macro BS via back-haul.

5.3 Analysis of Signal-to-Interference-plus-Noise Ratio (SINR)

Considering the downlink communication, This work consider the scenario where a UAV establishes a communication link with the typical user based on the strongest received signal and consequently provides the highest SINR for the user. Thus, for a typical user that is associated with the serving UAV, the received SINR at the typical user is given by

$$\mathrm{SINR}_{\mathrm{U,z}} = \frac{P_{\mathrm{U}} g_o \{L_{\mathrm{U,z}}(X_o)\}^{-1}}{\sigma^2 + \mathscr{I}_{\mathrm{U}} + \hat{\mathscr{I}}_{\mathrm{G}}}; \quad \mathrm{z} \in \{\mathrm{L},\mathrm{N}\}, \tag{5.5}$$

where X_o denotes the distance from the typical user to its serving UAV, $g_o \sim \exp(1)$ is the Rayleigh fading channel power with the unit mean for the desired link, σ^2 is the noise power, and the aggregate intra-tier interference is given by $\mathscr{I}_{\mathrm{U}} = \mathscr{I}_{\mathrm{U,C}} + \mathscr{I}_{\mathrm{U,N}}$ with

$$\mathscr{I}_{\mathrm{U,C}} = \sum_{\mathrm{z}\in\{\mathrm{L},\mathrm{N}\}} \sum\nolimits_{i\in\Phi_{\mathrm{U},k}\setminus\{o\}} P_{\mathrm{U}} g_i \{L_{\mathrm{U,z}}(X_i)\}^{-1}, \tag{5.6}$$

and

$$\mathscr{I}_{\mathrm{U,N}} = \sum\nolimits_{\mathrm{z}\in\{\mathrm{L,N}\}} \sum_{j\in\Phi_{\mathrm{U}}\setminus\Phi_{\mathrm{U},k}} P_{\mathrm{U}} g_j \{L_{\mathrm{U,z}}(X_j)\}^{-1}, \tag{5.7}$$

being the co-channel interferences for the UAVs with the propagation distance X_i and the point process $\Phi_{\mathrm{U},k}\setminus\{o\}$ corresponding to the density $b_k\lambda_{\mathrm{U}}$ that cache the k-th content, and for the UAVs with the propagation distance X_j and the point process $\Phi_{\mathrm{U}}\setminus\Phi_{\mathrm{U},k}$ corresponding to the density given by the independent thinning theorem $(1-b_k)\lambda_{\mathrm{U}}$ [205] that do not store the k-th content in their caches, respectively. Also, the aggregate inter-tier interference caused by the ground SBSs in tier G is given by

$$\hat{\mathscr{I}}_{\mathrm{G}} = \sum_{l\in\Phi_{\mathrm{G}}} P_{\mathrm{G}} g_l \{L_{\mathrm{G}}(Y_l)\}^{-1}, \tag{5.8}$$

where Y_l is the propagation distance between the typical user and the ground SBS, $g_i, g_j, g_l \sim \exp(1)$ are the interfering Rayleigh channel fading powers that follow the exponential distribution.

Similarly, the received SINR at the typical user from the ground SBSs in tier G is given by

$$\mathrm{SINR}_{\mathrm{G}} = \frac{P_{\mathrm{G}} g_o \{L_{\mathrm{G}}(Y_o)\}^{-1}}{\sigma^2 + \mathscr{I}_{\mathrm{G}} + \hat{\mathscr{I}}_{\mathrm{U}}}, \tag{5.9}$$

where the aggregate intra-tier interference is given by $\mathscr{I}_{\mathrm{G}} = \mathscr{I}_{\mathrm{G,C}} + \mathscr{I}_{\mathrm{G,N}}$ with

$$\mathscr{I}_{\mathrm{G,C}} = \sum\nolimits_{i\in\Phi_{\mathrm{G},k}\setminus\{o\}} P_{\mathrm{G}} g_i \{L_{\mathrm{G}}(Y_i)\}^{-1}, \tag{5.10}$$

and

$$\mathscr{I}_{\mathrm{G,N}} = \sum\nolimits_{j\in\Phi_{\mathrm{G}}\setminus\Phi_{\mathrm{G},k}} P_{\mathrm{G}} g_j \{L_{\mathrm{G}}(Y_j)\}^{-1}, \tag{5.11}$$

being the intra-tier interferences related to the ground SBSs with the ground distance

Y_i and the point process $\Phi_{\mathrm{G},k}\backslash\{o\}$ corresponding to the density $b_k\lambda_{\mathrm{G}}$ that stores the k-th content, and for the ground SBSs with the ground distance Y_j and the point process $\Phi_{\mathrm{G}}\backslash\Phi_{\mathrm{G},k}$ corresponding to the densities $(1-b_k)\lambda_{\mathrm{G}}$ that do not store the k-th file. Also, the aggregate inter-tier interference caused by all UAVs in tier U is given by

$$\hat{\mathscr{I}}_{\mathrm{U}} = \sum_{\mathrm{z}\in\{\mathrm{L},\mathrm{N}\}}\sum_{l\in\Phi_{\mathrm{U}}} P_{\mathrm{U}} g_l \{L_{\mathrm{U},\mathrm{z}}(X_l)\}^{-1}. \tag{5.12}$$

where X_l is the interfering propagation distance from UAVs in tier U.

5.4 Derivation of User Association Probability

User association accounts for both the content availability and the link reliability. Therefore, a user association method is introduced based on the maximum received signal power by the user from the UAV ($\mathbb{L}_{\mathrm{U},x}$) and the ground SBS ($\mathbb{L}_{\mathrm{G},y}$) with the following criterion

$$\mathbb{L}_{\mathrm{U},x} = P_{\mathrm{U}} g_o \Big(\sum_{\mathrm{z}\in\{\mathrm{L},\mathrm{N}\}} L_{\mathrm{U},\mathrm{z}}(r_x)^{-1} p_{\mathrm{z}}(r_x) \Big), \tag{5.13}$$

and

$$\mathbb{L}_{\mathrm{G},y} = P_{\mathrm{G}} g_o L_{\mathrm{G}}(r_y)^{-1}. \tag{5.14}$$

It is important to note that only the popular parts of all contents, i.e., $\mathscr{C}^{\mathrm{U}}$ and $\mathscr{C}^{\mathrm{G}}$, are cached at the UAV and ground SBSs due to their limited storage capacity. Hence, it is possible that a file requested by the user may be unavailable at SBSs, which has to be requested from a content database via the back-haul network. However, such situations arises occasionally and are omitted in analysis for mathematical tractability, similar to [207, 208]. A user is associated with the content-centric SBSs if the user requests file f_k and is served by UAV in tier U and SBS in tier G. Thus, when the user requests the file f_k,

the serving UAV and SBS denoted by $\mathbb{L}_k$ is defined as

$$\mathbb{L}_k = \begin{cases} \arg\max \left\{ \max\limits_{x\in\Phi_{\mathrm{U},k}} \mathbb{L}_{\mathrm{U},x}, \max\limits_{y\in\Phi_{\mathrm{G},k}} \mathbb{L}_{\mathrm{G},y} \right\}, f_k \in \{\mathscr{C}^{\mathrm{U}}, \mathscr{C}^{\mathrm{G}}\} \\ \arg\max\limits_{x\in\Phi_{\mathrm{U},k}} \mathbb{L}_{\mathrm{U},x}, f_k \in \mathscr{C}^{\mathrm{U}} \\ \arg\max\limits_{y\in\Phi_{\mathrm{G},k}} \mathbb{L}_{\mathrm{G},y}, f_k \in \mathscr{C}^{\mathrm{G}}. \end{cases} \tag{5.15}$$

Lemma 1: The probability that a typical user is associated with the nearest cache-enabled UAV with file f_k in LOS and NLOS conditions is given by

$$\mathscr{A}_{\mathrm{U}}^{k} = \sum\nolimits_{\mathrm{z}\in\{\mathrm{L},\mathrm{N}\}} \mathscr{A}_{\mathrm{U,z}}^{k}, \tag{5.16}$$

where, $\mathscr{A}_{\mathrm{U,L}}^{k}$ and $\mathscr{A}_{\mathrm{U,N}}^{k}$ are association probabilities for LOS and NLOS conditions, respectively, and $\mathscr{A}_{\mathrm{U,L}}^{k}$ is calculated as

$$\mathscr{A}_{\mathrm{U,L}}^{k} = 2\pi b_k \lambda_{\mathrm{U}} \int_h^{\infty} r_x \exp\Big(-\pi b_k \lambda_{\mathrm{G}} \Big(\frac{P_{\mathrm{G}}}{P_{\mathrm{U}}} {r_x}^{\alpha_{\mathrm{L}}}\Big)^{2/\alpha_{\mathrm{G}}} - 2\pi b_k \lambda_{\mathrm{U}} \int_h^{r_x} p_{\mathrm{L}}(l) l dl \Big) p_{\mathrm{L}}(r_x) dr_x. \tag{5.17}$$

Proof: Assume that r_x is the minimum propagation distance between the UAV with file f_k in tier U to the typical user and r_y is the distance from the ground SBS in tier G to the typical user. Thus, the user association probability for the UAV in the LOS condition $\mathscr{A}_{\mathrm{U,L}}^{k}$ is the probability that $L_{\mathrm{U,L}}(r_x) > L_{\mathrm{G}}(r_y)$. Therefore,

$$\mathscr{A}_{\mathrm{U,L}}^{k} = \mathrm{E}_{r_x}\big[\mathbb{P}[L_{\mathrm{U,L}}(r_x) > L_{\mathrm{G}}(r_y)]\big] = \int_h^{\infty} \mathbb{P}\Big[r_y > \Big(\frac{P_{\mathrm{G}}}{P_{\mathrm{U}}} r_x^{\alpha_{\mathrm{L}}}\Big)^{1/\alpha_{\mathrm{G}}} \Big] f_{r_x}^{\mathrm{L}}(r_x) dr_x. \tag{5.18}$$

To derive $\mathscr{A}_{\mathrm{U,L}}^{k}$, $\mathbb{P}[r_y > \left(\frac{P_{\mathrm{G}}}{P_{\mathrm{U}}} r_x^{\alpha_{\mathrm{L}}}\right)^{1/\alpha_{\mathrm{G}}}]$ is computed by using the void probability[3] of a 2D

[3]The probability that a typically chosen point (according to the Slivnyak theorem) is farther than r from its nearest neighbour is given by the void probability of the PPP and is given as $\exp(-\lambda\pi r^2)$, where λ is the intensity having unit of points/area [209].

Poisson process and is given as

$$\mathbb{P}\Big[r_y > \Big(\frac{P_{\mathrm{G}}}{P_{\mathrm{U}}} r_x^{\alpha_{\mathrm{L}}}\Big)^{1/\alpha_{\mathrm{G}}}\Big] = \exp\Big(-\pi b_k \lambda_{\mathrm{G}} \Big(\frac{P_{\mathrm{G}}}{P_{\mathrm{U}}} {r_x}^{\alpha_{\mathrm{L}}}\Big)^{2/\alpha_{\mathrm{G}}}\Big). \tag{5.19}$$

Furthermore, the PDF of r_x denoted by $f_{r_x}^{\mathrm{L}}(r_x)$ corresponds to the serving UAVs in LOS condition with probability $p_{\mathrm{L}}(r_x)$ that provides stronger signal to the typical user with the shortest distance. In this case, $f_{r_x}^{\mathrm{L}}(r_x)$ is derived by taking the derivative of $1 - \mathbb{P}[h < l < r_x]$ with respect to r_x and using the void probability of a 2D Poisson process, where $\mathbb{P}[h < l < r_x]$ is given as

$$\mathbb{P}[h < l < r_x] = \exp\big(-2\pi b_k \lambda_{\mathrm{U}} \int_h^{r_x} p_{\mathrm{L}}(l) l dl\big). \tag{5.20}$$

where l is the minimum propagation distance range. Then, by using Leibniz integral rule, $f_{r_x}^{\mathrm{L}}(r_x)$ is given by

$$f_{r_x}^{\mathrm{L}}(r_x) = 2\pi r_x b_k \lambda_{\mathrm{U}} p_{\mathrm{L}}(r_x) \times \exp\Big(-2\pi b_k \lambda_{\mathrm{U}} \int_h^{r_x} p_{\mathrm{L}}(l) l dl\Big). \tag{5.21}$$

By substituting (5.19) and (5.21) in (5.18), the result in (5.17) is obtained. Similarly, the association probability $\mathscr{A}_{\mathrm{U,N}}^k$ for the UAV in the NLOS condition can be derived by following the same steps as

$$\mathscr{A}_{\mathrm{U,N}}^k = 2\pi b_k \lambda_{\mathrm{U}} \int_h^{\infty} r_x \exp\Big(-\pi b_k \lambda_{\mathrm{G}} \Big(\frac{P_{\mathrm{G}}}{P_{\mathrm{U}}} {r_x}^{\alpha_{\mathrm{N}}}\Big)^{2/\alpha_{\mathrm{G}}} - 2\pi b_k \lambda_{\mathrm{U}} \int_h^{r_x} p_{\mathrm{N}}(l) l dl\Big) p_{\mathrm{N}}(r_x) dr_x. \tag{5.22}$$

Lemma 2: The probability that a typical user is associated with the nearest cache-

enabled ground SBS with file f_k is given by

$$\mathscr{A}_{\mathrm{G}} = 2\pi b_k \lambda_{\mathrm{G}} \sum_{\mathrm{z}\in\{\mathrm{L},\mathrm{N}\}} \int_0^{\infty} r_y \exp\Big(-\pi b_k \lambda_{\mathrm{G}} {r_y}^2 - 2\pi b_k \lambda_{\mathrm{U}} \int_h^{\left(\frac{P_{\mathrm{U}}}{P_{\mathrm{G}}} r_y^{\alpha_{\mathrm{G}}}\right)^{2/\alpha_{\mathrm{z}}}} p_{\mathrm{z}}(r_x) r_x dr_x \Big) dr_y, \tag{5.23}$$

Proof: Assume that the minimum distance between the ground SBS with file f_k in tier G to the typical user is r_y, and the propagation distance between the UAV in tier U to the typical user is r_x. Thus, the association probability $\mathscr{A}_{\mathrm{G}}$ is the probability that $L_{\mathrm{G}}(r_y) > L_{\mathrm{U,z}}(r_x)$. Therefore,

$$\mathscr{A}_{\mathrm{G}} = \mathrm{E}_{r_y}\big[\mathbb{P}[L_{\mathrm{G}}(r_y) > L_{\mathrm{U,z}}(r_x)]\big] = \int_0^{\infty} \mathbb{P}\Big[h < r_x < \Big(\frac{P_{\mathrm{U}}}{P_{\mathrm{G}}} r_y^{\alpha_{\mathrm{G}}}\Big)^{1/\alpha_{\mathrm{z}}}\Big] f_{r_y}^{\mathrm{G}}(r_y) dr_y. \tag{5.24}$$

Then using void probability of a 2D Poisson process, one has

$$\mathbb{P}\Big[h < r_x < \Big(\frac{P_{\mathrm{U}}}{P_{\mathrm{G}}} r_y^{\alpha_{\mathrm{G}}}\Big)^{1/\alpha_{\mathrm{z}}}\Big] = \exp\Big(-2\pi b_k \lambda_{\mathrm{U}} \int_h^{\left(\frac{P_{\mathrm{U}}}{P_{\mathrm{G}}} r_y^{\alpha_{\mathrm{G}}}\right)^{1/\alpha_{\mathrm{z}}}} p_{\mathrm{z}}(r_x) r_x dr_x \Big). \tag{5.25}$$

The PDF of the minimum ground distance r_y is given by

$$f_{r_y}^{\mathrm{G}}(r_y) = 2\pi b_k \lambda_{\mathrm{G}} r_y \exp\big(-\pi b_k \lambda_{\mathrm{G}} r_y^2 \big). \tag{5.26}$$

By substituting (5.25) and (5.27) in (5.24), the result in (5.23) is obtained.

5.5 The Successful Content Delivery Probability

The network performance is measured by the successful content delivery probability, which represents the probability that the file requested by a typical user is not only cached at UAV and SBS but also successfully transmitted by them over the wireless channel. For the density share scheme, the successful content delivery probability of the con-

sidered hybrid network is given by

$$\mathscr{P}_{\mathrm{SCD}}(\eta, b_k) = \mathscr{P}^{\mathrm{U}}_{\mathrm{SCD}}(\eta, b_k) + \mathscr{P}^{\mathrm{G}}_{\mathrm{SCD}}(\eta, b_k), \tag{5.27}$$

assuming that the content size of φ bits needs to be transmitted in τ seconds, the successful content delivery probability in the UAV is computed as

$$\mathscr{P}^{\mathrm{U}}_{\mathrm{SCD}}(\eta, b_k) = \sum_{k=1}^{J} m_k \mathbb{P}[\mathrm{SINR}_{\mathrm{U,z}} > \delta_{\mathrm{U}}], \tag{5.28}$$

with $\delta_{\mathrm{U}} = 2^{\frac{\varphi/\tau}{\mathscr{W}_{\mathrm{U}}}} - 1$ and $\mathscr{W}_{\mathrm{U}}$ being the UAV bandwidth. Furthermore, the successful content delivery probability for the ground SBS is calculated as

$$\mathscr{P}^{\mathrm{G}}_{\mathrm{SCD}}(\eta, b_k) = \sum_{k=1}^{J} m_k \mathbb{P}[\mathrm{SINR}_{\mathrm{G}} > \delta_{\mathrm{G}}], \tag{5.29}$$

where $\delta_{\mathrm{G}} = 2^{\frac{\varphi/\tau}{\mathscr{W}_{\mathrm{G}}}} - 1$, and $\mathscr{W}_{\mathrm{G}}$ is the ground SBS bandwidth. Next subsection will derive the successful content delivery probability for the UAV in tier U.

5.5.1 Successful Content Delivery Probability for the Cache-Enabled UAV Base Station

Lemma 3: The successful content delivery probability for the cache-enabled UAV with file f_k in tier U is given by

$$\mathscr{P}^{\mathrm{U}}_{\mathrm{SCD}}(\eta, b_k) = \sum_{k=1}^{J} m_k \mathscr{P}^{\mathrm{U}}_{\mathrm{Cov}}(\eta, b_k), \tag{5.30}$$

where $P^{\mathrm{U}}_{\mathrm{Cov}}(\eta, b_k) = P^{\mathrm{U,L}}_{\mathrm{Cov}}(\eta, b_k) + P^{\mathrm{U,N}}_{\mathrm{Cov}}(\eta, b_k)$ and $\mathscr{P}^{\mathrm{U,L}}_{\mathrm{Cov}}(\eta, b_k)$ and $\mathscr{P}^{\mathrm{U,N}}_{\mathrm{Cov}}(\eta, b_k)$ are the coverage probabilities to successfully delivered the file f_k with caching probability b_k to a typical user connected with the serving UAV in tier U with density $\lambda_{\mathrm{U}} = \eta\lambda_{\mathrm{S}}$ having LOS

and NLOS conditions, respectively, and are given as

$$\mathscr{P}_{\text{Cov}}^{\text{U,L}}(\eta, b_k) = \mathscr{L}_{\mathscr{I}_{\text{U,C}}}(s_{\text{L}}) \cdot \mathscr{L}_{\mathscr{I}_{\text{U,N}}}(s_{\text{L}}) \cdot \mathscr{L}_{\hat{\mathscr{I}}_{\text{G}}}(s_{\text{L}}) \cdot \exp -(s_{\text{L}}\sigma^2) \cdot \mathscr{A}_{\text{U,L}}^{k}, \tag{5.31}$$

$$\mathscr{P}_{\text{Cov}}^{\text{U,N}}(\eta, b_k) = \mathscr{L}_{\mathscr{I}_{\text{U,C}}}(s_{\text{N}}) \cdot \mathscr{L}_{\mathscr{I}_{\text{U,N}}}(s_{\text{N}}) \cdot \mathscr{L}_{\hat{\mathscr{I}}_{\text{G}}}(s_{\text{N}}) \cdot \exp -(s_{\text{N}}\sigma^2) \cdot \mathscr{A}_{\text{U,N}}^{k}, \tag{5.32}$$

respectively, where $s_{\text{z}} = \frac{\delta_{\text{U}}\beta_{\text{o}}}{P_{\text{U}}\sqrt{y^2+h^2}^{-\alpha_{\text{z}}}}$ for $\text{z} \in \{\text{L},\text{N}\}$, $\mathscr{A}_{\text{U,L}}^{k}$, and $\mathscr{A}_{\text{U,N}}^{k}$ are given in (5.17) and (5.22), respectively. Also, $\mathscr{L}_{\mathscr{I}_{\text{U,C}}}(\cdot)$, $\mathscr{L}_{\mathscr{I}_{\text{U,N}}}(\cdot)$, and $\mathscr{L}_{\hat{\mathscr{I}}_{\text{G}}}(\cdot)$ are the Laplace transforms of the interference generated by UAVs that cache with file f_k, UAVs that do not cache f_k, and ground network, respectively.

Proof: Given that a typical user is associated with the cache-enabled UAV in tier U in the LOS condition, the connection probability in the presence of the intra-tier interference from UAVs that cache and do not cache f_k and inter-tier interference from the ground network is given as

$$\begin{aligned}
\mathscr{P}_{\text{Cov}}^{\text{U,L}}(\eta, b_k) &= \mathbb{P}[\text{SINR}_{\text{U,L}} > \delta_{\text{U}}] = \mathbb{P}\Big[\frac{\text{P}_{\text{U}}\text{g}_{\text{o}}\text{L}_{\text{U,z}}{}^{-1}}{\sigma^2 + \mathscr{I}_{\text{U}} + \hat{\mathscr{I}}_{\text{G}}} > \delta_{\text{U}}\Big] \\
&= \mathbb{P}\Big[g_o > \frac{\delta_{\text{U}} L_{\text{U,z}}}{P_{\text{U}}}\big(\sigma^2 + \mathscr{I}_{\text{U,C}} + \mathscr{I}_{\text{U,N}} + \hat{\mathscr{I}}_{\text{G}}\big)\Big] \\
&= \exp -(s_{\text{L}}\sigma^2) \cdot \mathscr{L}_{\mathscr{I}_{\text{U,C}}}(s_{\text{L}}) \cdot \mathscr{L}_{\mathscr{I}_{\text{U,N}}}(s_{\text{L}}) \cdot \mathscr{L}_{\hat{\mathscr{I}}_{\text{G}}}(s_{\text{L}}),
\end{aligned} \tag{5.33}$$

where $s_{\text{L}} = \frac{\delta_{\text{U}}\beta_{\text{o}}}{P_{\text{U}}\sqrt{y^2+h^2}^{-\alpha_{\text{L}}}}$. In this work, the Laplace transforms of interferences can be determined by using probability generating function of a PPP and moment generating function. Thus, $\mathscr{L}_{\mathscr{I}_{\text{U,C}}}(s_{\text{L}})$ is given by

$$\begin{aligned}
\mathscr{L}_{\mathscr{I}_{\text{U,C}}}(s_{\text{L}}) &= \text{E}_{\Phi_{\text{U},k}\setminus\{o\}}\big[\exp -(s_{\text{L}}\mathscr{I}_{\text{U,C}})\big] \overset{(a)}{=} \\
&\exp\Big(-2\pi b_k \lambda_{\text{U}} \sum_{\text{z}\in\{\text{L},\text{N}\}} \int_{y}^{\infty} \Big(1 - \text{E}_{g_i}\Big[\exp\Big(\frac{-s_{\text{L}}P_{\text{U}}g_i\sqrt{x^2+h^2}^{-\alpha_{\text{z}}}}{\beta_{\text{o}}}\Big)\Big]\Big) x p_{\text{z}}(x')dx\Big) \\
&\overset{(b)}{=} \exp\Big(-2\pi b_k \lambda_{\text{U}} \sum_{\text{z}\in\{\text{L},\text{N}\}} \int_{y}^{\infty} \Big(\frac{s_{\text{L}}P_{\text{U}}\sqrt{x^2+h^2}^{-\alpha_{\text{z}}}}{\beta_{\text{o}} + s_{\text{L}}P_{\text{U}}\sqrt{x^2+h^2}^{-\alpha_{\text{z}}}}\Big) x p_{\text{z}}(x')dx\Big),
\end{aligned} \tag{5.34}$$

where $x' = \sqrt{x^2+h^2}$, (a) comes from the probability generating function of a PPP and (b) follows the moment generating function of the exponential distribution [194]. Likewise, $\mathscr{L}_{\mathscr{I}_{\mathrm{U,N}}}(s_{\mathrm{L}})$ is given as

$$\mathscr{L}_{\mathscr{I}_{\mathrm{U,N}}}(s_{\mathrm{L}}) = \exp\Big(-2\pi(1-b_k)\lambda_{\mathrm{U}} \sum_{\mathrm{z}\in\{\mathrm{L,N}\}} \int_{y}^{\infty} \Big(\frac{s_{\mathrm{L}} P_{\mathrm{U}} \sqrt{x^2+h^2}^{-\alpha_{\mathrm{z}}}}{\beta_{\mathrm{o}} + s_{\mathrm{L}} P_{\mathrm{U}} \sqrt{x^2+h^2}^{-\alpha_{\mathrm{z}}}}\Big) x p_{\mathrm{z}}(x') dx\Big). \quad (5.35)$$

where $x' = \sqrt{x^2+h^2}$, (a) comes from the probability generating function of a PPP and (b) follows the moment generating function of the exponential distribution [194]. Likewise, $\mathscr{L}_{\mathscr{I}_{\mathrm{U,N}}}(s_{\mathrm{L}})$ is given as

$$\mathscr{L}_{\mathscr{I}_{\mathrm{U,N}}}(s_{\mathrm{L}}) = \exp\Big(-2\pi(1-b_k)\lambda_{\mathrm{U}} \sum_{\mathrm{z}\in\{\mathrm{L,N}\}} \int_{y}^{\infty} \Big(\frac{s_{\mathrm{L}} P_{\mathrm{U}} \sqrt{x^2+h^2}^{-\alpha_{\mathrm{z}}}}{\beta_{\mathrm{o}} + s_{\mathrm{L}} P_{\mathrm{U}} \sqrt{x^2+h^2}^{-\alpha_{\mathrm{z}}}}\Big) x p_{\mathrm{z}}(x') dx\Big). \quad (5.36)$$

The Laplace transform for interference from the ground network is given as

$$\begin{aligned}
\mathrm{E}_{\Phi_{\mathrm{G}}}\big[\exp -(s_{\mathrm{L}}\hat{\mathscr{I}}_{\mathrm{G}})\big] &= \exp\Big(-2\pi\lambda_{\mathrm{G}} \int_0^{\infty} \Big(1 - \frac{1}{1+\frac{s_{\mathrm{L}} P_{\mathrm{G}} r^{-\alpha_{\mathrm{G}}}}{\beta_{\mathrm{o}}}}\Big) x dx\Big), \\
&= \exp\Big(-2\pi\lambda_{\mathrm{G}} \int_0^{\infty} \frac{\delta_{\mathrm{U}} P_{\mathrm{G}} \sqrt{y^2+h^2}^{\alpha_{\mathrm{L}}}}{P_{\mathrm{U}} r^{\alpha_{\mathrm{G}}} + \delta_{\mathrm{U}} P_{\mathrm{G}} \sqrt{y^2+h^2}^{\alpha_{\mathrm{L}}}} x dx\Big), \\
&= \exp\Big(-2\pi^2\lambda_{\mathrm{G}} \frac{\delta_{\mathrm{U}}^{2/\alpha_{\mathrm{G}}} (y^2+h^2)^{\alpha_{\mathrm{L}}/\alpha_{\mathrm{G}}} \csc\big(\frac{2\pi}{\alpha_{\mathrm{G}}}\big)}{\alpha_{\mathrm{G}} \big(\frac{P_{\mathrm{U}}}{P_{\mathrm{G}}}\big)^{2/\alpha_{\mathrm{G}}}}\Big). \quad (5.37)
\end{aligned}$$

where $\csc(\cdot)$ is the Cosecant trigonometry function.

Similarly, Laplace transforms of cached and un-cached UAVs in NLOS conditions can be computed by following the same steps. The next subsection will derive the successful content delivery probability for the ground SBS in tier G.

5.5.2 Successful Content Delivery Probability for the Cache-Enabled Small-Cell Base Station

Lemma 4: The successful content delivery probability for the cache-enabled ground SBS with file f_k in tier G is given by

$$\mathscr{P}^{\mathrm{G}}_{\mathrm{SCD}}(\eta, b_k) = \sum_{k=1}^{J} m_k \mathscr{P}^{\mathrm{G}}_{,\mathrm{Cov}}(\eta, b_k), \tag{5.38}$$

where $\mathscr{P}^{\mathrm{G}}_{\mathrm{Cov}}(\eta, b_k)$ is the coverage probability to successfully deliver the file f_k with caching probability b_k to the ground user connected with the serving ground SBS in tier G with SBS density $\lambda_{\mathrm{G}} = (1-\eta)\lambda_{\mathrm{S}}$ and is given as

$$\begin{aligned}\mathscr{P}^{\mathrm{G}}_{\mathrm{Cov}}(\eta, b_k) &= \mathbb{P}[\mathrm{SINR}_{\mathrm{G}} > \delta_{\mathrm{G}}] = \mathbb{P}\Big[\mathrm{g_o} > \frac{\delta_{\mathrm{G}} \mathrm{L_G}}{\mathrm{P_G}}\big(\sigma^2 + \mathscr{I}_{\mathrm{G,C}} + \mathscr{I}_{\mathrm{G,N}} + \hat{\mathscr{I}}_{\mathrm{U}}\big)\Big] \\ &= \mathscr{L}_{\mathscr{I}_{\mathrm{G,C}}}(s_{\mathrm{G}}) \cdot \mathscr{L}_{\mathscr{I}_{\mathrm{G,N}}}(s_{\mathrm{G}}) \cdot \mathscr{L}_{\hat{\mathscr{I}}_{\mathrm{U}}}(s_{\mathrm{G}}) \cdot \exp -(s_{\mathrm{G}}\sigma^2) \cdot \mathscr{A}_{\mathrm{G}},\end{aligned} \tag{5.39}$$

where $s_{\mathrm{G}} = \frac{\delta_{\mathrm{G}}\beta_{\mathrm{o}}}{P_{\mathrm{G}} x^{-\alpha_{\mathrm{G}}}}$, $\mathscr{A}_{\mathrm{G}}$ is given in (5.23), and $\mathscr{L}_{\mathscr{I}_{\mathrm{G,C}}}(\cdot)$, $\mathscr{L}_{\mathscr{I}_{\mathrm{G,N}}}(\cdot)$ and $\mathscr{L}_{\hat{\mathscr{I}}_{\mathrm{U}}}(\cdot)$ are the Laplace transforms of the intra-tier interference generated by ground SBSs that store f_k, ground SBSs that do not store f_k, and the UAV network, respectively.

Proof: The Laplace transform for the intra-tier interference generated by the ground SBSs that cache the file f_k is given as

$$\begin{aligned}\mathscr{L}_{\mathscr{I}_{\mathrm{G,C}}}(s_{\mathrm{G}}) &= \mathrm{E}_{\Phi_{\mathrm{G},k}\setminus\{o\}}[\exp(-s_{\mathrm{G}}\mathscr{I}_{\mathrm{G,C}})] \\ &= \exp\Big(-2\pi b_k \lambda_{\mathrm{G}} \int_y^{\infty} \Big(1 - \mathrm{E}_{g_i}\Big[\exp\Big(-\frac{s_{\mathrm{G}} P_{\mathrm{G}} g_i x^{-\alpha_{\mathrm{G}}}}{\beta_{\mathrm{o}}}\Big)\Big]\Big) x dx\Big) \\ &= \exp\Big(-2\pi b_k \lambda_{\mathrm{G}} \int_y^{\infty} \Big(\frac{s_{\mathrm{G}} P_{\mathrm{G}} r^{-\alpha_{\mathrm{G}}}}{\beta_{\mathrm{o}} + s_{\mathrm{G}} P_{\mathrm{G}} x^{-\alpha_{\mathrm{G}}}}\Big) x dx\Big) \\ &= \exp\Big(-2\pi b_k \lambda_{\mathrm{G}} \frac{\delta_{\mathrm{G}} y^2}{\alpha_{\mathrm{G}} - 2} {}_2F_1(1, 1 - \frac{2}{\alpha_{\mathrm{G}}}, 2 - \frac{2}{\alpha_{\mathrm{G}}}, -\delta_{\mathrm{G}})\Big).\end{aligned} \tag{5.40}$$

where ${}_2F_1\big(\cdot,\cdot,\cdot,\cdot\big)$ is the Gauss hypergeometric function. Likewise, $\mathscr{L}_{\mathscr{I}_{\mathrm{G,N}}}(s_{\mathrm{G}})$ is given as

$$\mathscr{L}_{\mathscr{I}_{\mathrm{G,N}}}(s_{\mathrm{G}}) = \exp\Big(-2\pi(1-b_k)\lambda_{\mathrm{G}}\frac{\delta_{\mathrm{G}}y^2}{\alpha_{\mathrm{G}}-2}{}_2F_1\big(1,1-\frac{2}{\alpha_{\mathrm{G}}},2-\frac{2}{\alpha_{\mathrm{G}}},-\delta_{\mathrm{G}}\big)\Big). \tag{5.41}$$

Using the proof of Lemma 3, $\mathscr{L}_{\hat{\mathscr{I}}_{\mathrm{U}}}(s_{\mathrm{G}})$ is given as

$$\mathscr{L}_{\hat{\mathscr{I}}_{\mathrm{U}}}(s_{\mathrm{G}}) = \exp\Big(-2\pi\lambda_{\mathrm{U}}\sum_{\mathrm{z}\in\{\mathrm{L,N}\}}\int_{y}^{\infty}\Big(\frac{s_{\mathrm{G}}P_{\mathrm{U}}\sqrt{x^2+h^2}^{-\alpha_{\mathrm{z}}}}{\beta_{\mathrm{o}}+s_{\mathrm{G}}P_{\mathrm{U}}\sqrt{x^2+h^2}^{-\alpha_{\mathrm{z}}}}\Big)xp_{\mathrm{z}}(x')dx\Big). \tag{5.42}$$

By substituting (5.40)-(5.42) in (5.39), the result in (5.38) is obtained.

5.6 Energy Efficiency of the Hybrid Network

Energy efficiency is a widely used performance indicator for the heterogeneous network with dense and random deployment of SBSs. Using (5.30) and (5.38), the successful content delivery probabilities for the UAV and ground networks is obtained, respectively. In this case, the throughput attained at a typical user by the UAV and ground SBS are given by $\sum_{k=1}^{J} m_k\mathbb{P}[\mathrm{SINR}_{\mathrm{U,z}}>\delta_{\mathrm{U}}]\log_2(1+\delta_{\mathrm{U}})$ and $\sum_{k=1}^{J} m_k\mathbb{P}[\mathrm{SINR}_{\mathrm{G}}>\delta_{\mathrm{G}}]\log_2(1+\delta_{\mathrm{G}})$, respectively, and the area spectral efficiency is taken over the UAV-user and ground SBS-user links in the network. Thus, for the UAV and ground homogeneous network, the area spectral efficiency is defined as $\lambda_{\mathrm{U}}\mathscr{P}^{\mathrm{U}}_{\mathrm{SCD}}(\eta,b_k)\log_2(1+\delta_{\mathrm{U}})$ and $\lambda_{\mathrm{G}}\mathscr{P}^{\mathrm{G}}_{\mathrm{SCD}}(\eta,b_k)\log_2(1+\delta_{\mathrm{G}})$, respectively. Finally, the energy efficiency of the hybrid network is defined as [210]

$$\mathrm{EE} = \frac{\Big[\lambda_{\mathrm{U}}\mathscr{P}^{\mathrm{U}}_{\mathrm{SCD}}(\eta,b_k)+\lambda_{\mathrm{G}}\mathscr{P}^{\mathrm{G}}_{\mathrm{SCD}}(\eta,b_k)\Big]\log_2(1+\delta)}{\lambda_{\mathrm{U}}\big(P_{\mathrm{U}}+P_{\mathrm{hov}}\big)+\lambda_{\mathrm{G}}\big(P_{\mathrm{G}}+\triangle_{\mathrm{G}}P_{\mathrm{RF}}\big)}, \tag{5.43}$$

where δ is a prescribed QoS requirement, P_{hov} is the power consumption of multi-rotor UAV in hovering state and given as [211]

$$P_{\mathrm{hov}} = \sqrt{\frac{\big(m_{\mathrm{U}}g\big)^3}{2\pi R^2 N_p\rho}}, \tag{5.44}$$

and m_{U} being the mass of UAV in kg, g is referred as acceleration of gravity in m/s^2, R and N_p denote the propeller radius and number of propellers, respectively, ρ denotes the air density in kg/m^3. This chapter adapted the power consumption model for small-cell wireless networks in [212], where $\triangle_{\mathrm{G}}$ is the load-dependent power consumption slope of the ground SBS and P_{RF} being the RF output power of the ground SBS.

5.7 The Proposed Content Caching Scheme

This section proposes a caching scheme where UAVs and ground SBSs in small-cell networks cache the contents according to their popularity. In particular, contents are segregated into three groups according to their popularity measure, corresponding to a placement probability of 1 ($b_k = 1$) for the most popular content files, a placement probability between 0 and 1 ($0 < b_k < 1$) for the files with moderate popularity, and a placement probability of 0 ($b_k = 0$) for unpopular files that do not need to be cached in the small-cell network. Thus, contents have their own popularity. Moreover, it is assumed that the content request follows the Zipf distribution where the content request probability is modeled as [213]

$$m_k = \frac{k^{-\nu}}{\sum_{s=1}^{K} s^{-\nu}}, \qquad \nu \geq 0, \tag{5.45}$$

where ν is the Zipf parameter defines the popularity distribution. For instance, $\nu = 0$ means that the content popularity is uniform and the larger value of ν indicates that the majority of the content requests accounts for the fewer popular contents.

This chapter seek to improve the overall successful content delivery performance of the hybrid network by the proposed caching scheme. Firstly, it is assumed that the content placement is made on the basis of most popular content scheme which stores the popular content in UAVs and ground SBSs with $b_k = 1$. In this case, the entire caching capacity is designated to store only the popular content and hence, successful content

delivery probability of a hybrid network can be given as

$$\mathscr{P}_{\mathrm{SCD}}^{\mathrm{MPC}}(\eta) = \sum_{k=1}^{J} m_k \mathscr{P}_{\mathrm{Cov}}^{\mathrm{U}}(\eta, b_k = 1) + \sum_{k=1}^{J} m_k \mathscr{P}_{\mathrm{Cov}}^{\mathrm{G}}(\eta, b_k = 1), \tag{5.46}$$

where $\mathscr{P}_{\mathrm{Cov}}^{\mathrm{U}}$ and $\mathscr{P}_{\mathrm{Cov}}^{\mathrm{G}}$ are given in (5.30) and (5.38), respectively.

Secondly, the improved caching scheme is proposed where a fraction of SBS caching capacity J_o is assigned to cache the most popular content and hence called the most popular content portion. Thereafter, the contents with moderate popularity are stored in the remaining portion of the caching capacity which is termed as the content diversity (CD) portion. In the CD portion, the disparity of the cached content with less popularity measures represents the content diversity. To this end, the successful content delivery probability of the hybrid network can be given as

$$\begin{aligned}\mathscr{P}_{\mathrm{SCD}}^{\mathrm{Hybrid}}(\eta) = &\sum_{k=1}^{J_{\mathrm{o}}} m_k \mathscr{P}_{\mathrm{Cov}}^{\mathrm{U}}(\eta, b_k = 1) + \sum_{k=J_{\mathrm{o}}+1}^{J} m_k \mathscr{P}_{\mathrm{Cov}}^{\mathrm{U}}(\eta, b'_k) + \\ &\sum_{k=1}^{J_{\mathrm{o}}} m_k \mathscr{P}_{\mathrm{Cov}}^{\mathrm{G}}(\eta, b_k = 1) + \sum_{k=J_{\mathrm{o}}+1}^{J} m_k \mathscr{P}_{\mathrm{Cov}}^{\mathrm{G}}(\eta, b'_k).\end{aligned} \tag{5.47}$$

where J_o is defined as the caching capacity in UAVs and ground SBSs to increase the content diversity and hence, improve the overall successful content delivery probability for the hybrid networks. In (5.47), contents $\{1, \cdots, J_{\mathrm{o}}\}$ are in the most popular content portion of the UAV and ground SBS caches with the placement probability $b_k = 1$ and contents $\{J_o + 1, \cdots, J\}$ are in the CD portion with the placement probability $0 < b'_k < 1$.

5.8 Numerical Results and Discussion

This section presents and discusses the numerical results. The user association probability in (5.16) and (5.23), respectively, analyze the performance of the typical user associated with the UAV and SBS that has cached the desired contents. The successful content delivery probabilities in (5.30) and (5.38), respectively, characterize the downlink transmission performance of the contents cached in the UAV and SBS. The energy efficiency

in (5.43) evaluates the power consumption performance of a hybrid network while successfully transmitting the most popular contents to the typical user. Furthermore, the successful content delivery performance of the proposed caching scheme in (5.47) is examined and compared with the popular caching scheme in (5.46) to characterize the impact of different network parameters as design guidelines.

The simulation and analytical results are plotted by using MATLAB. In this case, the simulation results are obtained by using a Monte Carlo technique with 10^5 runs, where 'poissrnd' in MATLAB is used to generate random deployment points according to the Poisson distribution. Furthermore, 'quadgk' in MATLAB is used to compute numerical integration in analytical expressions. The system parameters are given in Table 5.2, unless otherwise specified. In Table 5.2, the values for the PLEs and the environment specific parameters are adopted from [19] and [168], respectively, while speed of light is a fundamental constant, and other values are set for illustration purpose only.

Table 5.2: System parameters.

Parameters	**Values**
Transmit power of each UAV (P_{U})	1 W
Transmit power of each ground SBS (P_{G})	1 W
noise power (σ^2)	-170 dBm
frequency (f) and speed of light (c)	2 GHz, 3×10^8 m/s
PLEs (α_{L}, α_{N}, α_{G})	2.1, 3.7, 3.7 [168]
Environment parameter (a, b)	5.0188, 0.3511 (Suburban) [100]
Density of hybrid network (λ_{S})	10^{-4} 1/m^2
Bit rate of each file (φ/τ)	100 kbps
Bandwidth ($\mathcal{W}_{\mathrm{U}}$, $\mathcal{W}_{\mathrm{G}}$)	200 kHz
Database size (K)	10^4
Cache capacity of SBS (J)	100 files

5.8.1 User Association Probability

Fig. 5.2 investigates the impact of the density control parameter η on the user association probability for the cache-enabled UAV and ground SBSs in suburban environment. In the density sharing scheme of the UAV and SBS deployment, as η increases, the density of UAVs increases due to the factor $\lambda_{\mathrm{U}} = \eta\lambda_{\mathrm{S}}$. As a result, the user association probability with tier U UAVs monotonically increases with η. On the other hand, the density of the ground SBSs decreases, therefore, user association probability monotonically decreases with increase of η.

In Fig. 5.3, the impact of UAV altitude on the association probability of UAVs is investigated at different values of η in suburban environment. One can notice that the maximum association probability is 0.98 for $\eta = 0.7$ at the altitude of 25.50 meters and is 0.93 for $\eta = 0.2$ at the altitude of 46 meters. Thus, there exist an optimal UAV altitude to achieve higher association probability which depends on η and can be computed by searching (5.16) numerically. Finally, simulation results are plotted with the markers and agree well with the analytical results of Lemma 1 and Lemma 2 plotted with the solid lines, which validates the analysis.

5.8.2 Successful Content Delivery Performance

Fig. 5.4 and Fig. 5.5 analyze the impact of the density factor and the UAV altitude, respectively, on the coverage probability. In both cases, the optimal density control factor and the optimal UAV altitude exists for the UAV network. From Fig. 5.4, it is observed that, an optimal density control parameter exists for an adequate deployment of UAVs in a suburban, which leads to maximize the coverage probability. Furthermore, it is observed that an optimal η is a function of the given UAV altitude, for instance, η is 0.2 and 0.1 for the UAV altitude of 30 and 60 meters to achieve the maximum coverage probability of 0.8 and 0.7, respectively. On the other hand, the coverage performance of the ground network degrades as η increases. However, no significant improvement in the coverage

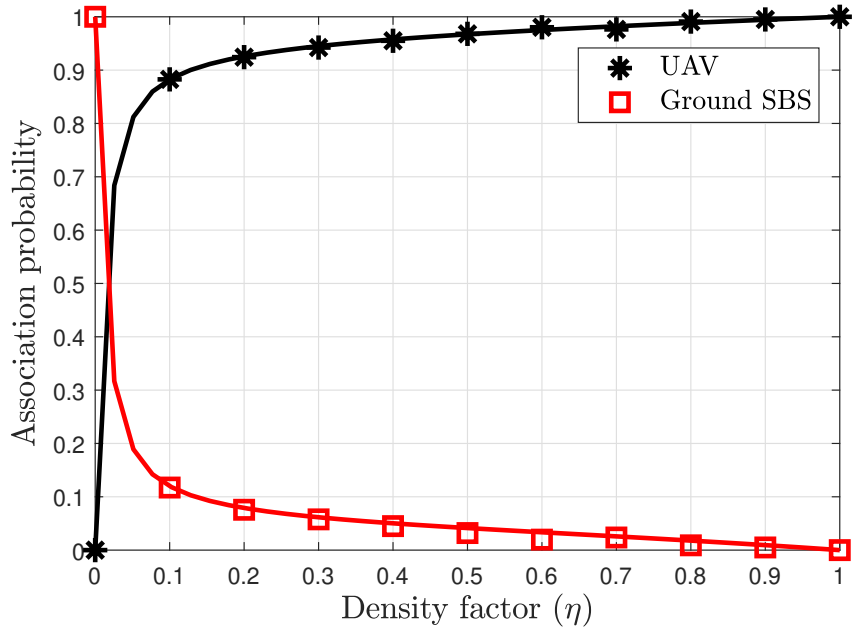

Figure 5.2: The impact of SBS density control parameter (η) on the user association probability for the UAV and the ground SBS in Suburban environment with $b_k = 1$.

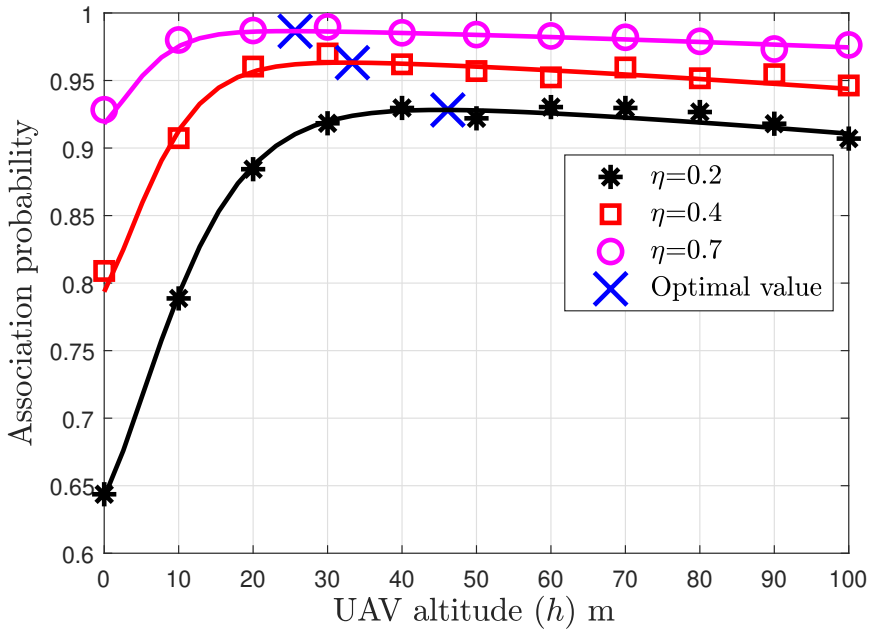

Figure 5.3: The impact of UAV altitude (h) on the user association probability for the UAVs with $b_k = 1$ and different η.

performance is observed for the SBS in the ground network.

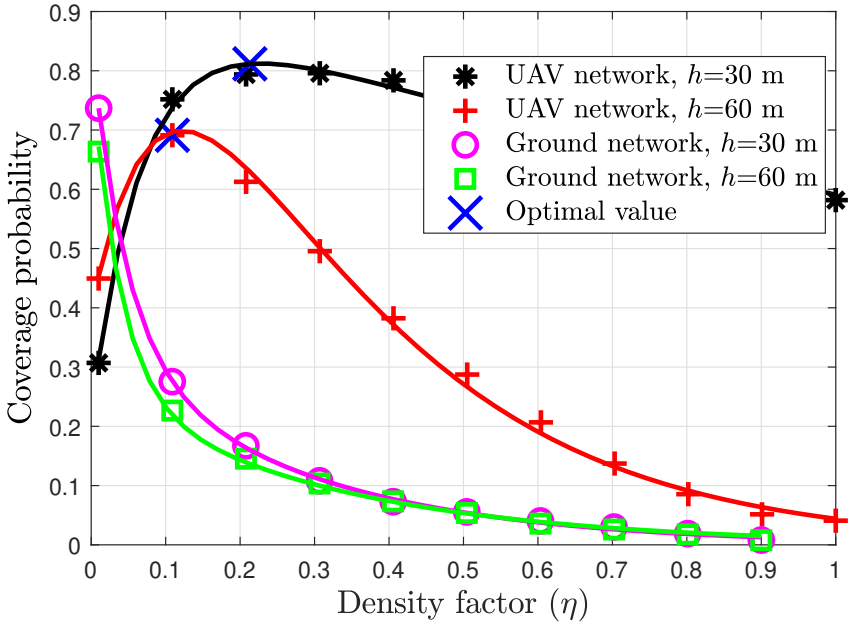

Figure 5.4: The impact of the density factor (η) on the coverage probability of the UAV and ground network for different altitudes.

For the given density control factor in Fig. 5.5, an optimal UAV altitude exists for suburban and urban environments. The higher optimal altitude is found in urban scenario experiencing more blockage. On the other hand, the UAVs should fly as low as possible in the suburban scenario where there are less blockages. In the suburban scenario, as η increases from 0.2 to 0.7, the number of UAVs increases, which increases the amount of co-channel interference generated by cache-enabled UAVs in a network. Therefore, the maximum coverage performance in the suburban scenario is achieved at the lower optimal altitudes and at the lesser density factor, for instance, h is 18, 22, and 28 meters for η of 0.2, 0.4, and 0.7 to achieve the coverage probability of 0.84. 0.82, and 0.8, respectively. Furthermore, the optimal altitude in urban environment is 63 meters for $\eta = 0.2$. In Fig. 5.4 and Fig. 5.5, the solid line represent the analytical results of Lemma 3 and Lemma 4 while the markers represent the simulation results.

Fig. 5.6 compares the successful content delivery performance for the networks

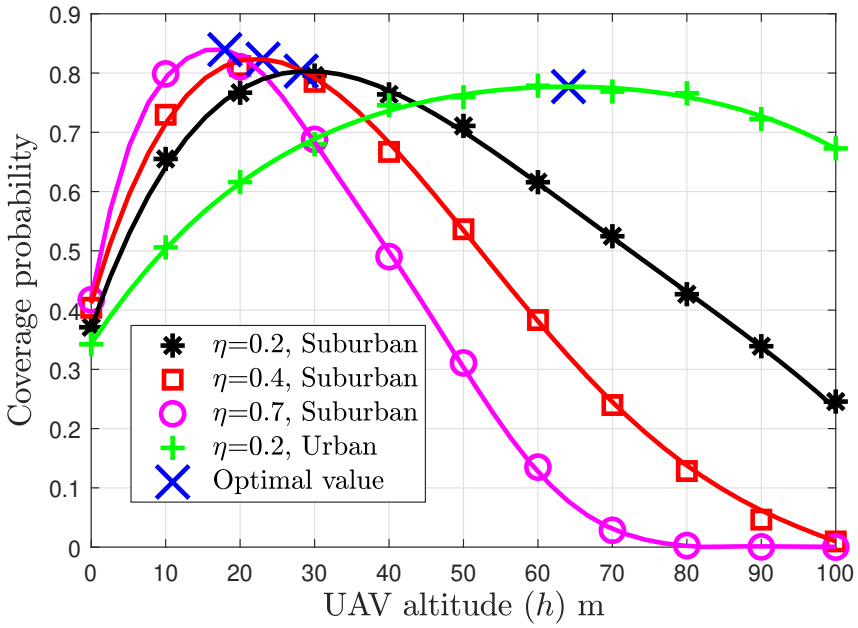

Figure 5.5: The impact of the UAV altitude (h) on the coverage probability of the UAV network for different density factor (η) in Suburban, and Urban ($a = 9.61$, $b = 0.16$) environments.

composed solely of UAV, ground SBS and hybrid network with different caching schemes. One can observe that the hybrid network operated with the proposed caching scheme outperform the popular caching scheme implemented for the UAV, ground and hybrid networks. This result is important which shows that the deployment of UAV and ground SBS alone does not meet the increasing content delivery demand in multi-tier heterogeneous network.

5.8.3 Energy Efficiency

Fig. 5.7 shows the comparison of the energy efficiency in the UAV, ground, and hybrid networks as a function of the density control factor with $\delta_{\mathrm{U}} = \delta_{\mathrm{G}} = \delta = 0$ dB. The parameters concerning the power consumption model of hovering UAV are adapted from [211] with $m_{\mathrm{U}} = 0.75$ Kg, $g = 9.8$ m/s^2, $R = 0.2$ m and $N_p = 4$ (quadcopter UAV), and $\rho = 1.225$ kg/m^3. Moreover, the parameters for the power consumption model of the ground SBS

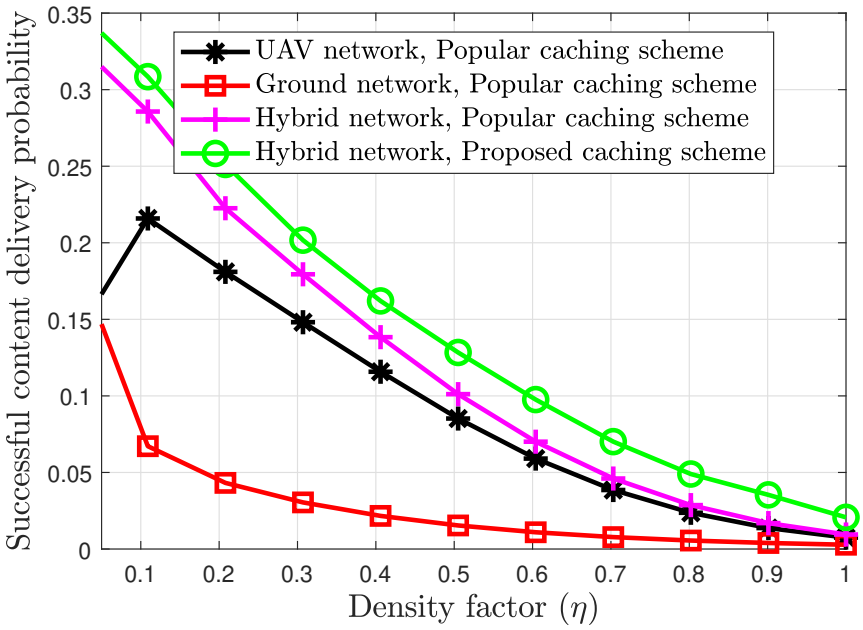

Figure 5.6: The impact of the density factor (η) on the successful content delivery probability of the UAV, ground and hybrid networks with J_o = 50 files, h = 60 meters, and v = 0.8 for different caching schemes.

are used for the femto-cell in [212] with P_{G} = 4.8 W, $\triangle_{\mathrm{G}}$ = 8.0, and P_{RF} = 0.05 W. The energy efficiency of the UAV network is worst due to its higher power expenditure to maintain hovering state of UAV, for example, with the given parameters, P_{hov} = 8.97 W for a single UAV. Thus, as density control factor increases, the overall energy consumption of the UAV network increases and hence, energy efficiency of the UAV network decreases. From Fig. 5.7, one can see that the energy efficiency of the ground network is better for femto-cell BS when compared to the UAV network, the reason for this behavior is that the RF power of ground SBSs is smaller than the hovering power of UAVs. Finally, it can be seen that expectedly, energy efficiency of the hybrid network is better than the UAV and ground networks, but beyond η = 0.5, the energy efficiency of the hybrid network is comparable with the ground network.

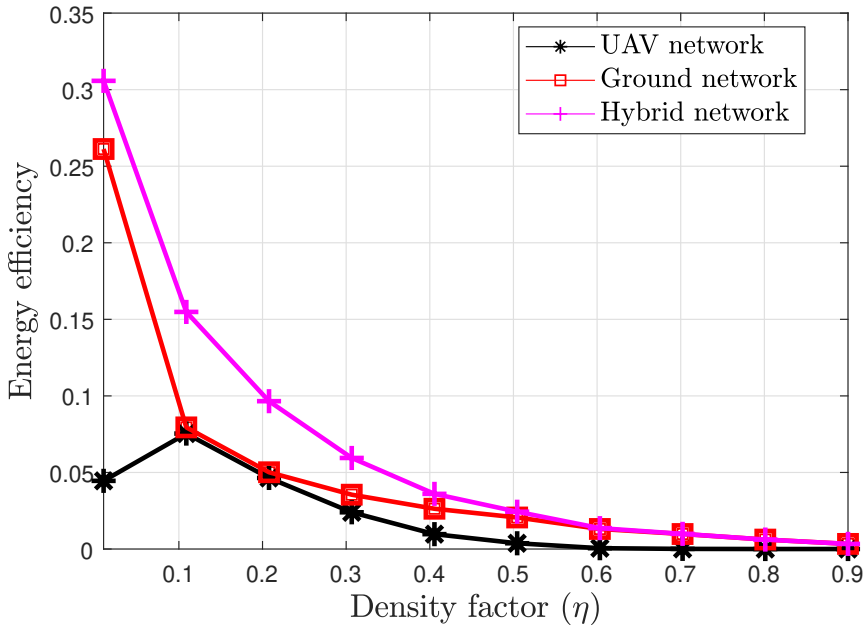

Figure 5.7: The impact of the density factor (η) on the energy efficiency of the UAV, ground and hybrid networks with $J = 100$ files, $h = 60$ meters, and $\upsilon = 0.8$.

5.8.4 Performance of the Proposed Caching Scheme

Fig. 5.8 - Fig. 5.11 illustrate the impact of caching size of each SBSs, Zipf parameter, UAVs altitude, and target data rate of content transmission, respectively, on the successful content delivery performance of the popular caching scheme [195–198] and the proposed caching schemes in a hybrid network for different content size in the database. The proposed caching scheme allow the caching of two types of files. First, the most popular files in the most popular content portion of the UAV and ground SBS with caching probability b_k. Second, the next most popular files with caching probability b'_k in the CD portion[4]. This work considers $J_o = 50$ files for an illustrative purpose only. This design parameter can be controlled by the network designer according to the need to cache the most popular files and the available caching capacity J in SBSs.

[4]Mostly, the beginning one minute of a YouTube video is much more popular than the remainder [194]. Therefore, in this work, such most popular contents are cached with $b_k = 1$ and remainder with $b'_k = 0.7$ (illustrative example to show that the average content popularity is 70 %).

In Fig. 5.8, it is observed that the proposed caching scheme performs better with an improvement of 26.6 % on average in comparison with the popular caching scheme which ignores the content diversity. When the content popularity is not uniform it is imperative to consider the content diversity in the probabilistic caching scheme to improve the the content delivery performance. In addition, more different file can be cached at UAVs and SBSs with the higher content diversity. In general, as the content size in the database decreases, the probability of the successful content delivery increases with the same performance gap.

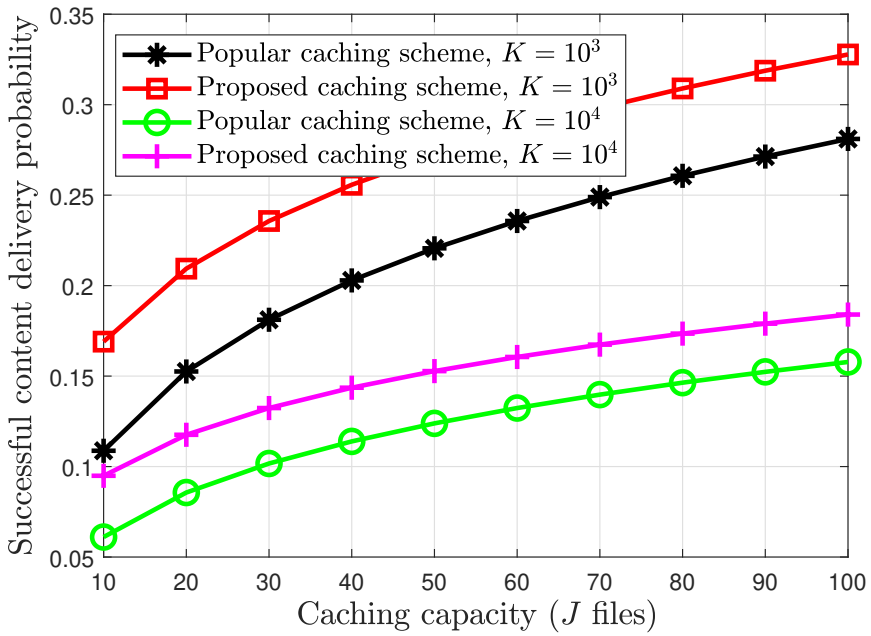

Figure 5.8: The impact of the caching capacity on the successful content delivery probability with $J_o = 50$ files, $\eta = 0.7$, $h = 60$ meters, and $\upsilon = 0.8$ for different caching schemes.

In Fig. 5.9, the successful content delivery performance depends on the skewness of the content popularity distribution defined by υ. However, for the highly skewed popular content e.g $\upsilon > 1.6$, the proposed scheme performs as well as popular content placement scheme. The reason for this behavior is that very few popular contents are requested by the majority of users and the optimal probabilistic caching scheme tends to store those contents.

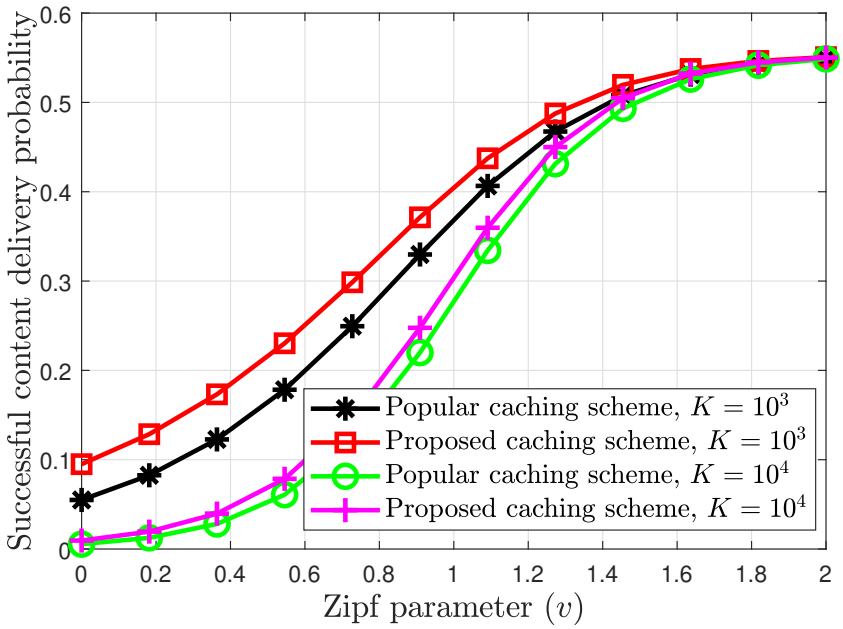

Figure 5.9: The impact of popularity skewness of contents on the successful content delivery probability for η = 0.7, h = 60 meters, and J_o = 50 files with different caching schemes.

In Fig. 5.10, one can see the existence of the optimal UAV altitude due to the trade-off by the altitude on the successful content delivery performance. When the LOS probability increases, for example, from 10 to 15 meters, the content delivery performance improves due to lesser shadowing. However, beyond 15 meters, the adverse effect on performance occurs due to the greater link distance between UAV and the ground user which corresponds to higher path loss. In Fig. 5.11, it is observed that the content delivery probability increases as the target data rate reduces due to the decrease of the SINR threshold and thus, decreases the QoS of the typical user.

5.9 Conclusion

This chapter derived the user association probability and the successful content delivery probability by using tools of stochastic geometry. The successful content delivery performance of the popular and the proposed caching schemes is compared in the con-

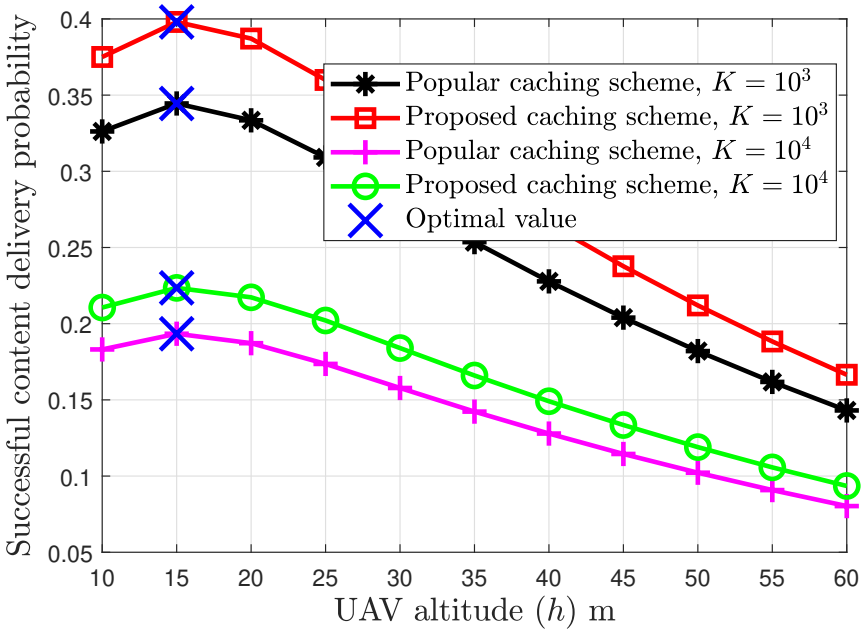

Figure 5.10: The impact of the UAV altitude on the successful content delivery probability for $\eta = 0.7$, $h = 60$ meters, $\nu = 0.8$, and $J_o = 50$ files with different caching schemes.

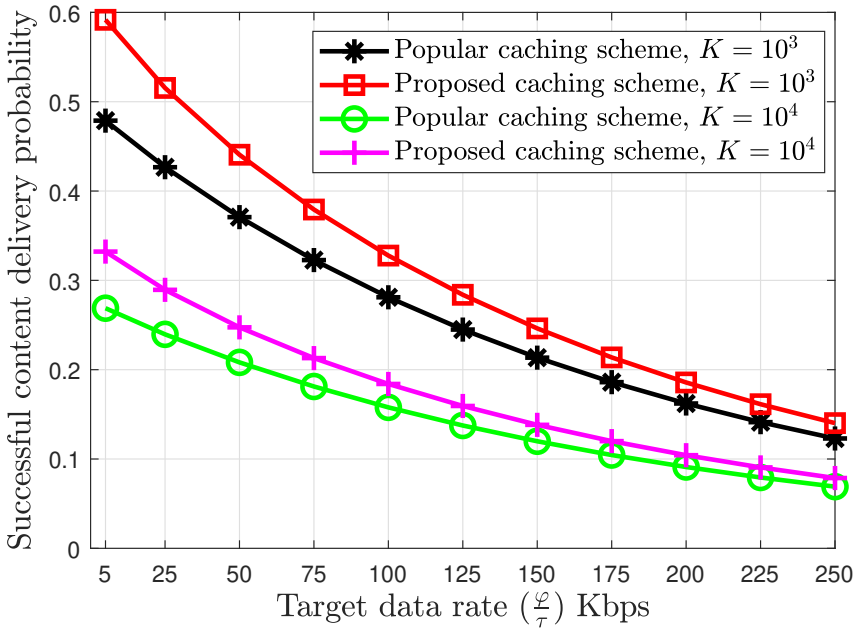

Figure 5.11: The impact of target data rate of the link on the successful content delivery probability for $\eta = 0.7$, $h = 60$ meters, $\nu = 0.8$, and $J_o = 50$ files with different caching schemes.

sidered hybrid cache-enabled network. Thus, found that the successful content delivery performance is improved by 26.6 % on average with the proposed hybrid caching scheme which considers the content diversity. Also, the performance is dependent on the caching capacity of SBSs, popularity distribution of the content, UAV altitude, and target data rate of the link. Furthermore, the cache-enabled hybrid network is more energy efficient as compared to the separate UAV and ground networks while caching the same contents. Future extension of this work includes the study of the cooperative caching scheme in a hybrid network where participating UAVs and ground SBSs cache different contents.

Chapter 6

Conclusions and Future of UAV Communications

6.1 Summary

The main body of the work presented in this thesis are summarized as follows:

- **Chapter 1** discussed the potential benefits and applications of UAVs for enabling wireless communication. Moreover, types of UAVs were categorized based on their operational altitudes, and structural design. This chapter highlighted the basic requirements of UAV communications and categorized the communication types as payload and non-payload communications. Then, frameworks of UAV-assisted communication and cellular-controlled UAV networks were presented along with their applications. Finally, some of the major design challenges of UAV communication were thoroughly investigated and accordingly presented as research motivation of this thesis.

- **Chapter 2** provided an extensive review of the measurement methods proposed for UAV channel modeling that use LAPs and discussed various channel characterization efforts. Also, this chapter reviewed UAV channel modeling approaches

from a contemporary perspective, and categorized these as deterministic, stochastic and geometric-stochastic models. Finally, the future research challenges were outlined for developing accurate and realistic UAV channel models.

- **Chapter 3** studied a coordinated deployment strategy of multiple UAVs in two scenarios. In the first scenario, symmetric placement of UAVs was assumed at a common optimal altitude and transmit power. In the second scenario, asymmetric deployment of UAVs with different altitudes and transmit powers was assumed. Then, the coverage area performance was investigated as a function of separation distance between UAVs which were deployed in a certain geographical area to satisfy a target SINR threshold at the cell boundary. Finally, the system-level performance of a boundary user was studied in terms of the coverage probability. Numerical results unveiled that the SINR threshold, the separation distance, and the number of UAVs and their formations should be carefully selected to achieve the maximum coverage area inside and to reduce unnecessary expansion outside the target area. Thus, this chapter provided important design guidelines for the deployment of multiple UAVs in presence of downlink co-channel interference.

- **Chapter 4** analytically characterized the impact of ground user mobility, propagation environment and channel fading on the performance of uplink UAV communications. Closed-form expressions for the outage probability and the average BER using the RWP model for ground user mobility, UAV channel models for different propagation environments and the Nakagami-m model for fading channel were derived. Furthermore, the outage analysis took into account both static and mobile interfering users by employing the Gamma approximation. Numerical results were presented to demonstrate the interplay between the communication performance and the system parameters.

- **Chapter 5** developed the analytical framework of the hybrid caching network comprising UAVs and SBSs, where UAVs were preferred because of their flexible deploy-

ment and elevated platform which offered better downlink propagation with LOS conditions. First, the association probability for the ground user affiliated with a UAV and ground SBS was derived. Then the successful content delivery probability is derived by considering both the downlink inter-cell and intra-cell interferences. Then the energy efficiency was analyzed for the hybrid network and compared with the separate UAV and ground networks. Furthermore, this chapter proposed a caching scheme to improve the successful content delivery performance by managing the content popularity, where part of the caching capacity in each UAV and ground SBS is reserved to store the most popular content, while the remaining portion stores the less popular contents. Numerical results unveiled that the proposed caching scheme performs better with an improvement of 26.6 % in comparison with the most popular content caching scheme which overlooks the impact of content diversity during caching.

6.2 Future Works and Challenges

During study, interesting problems have been figured out that need to be addressed for better insight of the integration of UAVs into existing communication networks. Some of the open problems have been pointed out as follows:

- **Channel Modeling**: A proper understanding of UAV channel models is imperative for the widespread applicability of UAVs in different propagation scenarios. Therefore, adequate measurement campaigns are required for the validation of UAV channel models. In addition to the research papers published on UAV channel modeling, the 3GPP gathered the key stakeholders from industries to launch the systematic measurement campaigns for accurate channel modeling. However, most of these efforts are limited to a single UAV in a very specific environment. In this regard, broader channel measurement campaigns are needed that can cut across rural and urban environments, as well as different operational en-

vironments, such as different weather conditions. In addition, the use of UAVs at lower altitudes is of high importance when UAV act as BSs, UEs, and relays, thus, one must have more insight related to both the air-to-ground and air-to-air channel modeling. Particularly, UAV channel models must capture the time-varying effects of airframe shadowing and Doppler spread due to the mobility of UAVs.

- **Regulations and Standardization**: Regulations for aeronautical communications are explicitly and clearly defined for manned aircraft traveling at thousands of meters above ground level. However, these rules and regulations are not well matured for UAVs that fly at lower altitudes. Recent efforts related to UAV regulations are restricted to specifying the UAV operational altitude for hobbyist and commercial use, and not for providing on-demand wireless communication services. It is also important to frame regulations to allow UAVs to fly above private properties or no-fly zones, such as airports and to keep safe distance from people. Furthermore, regulations should be placed to guarantee safe and reliable flight operation during the night time. Also, wireless access standard has not yet been introduced for UAV communications or FANETs as it has been well defined for vehicular communication systems or vehicular ad hoc networks (VANETs) in the form of IEEE 802.11p.

- **UAV Battery Lifetime**: Another unique challenge of UAV communications is the low battery lifetime of UAV nodes. Most of the UAV energy is consumed on its flight operation and less energy is needed for communication purposes. Thus, limited battery lifetime is a major hurdle that curtail the UAV endurance (flight time) and designing the UAV trajectory.

- **UAV Deployment**: New solutions are needed for the optimal 3D deployment of UAVs while taking into account their unique attributes. For example, one key research challenge is the optimal 3D deployment of UAVs in the presence of terrestrial networks in urban areas. In this case, there is a need to study the impact of co-channel interference from the cellular networks while keeping the safe distance

from the buildings and other ground obstacles. UAV deployment will be further aggravated when multiple UAVs are operating in the same area. Other major deployment problem includes, the joint optimization of bandwidth allocation and 3D deployment of UAV for low latency communication, and joint optimization of 3D deployment and cell association for minimizing flight time.

- **Performance Analysis**: The fundamental analysis is intended to capture the spatial and temporal variations on the received signal, and determine its impact on various performance metrics. A number of open research problems are related to the performance analysis of UAV networks that still need to be studied. For example, one must completely characterize the performance of different digital modulation schemes in UAV-enabled wireless networks, that comprises of both aerial and terrestrial UEs and BSs, in terms of capacity, coverage, and error performances. Specifically, there is a need for tractable analysis for coverage probability and spectral efficiency in hybrid UAV-terrestrial communication networks. Moreover, fundamental performance analysis needs to be performed to understand the intrinsic trade-offs between the spectral efficiency and energy efficiency in the UAV-enabled networks. Another important problem is to analyze the performance of UAV networks where both the UAV and ground users are mobile.

- **UAV Trajectory Optimization**: Optimal trajectory design for mobile UAV is an important issue in UAV communications. Specifically, optimal path planning is crucial for UAVs operating for data collection from ground-based sensors and caching scenarios. UAV trajectory planning is mostly dependent on the dimension of the target area, flight duration of mission, QoS requirement by the ground users, energy constraints, and resource allocation. Apart from physical parameters, UAV trajectory optimization is analytically a challenging problem because it involves a fixed number of optimization variables related to the UAV locations. In addition, the UAV trajectory optimization requires coupling between different QoS metrics

in wireless communication with the mobility of UAV. Recently, there has been number of studies on the joint trajectory optimization of UAV with its wireless communication metrics such as, throughput maximization in [214–216], and energy-efficient UAV communication in [217, 218].

6.3 Future Applications of UAV Communication

6.3.1 Defending 5G Networks using UAVs

Security encompasses a number of qualities that are necessary for any communications system to protect user identity, the information and services from being adversely manipulated, misused, or blocked. In general, wireless communications are more susceptible to security threats because the information is being broadcast over the air and may not be completely shielded. In particular, the 5G networks are extensive, customizable, and mostly software-defined. Consequently, their attack surface is much wider than 4G networks and they could impose larger and severe danger if breached. Also, 5G networks are more appealing to attack since they support critical applications in healthcare management, safety, and autonomous driving. Thus, it is important to defend 5G networks to reduce their threats to the public. Despite dedicated research efforts to safeguard 5G networks, security deficiencies also evolve as attackers can device new and innovative strategies to gain illegitimate access to 5G operations. Some of the popular attack types to cellular networks are eavesdropping, jamming, and spoofing. These attacks can be more lethal in 5G-enabled UAV communications, because compared to terrestrial radio channels that mostly experience severe path-loss, shadowing, and multipath fading, air-to-ground channels generally encounter dominant LOS between high-altitude UAVs and the ground devices, which can be exploited by eavesdroppers and jammers as shown in Fig. 6.1. Thus, UAVs can be envisioned to use in the defender role to protect 5G networks. Most existing approaches nationally and internationally adopt ground-based solutions. However, aerial platforms, such as UAVs, allow better channel conditions and agile de-

ployment and thus, they have great advantages over ground-based solutions. Specifically, this section proposes following solutions:

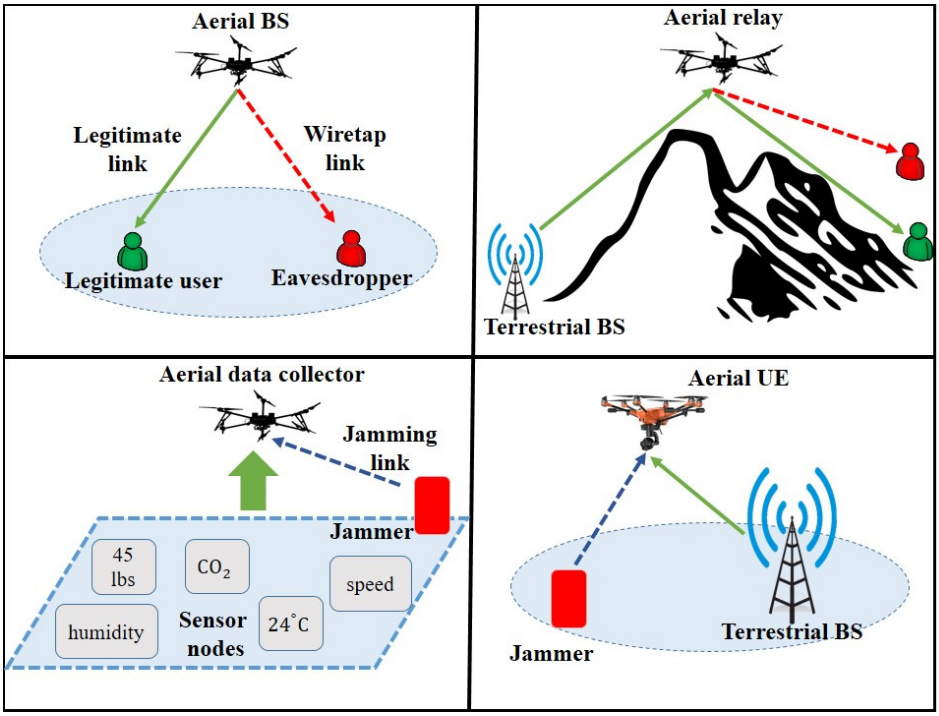

Figure 6.1: Security threats to the UAV-enabled 5G networks.

- **UAV-Assisted 3D Beam-forming**: The proposed countermeasure scheme to prevent terrestrial eavesdropping is depicted in Fig. 6.2. In this scheme, UAV-enabled 3D beam-forming technique will be used to adjust the beam pattern in azimuth and elevation planes to achieve significant improvement in the SINR at the receiver side. Also, 3D beam-forming will be jointly employed with artificial noise transmitted from UAV to deliberately impair the channels of terrestrial eavesdropper for 5G security provisioning. In this scheme, the UAV-enabled 3D beam-forming solution is preferred over the terrestrial 2D beam-forming because the UAVs can exploit the elevation angle separation to differentiate the legitimate user and eavesdropper located apart on the same horizontal plane. For example, as shown in Fig. 6.3, when both the legitimate user and the eavesdropper are located in the same

direction with different horizontal distances, any attempt to jam the eavesdropper by transmitting artificial noise from the terrestrial BS will also nullify the signal reception at the legitimate user. Another reason to prefer UAV-enabled 3D beamforming solution is to leverage the UAV mobility to get closer to the legitimate user and then use high-resolution information beams to transmit confidential information via joint optimization of UAV positioning, resource allocation, and 3D beamforming.

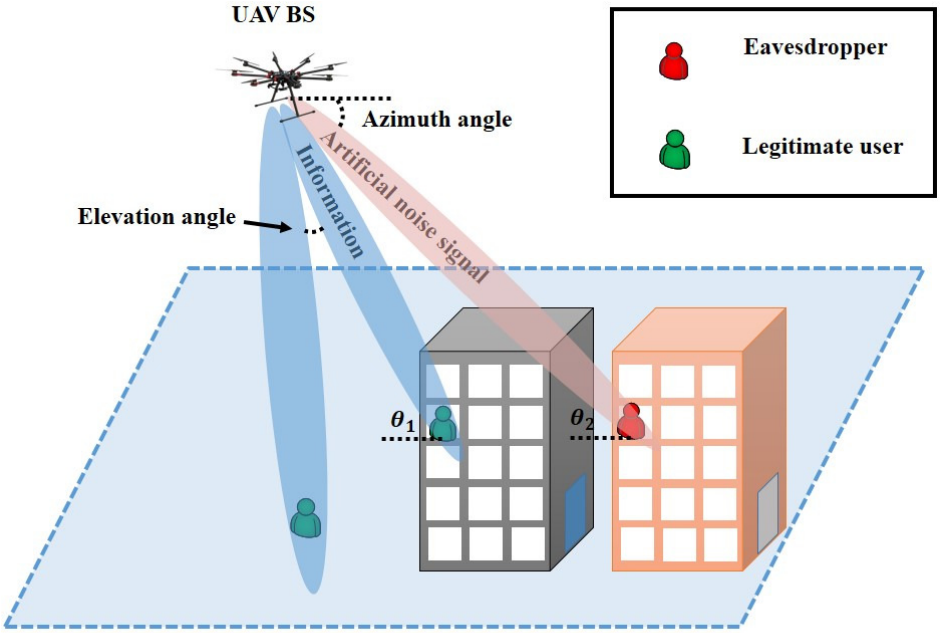

Figure 6.2: UAV-assisted 3D beam-forming to prevent eavesdropping attacks.

- **UAV-Assisted Cooperative Multipoint (CoMP) Transmission**: The proposed countermeasure scheme to prevent terrestrial jamming is depicted in Fig. 6.4. This scheme will use cooperative multipoint (CoMP) transmission in the form of 3D beam-forming with multiple UAVs. In jamming attacks, the terrestrial adversary nodes send artificial noise to interfere with aerial UE and hence reduce its SINR for decoding. The proposed scheme will jointly optimize positioning of multiple

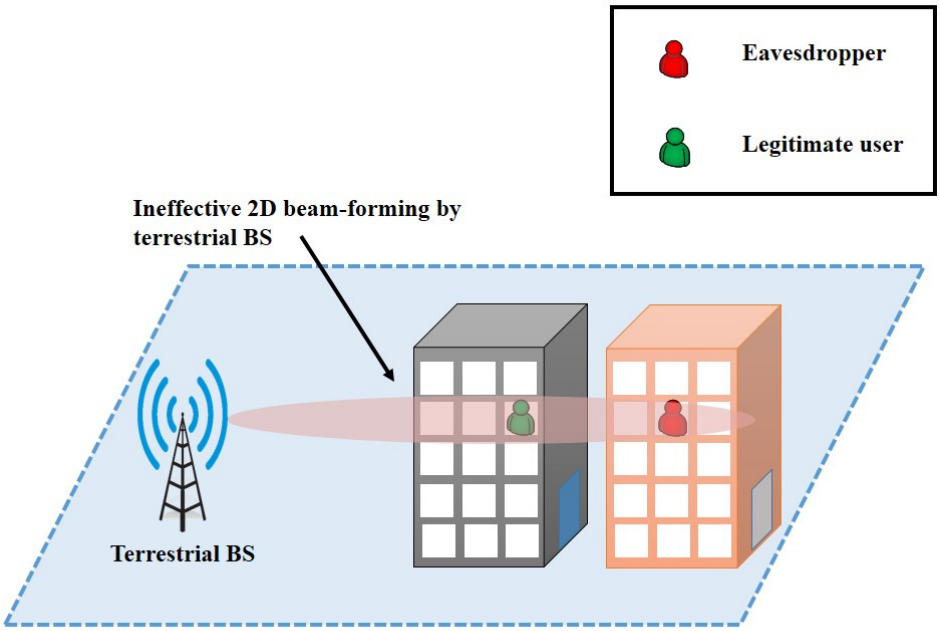

Figure 6.3: Ineffective 2D Beam-forming with terrestrial network.

UAVs, where some UAVs transmit high-resolution beams to significantly improve SINR of legitimate links while others transmit artificial noise to jam eavesdropper.

- **UAV-Assisted Reconfigurable Intelligent Surface (RIS)**: The proposed alternative countermeasure scheme to prevent terrestrial eavesdropping is depicted in Fig. 6.5. This scheme will use a reconfigurable intelligent surface (RIS), a recent advance in wireless communications for 'smart' channels, to enhance physical-layer security. The proposed scheme comprises of UAV-mounted RIS, terrestrial BS, legitimate user, and eavesdropper. A RIS is a meta-surface that contains the low-power-consuming and electronically-controllable analog processing elements. Using a RIS, the phase of the reflected signals can be adjusted in real-time to maximize the effective channel gain. Recently, RISs have received extensive attention to ameliorate wireless propagation conditions and enhance communication qual-

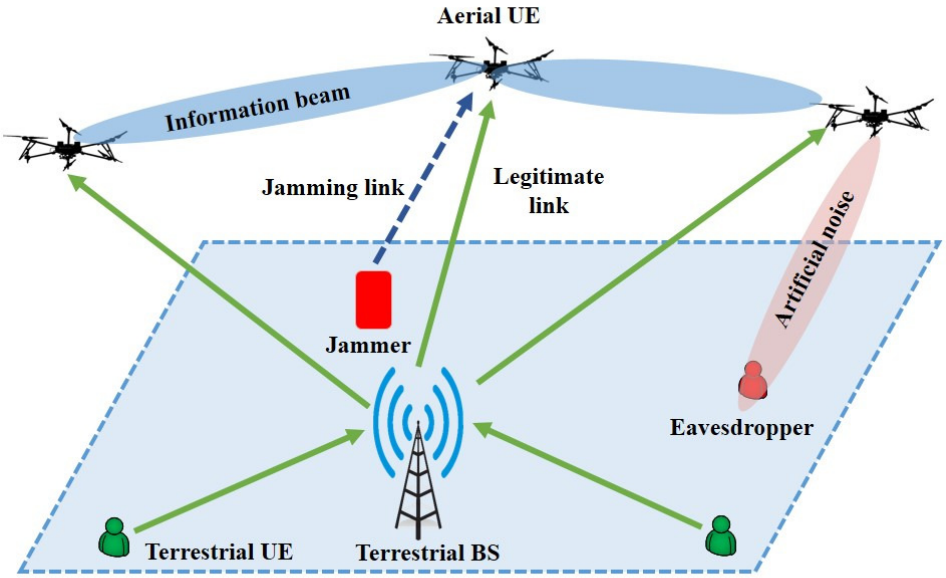

Figure 6.4: UAV-assisted CoMP network to prevent jamming and eavesdropping attacks.

ity. For instance, in [219], the authors presented the applications, challenges, and opportunities of the UAV-mounted RIS. However, this work is limited to conceptual framework and no performance analysis was provided. In [220], the authors jointly designed UAV position and passive beam-forming using RIS. However, the RIS was not mounted on UAV and instead it was located on buildings. In particular, the proposed countermeasure technique will examine joint optimization of the phase-shifter at the UAV-assisted RIS, and the beam-forming and artificial noise covariance matrix at the terrestrial BS. This strategy will significantly increase the system sum-rate by constructively adding the reflected in-phase signals.

6.3.2 UAV-Enabled 5G Radio Sensing

The 5G signals have unique merits such as, high carrier frequency with large channel bandwidth, and unprecedented number of antennas due to massive MIMO technology.

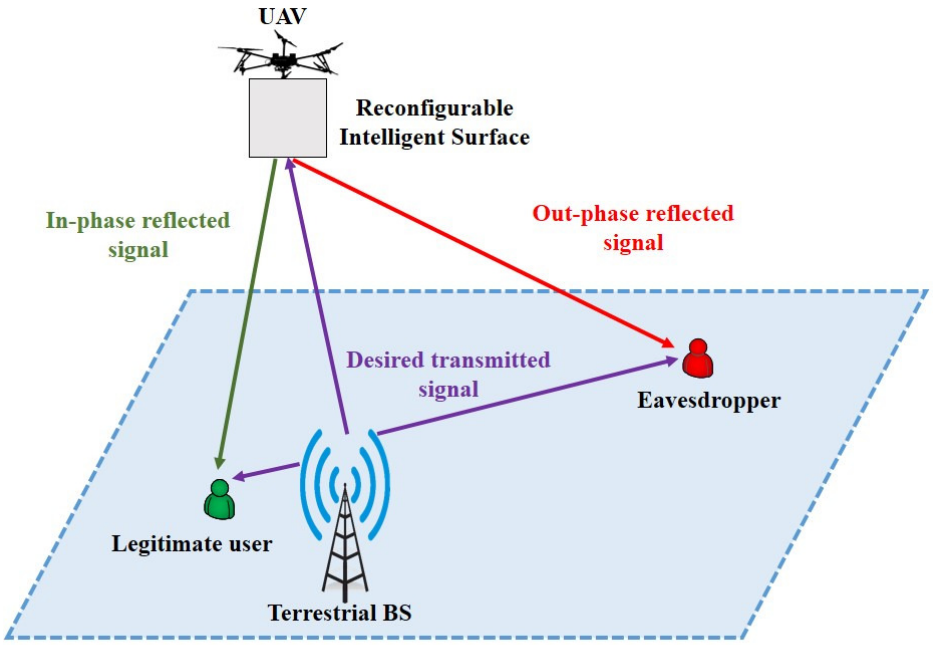

Figure 6.5: UAV-assisted reconfigurable intelligent surface (RIS) technique to prevent eavesdropping.

Therefore, many studies [221–225] have shown the ability of using 5G signals to sense the ambient environment and thereby realize a set of emerging applications, such as object imaging in [221], post-surgical fall detection in [222], walking speed recognition in [223], vital sign monitoring in [224], and vehicular tracking in [225]. However, there are not many studies available nationally and internationally to use UAV-enabled 5G radio sensing technique. Some of the UAV-enabled 5G radio sensing applications include, monitoring and surveillance for real-time traffic management, search for survivors trapped beneath the collapsed buildings or rubble during natural disasters, and material inspection of hard-to-reach assets and critical infrastructure.

References

[1] *DJI-Spreading Wings S1000*. https://www.dji.com/spreading-wings-s1000/spec. Launched: February 2014.

[2] *Yuneec-H520E/520*. https://america.yuneec.com/h520-series/info. Launched: November 2020.

[3] *Parrot Disco*. https://dronerush.com/product/parrot-disco/. Launched: October 2016.

[4] *General Atomics MQ-9 Reaper*. https://www.ga-asi.com/remotely-piloted-aircraft/mq-9a. Launched: 2001.

[5] *Characteristics of Unmanned Aircraft Systems and Spectrum Requirements to Support Their Safe Operation in Non-Segregated Airspace*. document M.2171. International Telecommunication Union, 2009.

[6] *Technical Specification Group Radio Access Network: Study on enhanced LTE Support for Aerial Vehicles*. document 3GPP TR 36.777 V15.0.0. 3rd Generation Partnership Project, Dec. 2017.

[7] *Ericsson and China Mobile conduct world's first 5G drone prototype field trial*. https://www.ericsson.hr/en/20160906-5g-drone. 2016.

[8] *LTE unmanned aircraft systems*. Tech. Rep. Qualcomm Technologies, Inc., May 2017.

[9] *Propagation data and prediction methods for the design of terrestrial broadband millimetric radio access systems*. P.1410-2, P Series, Radiowave Propagation. International Telecommunication Union, 2003.

[10] S. Karapantazis and F. Pavlidou. “Broadband communications via high-altitude platforms: A survey”. In: *IEEE Communications Surveys & Tutorials* 7.1 (2005), pp. 2–31.

[11] L. Gupta, R. Jain, and G. Vaszkun. “Survey of Important Issues in UAV Communication Networks”. In: *IEEE Communications Surveys & Tutorials* 18.2 (2016), pp. 1123–1152.

[12] Ilker Bekmezci, Ozgur Koray Sahingoz, and Şamil Temel. “Flying ad-hoc networks (FANETs): A survey”. In: *Ad Hoc Networks* 11.3 (2013), pp. 1254–1270.

[13] S. Hayat, E. Yanmaz, and R. Muzaffar. “Survey on Unmanned Aerial Vehicle Networks for Civil Applications: A Communications Viewpoint”. In: *IEEE Communications Surveys & Tutorials* 18.4 (2016), pp. 2624–2661.

[14] N. Hossein Motlagh, T. Taleb, and O. Arouk. “Low-Altitude Unmanned Aerial Vehicles-Based Internet of Things Services: Comprehensive Survey and Future Perspectives”. In: *IEEE Internet of Things Journal* 3.6 (2016), pp. 899–922.

[15] B. Li, Z. Fei, and Y. Zhang. “UAV Communications for 5G and Beyond: Recent Advances and Future Trends”. In: *IEEE Internet of Things Journal* 6.2 (2019), pp. 2241–2263.

[16] H. Shakhatreh et al. “Unmanned Aerial Vehicles (UAVs): A Survey on Civil Applications and Key Research Challenges”. In: *IEEE Access* 7 (2019), pp. 48572–48634.

[17] A. Fotouhi et al. “Survey on UAV Cellular Communications: Practical Aspects, Standardization Advancements, Regulation, and Security Challenges”. In: *IEEE Communications Surveys & Tutorials* 21.4 (2019), pp. 3417–3442.

[18] H. Wang et al. “Survey on Unmanned Aerial Vehicle Networks: A Cyber Physical System Perspective”. In: *IEEE Communications Surveys & Tutorials* 22.2 (2020), pp. 1027–1070.

[19] A. Al-Hourani, S. Kandeepan, and S. Lardner. “Optimal LAP Altitude for Maximum Coverage”. In: *IEEE Wireless Communications Letters* 3.6 (2014), pp. 569–572.

[20] M. Mozaffari et al. “Drone Small Cells in the Clouds: Design, Deployment and Performance Analysis”. In: *2015 IEEE Global Communications Conference (GLOBECOM)*. 2015, pp. 1–6.

[21] E. Kalantari, H. Yanikomeroglu, and A. Yongacoglu. “On the Number and 3D Placement of Drone Base Stations in Wireless Cellular Networks”. In: *2016 IEEE 84th Vehicular Technology Conference (VTC-Fall)*. 2016, pp. 1–6.

[22] I. Bor-Yaliniz and H. Yanikomeroglu. “The New Frontier in RAN Heterogeneity: Multi-Tier Drone-Cells”. In: *IEEE Communications Magazine* 54.11 (2016), pp. 48–55.

[23] A. M. Hayajneh et al. “Drone Empowered Small Cellular Disaster Recovery Networks for Resilient Smart Cities”. In: *2016 IEEE International Conference on Sensing, Communication and Networking (SECON Workshops)*. 2016, pp. 1–6.

[24] J. Košmerl and A. Vilhar. “Base stations placement optimization in wireless networks for emergency communications”. In: *2014 IEEE International Conference on Communications Workshops (ICC)*. 2014, pp. 200–205.

[25] M. Mozaffari et al. “Unmanned Aerial Vehicle With Underlaid Device-to-Device Communications: Performance and Tradeoffs”. In: *IEEE Transactions on Wireless Communications* 15.6 (2016), pp. 3949–3963.

[26] M. M. Azari et al. “Ultra Reliable UAV Communication Using Altitude and Cooperation Diversity”. In: *IEEE Transactions on Communications* 66.1 (2018), pp. 330–344.

[27] P. K. Sharma and D. I. Kim. “Random 3D Mobile UAV Networks: Mobility Modeling and Coverage Probability”. In: *IEEE Transactions on Wireless Communications* 18.5 (2019), pp. 2527–2538.

[28] Y. Qin, M. A. Kishk, and M. -S. Alouini. “Performance Evaluation of UAV-Enabled Cellular Networks With Battery-Limited Drones”. In: *IEEE Communications Letters* 24.12 (2020), pp. 2664–2668.

[29] V. A. Aalo, C. Mukasa, and G. P. Efthymoglou. “Effect of Mobility on the Outage and BER Performances of Digital Transmissions over Nakagami-m Fading Channels”. In: *IEEE Transactions on Vehicular Technology* 65.4 (2016), pp. 2715–2721.

[30] V. A. Aalo, P. S. Bithas, and G. P. Efthymoglou. “On the Impact of User Mobility on the Performance of Wireless Receivers”. In: *IEEE Access* 8 (2020), pp. 197300–197311.

[31] A. Gupta and P. Garg. “Statistics of SNR for an Indoor VLC System and Its Applications in System Performance”. In: *IEEE Communications Letters* 22.9 (2018), pp. 1898–1901.

[32] M. A. Arfaoui et al. “Measurements-Based Channel Models for Indoor LiFi Systems”. In: *IEEE Transactions on Wireless Communications* 20.2 (2021), pp. 827–842.

[33] N. Zhao et al. “Caching Unmanned Aerial Vehicle-Enabled Small-Cell Networks: Employing Energy-Efficient Methods That Store and Retrieve Popular Content”. In: *IEEE Vehicular Technology Magazine* 14.1 (2019), pp. 71–79.

[34] T. Zhang et al. “Cache-Enabling UAV Communications: Network Deployment and Resource Allocation”. In: *IEEE Transactions on Wireless Communications* 19.11 (2020), pp. 7470–7483.

[35] *Minimum Operational Performance Standards for Unmanned Aircraft Systems*. SC-228. Radio Technical Commission for Aeronautics (RTCA), May 2013.

[36] Hoot Gibson. *Overview of Drone Advisory Committee (DAC) Objectives*. https://www.rtca.org/drone-advisory-committee/. Sept. 2016.

[37] *UAS Traffic Management (UTM) Project*. https://www.nasa.gov/utm. Jan. 2020.

[38] A. D. Panagopoulos, P. M. Arapoglou, and P. G. Cottis. "Satellite communications at KU, KA, and V bands: Propagation impairments and mitigation techniques". In: *IEEE Communications Surveys & Tutorials* 6.3 (2004), pp. 2–14.

[39] Paolo Chini, Giovanni Giambene, and Sastri Kota. "A survey on mobile satellite systems". In: *International Journal of Satellite Communications and Networking* 28.1 (2010), pp. 29–57.

[40] K. Daniel et al. "Three dimensional channel characterization for low altitude aerial vehicles". In: *2010 7th International Symposium on Wireless Communication Systems*. 2010, pp. 756–760.

[41] Qixing Feng et al. "Path Loss Models for Air-to-Ground Radio Channels in Urban Environments". In: *2006 IEEE 63rd Vehicular Technology Conference*. Vol. 6. 2006, pp. 2901–2905.

[42] Q. Feng et al. "Modelling the Likelihood of Line-of-Sight for Air-to-Ground Radio Propagation in Urban Environments". In: *IEEE Globecom 2006*. 2006, pp. 1–5.

[43] A. Al-Hourani, S. Kandeepan, and A. Jamalipour. "Modeling air-to-ground path loss for low altitude platforms in urban environments". In: *2014 IEEE Global Communications Conference*. 2014, pp. 2898–2904.

[44] A. AL-Hourani et al. "Coverage and rate analysis of aerial base stations [Letter]". In: *IEEE Transactions on Aerospace and Electronic Systems* 52.6 (2016), pp. 3077–3081.

[45] M. Mozaffari et al. “Efficient Deployment of Multiple Unmanned Aerial Vehicles for Optimal Wireless Coverage”. In: *IEEE Communications Letters* 20.8 (2016), pp. 1647–1650. DOI: 10.1109/LCOMM.2016.2578312.

[46] David W Matolak and Ruoyu Sun. “Air–ground channel characterization for unmanned aircraft systems—Part I: Methods, measurements, and models for over-water settings”. In: *IEEE Transactions on Vehicular Technology* 66.1 (2016), pp. 26–44.

[47] Ruoyu Sun and David W Matolak. “Air–ground channel characterization for unmanned aircraft systems-Part II: Hilly and mountainous settings”. In: *IEEE Transactions on Vehicular Technology* 66.3 (2016), pp. 1913–1925.

[48] David W Matolak and Ruoyu Sun. “Air–ground channel characterization for unmanned aircraft systems—Part III: The suburban and near-urban environments”. In: *IEEE Transactions on Vehicular Technology* 66.8 (2017), pp. 6607–6618.

[49] W. G. Newhall and J. H. Reed. “A geometric air-to-ground radio channel model”. In: *MILCOM 2002. Proceedings*. Vol. 1. 2002, pp. 632–636.

[50] Michael Wentz and Milica Stojanovic. “A MIMO radio channel model for low-altitude air-to-ground communication systems”. In: *2015 IEEE 82nd Vehicular Technology Conference (VTC 2015 Fall)*. 2015, pp. 1–6.

[51] Mostafa Ibrahim and Huseyin Arslan. “Air-ground Doppler-delay spread spectrum for dense scattering environments”. In: *MILCOM 2015-2015 IEEE Military Communications Conference*. 2015, pp. 1661–1666.

[52] Sardar Muhammad Gulfam et al. “On the spatial characterization of 3-D air-to-ground radio communication channels”. In: *2015 IEEE International Conference on Communications (ICC)*. 2015, pp. 2924–2930.

[53] Linzhou Zeng et al. “A 3D geometry-based stochastic channel model for UAV-MIMO channels”. In: *2017 IEEE Wireless Communications and Networking Conference (WCNC)*. 2017, pp. 1–5.

[54] Vishnu Vardhan Chetlur and Harpreet S Dhillon. “Downlink coverage analysis for a finite 3-D wireless network of unmanned aerial vehicles”. In: *IEEE Transactions on Communications* 65.10 (2017), pp. 4543–4558.

[55] Abbas Mohammed et al. “The role of high-altitude platforms (HAPs) in the global wireless connectivity”. In: *Proceedings of the IEEE* 99.11 (2011), pp. 1939–1953.

[56] *Roadmap for the Integration of Civil Remotely-Piloted Aircraft Systems into the European Aviation System*. Tech. Rep. https://publicintelligence.net/eu-rpa-roadmap/.: EUROCONTROL, 2013.

[57] *Integration of Civil Unmanned Aircraft Systems (UAS) in the National Airspace System (NAS) Roadmap*. Tech. rep. http://www.faa.gov/uas/media/uas_roadmap_2013.pdf: US Department of Transportation Federal Aviation Authority, 2013.

[58] *Flying drones or model aircraft recreationally*. `https://www.casa.gov.au/modelaircraft`.

[59] *Flying in the open category*. `https://www.caa.co.uk/Consumers/Unmanned-aircraft/Recreational-drones/Flying-in-the-open-category/`.

[60] Matthias Holzbock and Christian Senninger. “An aeronautical multimedia service demonstration at high frequencies”. In: *IEEE MultiMedia* 6.4 (1999), pp. 20–29.

[61] Yee Hui Lee, Yu Song Meng, and Yew Heng Heng. “Experimental characterizations of an air to land channel over sea surface in C band”. In: *Proc. XXIXth URSI General Assembly* (2008).

[62] Yu Song Meng and Yee Hui Lee. “Study of shadowing effect by aircraft maneuvering for air-to-ground communication”. In: *AEU-International Journal of Electronics and Communications* 66.1 (2012), pp. 7–11.

[63] J Kunisch et al. “Wideband time-variant air-to-ground radio channel measurements at 5 GHz”. In: *Proceedings of the 5th European Conference on Antennas and Propagation (EUCAP)*. 2011, pp. 1386–1390.

[64] Ruoyu Sun, David W Matolak, and William Rayess. “Air-ground channel characterization for unmanned aircraft systems—Part IV: Airframe shadowing”. In: *IEEE Transactions on Vehicular Technology* 66.9 (2017), pp. 7643–7652.

[65] Jesse Chen, Babak Daneshrad, and Weijun Zhu. “MIMO performance evaluation for airborne wireless communication systems”. In: *MILCOM 2011 Military Communications Conference*. 2011, pp. 1827–1832.

[66] Michael Rice and Michael Jensen. “Multipath propagation for helicopter-to-ground MIMO links”. In: *MILCOM 2011 Military Communications Conference*. 2011, pp. 447–452.

[67] Michael Rice and Mohammad Saquib. “MIMO equalization for helicopter-to-ground communications”. In: *MILCOM 2011 Military Communications Conference*. 2011, pp. 501–506.

[68] Yi Jiang et al. “MIMO for airborne communications [Industry Perspectives]”. In: *IEEE Wireless Communications* 21.5 (2014), pp. 4–6.

[69] W Vergara, J Levatich, and T Carroll. “VHF air-ground propagation far beyond the horizon and tropospheric stability”. In: *IRE Transactions on Antennas and Propagation* 10.5 (1962), pp. 608–621.

[70] KENT Chamberlin. “The effect of tree cover on air-ground, VHF propagation path loss”. In: *IEEE transactions on communications* 34.9 (1986), pp. 958–962.

[71] JR Child. “Air-to-ground propagation at 900 MHz”. In: *35th IEEE Vehicular Technology Conference*. Vol. 35. 1985, pp. 73–80.

[72] Michael Rice, Ricky Dye, and Kenneth Welling. “Narrowband channel model for aeronautical telemetry”. In: *IEEE transactions on Aerospace and electronic systems* 36.4 (2000), pp. 1371–1376.

[73] William G Newhall et al. “Wideband air-to-ground radio channel measurements using an antenna array at 2 GHz for low-altitude operations”. In: *IEEE Military Communications Conference, 2003. MILCOM 2003.* Vol. 2. 2003, pp. 1422–1427.

[74] Michael Rice, Adam Davis, and Christian Bettweiser. “Wideband channel model for aeronautical telemetry”. In: *IEEE Transactions on aerospace and Electronic systems* 40.1 (2004), pp. 57–69.

[75] Michal Simunek, Fernando Pérez Fontán, and Pavel Pechac. “The UAV low elevation propagation channel in urban areas: Statistical analysis and time-series generator”. In: *IEEE Transactions on Antennas and Propagation* 61.7 (2013), pp. 3850–3858.

[76] Michal Simunek, Pavel Pechac, and Fernando P Fontán. “Excess loss model for low elevation links in urban areas for UAVs”. In: *Radio engineering* 20.3 (2011), pp. 561–568.

[77] Michal Simunek et al. “Space diversity gain in urban area low elevation links for surveillance applications”. In: *IEEE transactions on antennas and propagation* 61.12 (2013), pp. 6255–6260.

[78] Michal Simunek, Pavel Pechac, and Fernando P Fontan. “Feasibility of UAV link space diversity in wooded areas”. In: *International Journal of Antennas and Propagation* 2013 (2013).

[79] Xuesong Cai et al. “Low altitude UAV propagation channel modelling”. In: *2017 11th European Conference on Antennas and Propagation (EUCAP)*. 2017, pp. 1443–1447.

[80] Xiaokang Ye et al. “Air-to-ground big-data-assisted channel modeling based on passive sounding in LTE networks”. In: *2017 IEEE Globecom Workshops (GC Wkshps)*. 2017, pp. 1–6.

[81] Wahab Khawaja, Ismail Guvenc, and David Matolak. “UWB channel sounding and modeling for UAV air-to-ground propagation channels”. In: *2016 IEEE global communications conference (GLOBECOM)*. 2016, pp. 1–7.

[82] Zhi Yang et al. “Channel model in the urban environment for unmanned aerial vehicle communications”. In: *12th European Conference on Antennas and Propagation (EuCAP 2018)*. 2018, pp. 1–5.

[83] Richard M Gutierrez et al. “Time and frequency dispersion characteristics of the UAS wireless channel in residential and mountainous desert terrains”. In: *2017 14th IEEE Annual Consumer Communications & Networking Conference (CCNC)*. 2017, pp. 516–521.

[84] R. M. Gutierrez et al. “Comparison of UAS-to-Ground Small-Scale Fading in Residential and Mountainous Desert Terrains”. In: *IEEE Transactions on Vehicular Technology* 68.10 (2019), pp. 9348–9358.

[85] Eric W Frew and Timothy X Brown. “Airborne communication networks for small unmanned aircraft systems”. In: *Proceedings of the IEEE* 96.12 (2008).

[86] Niklas Goddemeier, Sebastian Rohde, and Christian Wietfeld. “Experimental validation of RSS driven UAV mobility behaviors in IEEE 802.11 s networks”. In: *2012 IEEE Globecom Workshops*. 2012, pp. 1550–1555.

[87] Evşen Yanmaz et al. “Experimental performance analysis of two-hop aerial 802.11 networks”. In: *2014 IEEE Wireless Communications and Networking Conference (WCNC)*. 2014, pp. 3118–3123.

[88] Samira Hayat, Evşen Yanmaz, and Christian Bettstetter. “Experimental analysis of multipoint-to-point UAV communications with IEEE 802.11 n and 802.11 ac”. In:

2015 IEEE 26th Annual International Symposium on Personal, Indoor, and Mobile Radio Communications (PIMRC). 2015, pp. 1991–1996.

[89] Jude Allred et al. “Sensorflock: an airborne wireless sensor network of micro-air vehicles”. In: *Proceedings of the 5th international conference on Embedded networked sensor systems*. 2007, pp. 117–129.

[90] Apratim Shaw and Kamran Mohseni. “A fluid dynamic based coordination of a wireless sensor network of unmanned aerial vehicles: 3-D simulation and wireless communication characterization”. In: *IEEE Sensors Journal* 11.3 (2010), pp. 722–736.

[91] Nadeem Ahmed, Salil S Kanhere, and Sanjay Jha. “On the importance of link characterization for aerial wireless sensor networks”. In: *IEEE Communications Magazine* 54.5 (2016), pp. 52–57.

[92] Niklas Goddemeier and Christian Wietfeld. “Investigation of air-to-air channel characteristics and a UAV specific extension to the rice model”. In: *2015 IEEE Globecom Workshops (GC Wkshps)*. 2015, pp. 1–5.

[93] Evşen Yanmaz, Robert Kuschnig, and Christian Bettstetter. “Channel measurements over 802.11 a-based UAV-to-ground links”. In: *2011 IEEE GLOBECOM Workshops (GC Wkshps)*. 2011, pp. 1280–1284.

[94] Evşen Yanmaz, Robert Kuschnig, and Christian Bettstetter. “Achieving air-ground communications in 802.11 networks with three-dimensional aerial mobility”. In: *2013 Proceedings IEEE INFOCOM*. 2013, pp. 120–124.

[95] Chen-Mou Cheng et al. “Performance measurement of 802.11 a wireless links from UAV to ground nodes with various antenna orientations”. In: *Proceedings of 15th International Conference on Computer Communications and Networks*. 2006, pp. 303–308.

[96] Dan Hague, HT Kung, and Bruce Suter. “Field experimentation of cots-based UAV networking”. In: *IEEE Military Communications Conference, 2006. MILCOM 2006*. 2006, pp. 1–7.

[97] Niklas Goddemeier, Kai Daniel, and Christian Wietfeld. “Coverage evaluation of wireless networks for unmanned aerial systems”. In: *2010 IEEE Globecom Workshops*. 2010, pp. 1760–1765.

[98] Tiago Tavares et al. “Generalized LUI propagation model for UAVs communications using terrestrial cellular networks”. In: *2015 IEEE 82nd Vehicular Technology Conference (VTC2015-Fall)*. IEEE. 2015, pp. 1–6.

[99] Rafhael Amorim et al. “Radio channel modeling for UAV communication over cellular networks”. In: *IEEE Wireless Communications Letters* 6.4 (2017), pp. 514–517.

[100] Akram Al-Hourani and Karina Gomez. “Modeling cellular-to-UAV path-loss for suburban environments”. In: *IEEE Wireless Communications Letters* 7.1 (2017), pp. 82–85.

[101] Ervin Teng, João Diogo Falcão, and Bob Iannucci. “Holes-in-the-Sky: A field study on cellular-connected UAS”. In: *2017 International Conference on Unmanned Aircraft Systems (ICUAS)*. 2017, pp. 1165–1174.

[102] M. D. Villaluz et al. “Preliminary 4.5G Cellular Network Assessment with Calibrated Standard Propagation Model (SPM) for uTM-UAS Operations in Singapore Airspace”. In: *2018 International Conference on Unmanned Aircraft Systems (ICUAS)*. 2018, pp. 796–805.

[103] X. Ye et al. “Air-to-Ground Big-Data-Assisted Channel Modeling Based on Passive Sounding in LTE Networks”. In: *2017 IEEE Globecom Workshops (GC Wkshps)*. 2017, pp. 1–6.

[104] T. Liu et al. “Measurement-Based Characterization and Modeling for Low-Altitude UAV Air-to-Air Channels”. In: *IEEE Access* 7 (2019), pp. 98832–98840.

[105] J. Rodríguez-Piñeiro et al. “Air-to-Ground Channel Characterization for Low-Height UAVs in Realistic Network Deployments”. In: *IEEE Transactions on Antennas and Propagation* 69.2 (2021), pp. 992–1006.

[106] Y. Shi et al. “Measurement-based characterization of LOS and NLOS drone-to-ground channels”. In: *2018 IEEE Wireless Communications and Networking Conference (WCNC)*. 2018, pp. 1–6.

[107] Seilendria A. Hadiwardoyo et al. “Experimental characterization of UAV-to-car communications”. In: *Computer Networks* 136 (2018), pp. 105–118.

[108] G. Zhang et al. “A USRP-Based Channel Sounder for UAV Communications”. In: *2020 14th European Conference on Antennas and Propagation (EuCAP)*. 2020, pp. 1–4.

[109] H. Zeyu et al. “Empirical Dynamic Modeling for Low-Altitude UAV Propagation Channels”. In: *IEEE Transactions on Wireless Communications* (2021).

[110] HT Kung et al. “Measuring diversity on a low-altitude UAV in a ground-to-air wireless 802.11 mesh network”. In: *2010 IEEE Globecom Workshops*. IEEE. 2010, pp. 1799–1804.

[111] Tricia J Willink et al. “Measurement and characterization of low-altitude air-to-ground MIMO channels”. In: *IEEE Transactions on Vehicular Technology* 65.4 (2015), pp. 2637–2648.

[112] David W Matolak. “Air-ground channels & models: Comprehensive review and considerations for unmanned aircraft systems”. In: *2012 IEEE aerospace conference*. IEEE. 2012, pp. 1–17.

[113] Luis Afonso et al. “Cellular for the skies: Exploiting mobile network infrastructure for low altitude air-to-ground communications”. In: *IEEE Aerospace and Electronic Systems Magazine* 31.8 (2016), pp. 4–11.

[114] Irem Bor-Yaliniz and Halim Yanikomeroglu. “The New Frontier in RAN Heterogeneity: Multi-Tier Drone-Cells”. In: *IEEE Communications Magazine* 54.11 (2016), pp. 48–55.

[115] Asaad Kaadan, Hazem H. Refai, and Peter G. LoPresti. “Multielement FSO Transceivers Alignment for Inter-UAV Communications”. In: *Journal of Lightwave Technology* 32.24 (2014), pp. 4785–4795.

[116] Zhenyu Xiao, Pengfei Xia, and Xiang-gen Xia. “Enabling UAV cellular with millimeter-wave communication: potentials and approaches”. In: *IEEE Communications Magazine* 54.5 (2016), pp. 66–73. DOI: 10.1109/MCOM.2016.7470937.

[117] Ibrahim Y. Abualhaol and Mustafa M. Matalgah. “Performance analysis of multi-carrier relay-based UAV network over fading channels”. In: *2010 IEEE Globecom Workshops*. 2010, pp. 1811–1815.

[118] Feng Jiang and A. Lee Swindlehurst. “Optimization of UAV Heading for the Ground-to-Air Uplink”. In: *IEEE Journal on Selected Areas in Communications* 30.5 (2012), pp. 993–1005.

[119] Yifeng Zhou et al. “Modeling of packet dropout for UAV wireless communications”. In: *2012 International Conference on Computing, Networking and Communications (ICNC)*. 2012, pp. 677–682.

[120] Indranil Sen and David W. Matolak. “Vehicle–Vehicle Channel Models for the 5-GHz Band”. In: *IEEE Transactions on Intelligent Transportation Systems* 9.2 (2008), pp. 235–245.

[121] James J Jong Hyuk Park et al. *Multimedia and ubiquitous Engineering*. Vol. 308. Springer Science & Business, 2014.

[122] Irem Bor-Yaliniz, Sebastian S. Szyszkowicz, and Halim Yanikomeroglu. “Environment-Aware Drone-Base-Station Placements in Modern Metropolitans”. In: *IEEE Wireless Communications Letters* 7.3 (2018), pp. 372–375.

[123] Ali Mohammad Hayajneh et al. “Optimal Dimensioning and Performance Analysis of Drone-Based Wireless Communications”. In: *2016 IEEE Globecom Workshops (GC Wkshps)*. 2016, pp. 1–6.

[124] Mohamed Alzenad et al. “3-D Placement of an Unmanned Aerial Vehicle Base Station (UAV-BS) for Energy-Efficient Maximal Coverage”. In: *IEEE Wireless Communications Letters* 6.4 (2017), pp. 434–437.

[125] Mohammad Mozaffari et al. “Optimal transport theory for power-efficient deployment of unmanned aerial vehicles”. In: *2016 IEEE International Conference on Communications (ICC)*. 2016, pp. 1–6.

[126] Jiaxun Lu et al. “Energy-Efficient 3D UAV-BS Placement versus Mobile Users Density and Circuit Power”. In: *2017 IEEE Globecom Workshops (GC Wkshps)*. 2017, pp. 1–6.

[127] Mohammad Mozaffari et al. “Drone Small Cells in the Clouds: Design, Deployment and Performance Analysis”. In: *2015 IEEE Global Communications Conference (GLOBECOM)*. 2015, pp. 1–6.

[128] Mohammad Mozaffari et al. “Optimal Transport Theory for Cell Association in UAV-Enabled Cellular Networks”. In: *IEEE Communications Letters* 21.9 (2017), pp. 2053–2056.

[129] Mohammad Mozaffari et al. “Wireless Communication Using Unmanned Aerial Vehicles (UAVs): Optimal Transport Theory for Hover Time Optimization”. In: *IEEE Transactions on Wireless Communications* 16.12 (2017), pp. 8052–8066.

[130] Yunfei Chen, Wei Feng, and Gan Zheng. “Optimum Placement of UAV as Relays”. In: *IEEE Communications Letters* 22.2 (2018), pp. 248–251.

[131] R. Irem Bor-Yaliniz, Amr El-Keyi, and Halim Yanikomeroglu. “Efficient 3-D placement of an aerial base station in next generation cellular networks”. In: *2016 IEEE International Conference on Communications (ICC)*. 2016, pp. 1–5.

[132] Mingzhe Chen et al. “Caching in the Sky: Proactive Deployment of Cache-Enabled Unmanned Aerial Vehicles for Optimized Quality-of-Experience”. In: *IEEE Journal on Selected Areas in Communications* 35.5 (2017), pp. 1046–1061. DOI: 10.1109/JSAC.2017.2680898.

[133] Yong Zeng, Rui Zhang, and Teng Joon Lim. “Wireless communications with unmanned aerial vehicles: opportunities and challenges”. In: *IEEE Communications Magazine* 54.5 (2016), pp. 36–42.

[134] John David Parsons. *The mobile radio propagation channel*. Wiley, 2000.

[135] S.M. Elnoubi. “A simplified stochastic model for the aeronautical mobile radio channel”. In: *[1992 Proceedings] Vehicular Technology Society 42nd VTS Conference - Frontiers of Technology*. 1992, 960–963 vol.2. DOI: 10.1109/VETEC.1992.245268.

[136] Mohammad Asif Zaman et al. “Modeling VHF air-to-ground multipath propagation channel and analyzing channel characteristics and BER performance”. In: *2010 IEEE Region 8 International Conference on Computational Technologies in Electrical and Electronics Engineering (SIBIRCON)*. 2010, pp. 335–338.

[137] Yang Ding et al. “A time-varying transition channel model for air-ground communication”. In: *2017 IEEE/AIAA 36th Digital Avionics Systems Conference (DASC)*. 2017, pp. 1–8.

[138] Steve Blandino, Florian Kaltenberger, and Michael Feilen. “Wireless Channel Simulator Testbed for Airborne Receivers”. In: *2015 IEEE Globecom Workshops (GC Wkshps)*. 2015, pp. 1–6. DOI: 10.1109/GLOCOMW.2015.7413991.

[139] Xijun Gao, Zili Chen, and Yongjiang Hu. “Analysis of unmanned aerial vehicle MIMO channel capacity based on aircraft attitude”. In: *WSEAS Transactions on Information Science and Applications* 10.2 (2013), pp. 58–67.

[140] Faraj Lagum, Irem Bor-Yaliniz, and Halim Yanikomeroglu. “Strategic Densification With UAV-BSs in Cellular Networks”. In: *IEEE Wireless Communications Letters* 7.3 (2018), pp. 384–387.

[141] Mohammad Mozaffari et al. “Unmanned Aerial Vehicle With Underlaid Device-to-Device Communications: Performance and Tradeoffs”. In: *IEEE Transactions on Wireless Communications* 15.6 (2016), pp. 3949–3963.

[142] Bertold Van Der Bergh, Alessandro Chiumento, and Sofie Pollin. “LTE in the sky: trading off propagation benefits with interference costs for aerial nodes”. In: *IEEE Communications Magazine* 54.5 (2016), pp. 44–50.

[143] Wahab Khawaja, Ozgur Ozdemir, and Ismail Guvenc. “UAV Air-to-Ground Channel Characterization for mmWave Systems”. In: *2017 IEEE 86th Vehicular Technology Conference (VTC-Fall)*. 2017, pp. 1–5.

[144] Tryphon T Georgiou. “Distances and Riemannian metrics for spectral density functions”. In: *IEEE Transactions on Signal Processing* 55.8 (2007), pp. 3995–4003.

[145] Tricia J. Willink. “Wide-Sense Stationarity of Mobile MIMO Radio Channels”. In: *IEEE Transactions on Vehicular Technology* 57.2 (2008), pp. 704–714.

[146] Mohammad Mahdi Azari et al. “Optimal UAV Positioning for Terrestrial-Aerial Communication in Presence of Fading”. In: *2016 IEEE Global Communications Conference (GLOBECOM)*. 2016, pp. 1–7.

[147] Mohamed Alzenad, Amr El-Keyi, and Halim Yanikomeroglu. “3-D Placement of an Unmanned Aerial Vehicle Base Station for Maximum Coverage of Users With Different QoS Requirements”. In: *IEEE Wireless Communications Letters* 7.1 (2018), pp. 38–41.

[148] Jiangbin Lyu et al. “Placement Optimization of UAV-Mounted Mobile Base Stations”. In: *IEEE Communications Letters* 21.3 (2017), pp. 604–607.

[149] Mohammad Mozaffari et al. “Mobile Internet of Things: Can UAVs Provide an Energy-Efficient Mobile Architecture?” In: *2016 IEEE Global Communications Conference (GLOBECOM)*. 2016, pp. 1–6.

[150] Sidharth Kumar, Suraj Suman, and Swades De. “Backhaul and delay-aware placement of UAV-enabled base station”. In: *IEEE INFOCOM 2018 - IEEE Conference on Computer Communications Workshops (INFOCOM WKSHPS)*. 2018, pp. 634–639.

[151] Markus Gruber. “Role of altitude when exploring optimal placement of UAV access points”. In: *2016 IEEE Wireless Communications and Networking Conference*. 2016, pp. 1–5.

[152] Wei Feng et al. “When mmWave Communications Meet Network Densification: A Scalable Interference Coordination Perspective”. In: *IEEE Journal on Selected Areas in Communications* 35.7 (2017), pp. 1459–1471.

[153] Istvan Kovacs et al. “Interference Analysis for UAV Connectivity over LTE Using Aerial Radio Measurements”. In: *2017 IEEE 86th Vehicular Technology Conference (VTC-Fall)*. 2017, pp. 1–6.

[154] Sebastian Rohde and Christian Wietfeld. “Interference Aware Positioning of Aerial Relays for Cell Overload and Outage Compensation”. In: *2012 IEEE Vehicular Technology Conference (VTC Fall)*. 2012, pp. 1–5.

[155] Daniele Giovanni Cileo, Navuday Sharma, and Maurizio Magarini. “Coverage, capacity and interference analysis for an aerial base station in different environments”. In: *2017 International Symposium on Wireless Communication Systems (ISWCS)*. 2017, pp. 281–286.

[156] Nan Zhao et al. “Caching UAV Assisted Secure Transmission in Hyper-Dense Networks Based on Interference Alignment”. In: *IEEE Transactions on Communications* 66.5 (2018), pp. 2281–2294.

[157] Jingcong Sun and Christos Masouros. “Deployment Strategies of Multiple Aerial BSs for User Coverage and Power Efficiency Maximization”. In: *IEEE Transactions on Communications* 67.4 (2019), pp. 2981–2994.

[158] Qingqing Wu, Yong Zeng, and Rui Zhang. “Joint Trajectory and Communication Design for Multi-UAV Enabled Wireless Networks”. In: *IEEE Transactions on Wireless Communications* 17.3 (2018), pp. 2109–2121.

[159] Mohammad Mahdi Azari et al. “Coverage maximization for a poisson field of drone cells”. In: *2017 IEEE 28th Annual International Symposium on Personal, Indoor, and Mobile Radio Communications (PIMRC)*. 2017, pp. 1–6.

[160] Liang Liu, Shuowen Zhang, and Rui Zhang. “Cooperative Interference Cancellation for Multi-Beam UAV Uplink Communication: A DoF Analysis”. In: *2018 IEEE Globecom Workshops (GC Wkshps)*. 2018, pp. 1–6.

[161] Nan Zhao et al. “Communications, caching, and computing oriented small cell networks with interference alignment”. In: *IEEE Communications Magazine* 54.9 (2016), pp. 29–35.

[162] Fen Cheng et al. “Power Allocation for Cache-Aided Small-Cell Networks With Limited Backhaul”. In: *IEEE Access* 5 (2017), pp. 1272–1283.

[163] Liang Liu, Shuowen Zhang, and Rui Zhang. “CoMP in the Sky: UAV Placement and Movement Optimization for Multi-User Communications”. In: *IEEE Transactions on Communications* 67.8 (2019), pp. 5645–5658.

[164] Ralf Irmer et al. “Coordinated multipoint: Concepts, performance, and field trial results”. In: *IEEE Communications Magazine* 49.2 (2011), pp. 102–111.

[165] Ursula Challita, Walid Saad, and Christian Bettstetter. “Interference Management for Cellular-Connected UAVs: A Deep Reinforcement Learning Approach”. In: *IEEE Transactions on Wireless Communications* 18.4 (2019), pp. 2125–2140.

[166] Weidong Mei and Rui Zhang. “Uplink Cooperative NOMA for Cellular-Connected UAV”. In: *IEEE Journal of Selected Topics in Signal Processing* 13.3 (2019), pp. 644–656.

[167] Wei Feng et al. “UAV-Aided MIMO Communications for 5G Internet of Things”. In: *IEEE Internet of Things Journal* 6.2 (2019), pp. 1731–1740.

[168] M. Mahdi Azari, Fernando Rosas, and Sofie Pollin. “Cellular Connectivity for UAVs: Network Modeling, Performance Analysis, and Design Guidelines”. In: *IEEE Transactions on Wireless Communications* 18.7 (2019), pp. 3366–3381.

[169] Shaohui Sun et al. “Interference management through CoMP in 3GPP LTE-advanced networks”. In: *IEEE Wireless Communications* 20.1 (2013), pp. 59–66.

[170] Kannan Govindan, Kai Zeng, and Prasant Mohapatra. “Probability Density of the Received Power in Mobile Networks”. In: *IEEE Transactions on Wireless Communications* 10.11 (2011), pp. 3613–3619.

[171] Tracy Camp, Jeff Boleng, and Vanessa Davies. “A survey of mobility models for ad hoc network research”. In: *Wireless communications and mobile computing* 2.5 (2002), pp. 483–502.

[172] E. Hyytia, P. Lassila, and J. Virtamo. “Spatial node distribution of the random waypoint mobility model with applications”. In: *IEEE Transactions on Mobile Computing* 5.6 (2006), pp. 680–694.

[173] Jie Tang et al. “Impact of Mobility on Physical Layer Security Over Wireless Fading Channels”. In: *IEEE Transactions on Wireless Communications* 17.12 (2018), pp. 7849–7864.

[174] Ning Cao, Yunfei Chen, and Zhutian Yang. “Secrecy Outage Probability With Randomly Moving Interferers in Nakagami- m Fading”. In: *IEEE Communications Letters* 23.1 (2019), pp. 76–79.

[175] Pankaj K. Sharma and Dong In Kim. “Coverage Probability of 3-D Mobile UAV Networks”. In: *IEEE Wireless Communications Letters* 8.1 (2019), pp. 97–100.

[176] Hazem Sallouha, Mohammad Mahdi Azari, and Sofie Pollin. “Energy-Constrained UAV Trajectory Design for Ground Node Localization”. In: *2018 IEEE Global Communications Conference (GLOBECOM)*. 2018, pp. 1–7.

[177] Theodore S Rappaport et al. *Wireless communications: principles and practice*. Vol. 2. prentice hall PTR New Jersey, 1996.

[178] Izrail Solomonovich Gradshteyn and Iosif Moiseevich Ryzhik. *Table of integrals, series, and products*. Academic press, 2014.

[179] Marvin K Simon and Mohamed-Slim Alouini. *Digital communication over fading channels*. Vol. 95. John Wiley & Sons, 2005.

[180] Xiaohu Ge et al. “5G wireless backhaul networks: challenges and research advances”. In: *IEEE Network* 28.6 (2014), pp. 6–11.

[181] Karthikeyan Shanmugam et al. “FemtoCaching: Wireless Content Delivery Through Distributed Caching Helpers”. In: *IEEE Transactions on Information Theory* 59.12 (2013), pp. 8402–8413.

[182] Negin Golrezaei et al. “Femtocaching and device-to-device collaboration: A new architecture for wireless video distribution”. In: *IEEE Communications Magazine* 51.4 (2013), pp. 142–149.

[183] Tony Q. S. Quek, Wang Chi Cheung, and Marios Kountouris. “Energy Efficiency Analysis of Two-Tier Heterogeneous Networks”. In: *17th European Wireless 2011 - Sustainable Wireless Technologies*. 2011, pp. 1–5.

[184] Aziz A. Khuwaja et al. “Optimum Deployment of Multiple UAVs for Coverage Area Maximization in the Presence of Co-Channel Interference”. In: *IEEE Access* 7 (2019), pp. 85203–85212.

[185] Chiya Zhang and Wei Zhang. “Spectrum Sharing in Drone Small Cells”. In: *2016 IEEE Global Communications Conference (GLOBECOM)*. 2016, pp. 1–6.

[186] Lin Qi, Shi Yan, and Mugen Peng. “Modeling and Performance Analysis in UAV Assisted Ultra Dense Networks”. In: *2018 IEEE International Conference on Communications Workshops (ICC Workshops)*. 2018, pp. 1–6.

[187] Huici Wu et al. “Cooperative UAV Cluster-Assisted Terrestrial Cellular Networks for Ubiquitous Coverage”. In: *IEEE Journal on Selected Areas in Communications* 36.9 (2018), pp. 2045–2058.

[188] Esma Turgut and M. Cenk Gursoy. “Downlink Analysis in Unmanned Aerial Vehicle (UAV) Assisted Cellular Networks With Clustered Users”. In: *IEEE Access* 6 (2018), pp. 36313–36324.

[189] Dongsun Kim, Jemin Lee, and Tony Q. S. Quek. “Multi-layer Unmanned Aerial Vehicle Networks: Modeling and Performance Analysis”. In: *IEEE Transactions on Wireless Communications* 19.1 (2020), pp. 325–339.

[190] Xiaosheng Lin, Junjuan Xia, and Zhi Wang. “Probabilistic Caching Placement in UAV-assisted Heterogeneous Wireless Networks”. In: *Physical Communication* 33 (2019), pp. 54–61.

[191] Ramy Amer et al. “Caching to the Sky: Performance Analysis of Cache-Assisted CoMP for Cellular-Connected UAVs”. In: *2019 IEEE Wireless Communications and Networking Conference (WCNC)*. 2019, pp. 1–6.

[192] M. G. Khoshkholgh et al. “Randomized Caching in Cooperative UAV-Enabled Fog-RAN”. In: *2019 IEEE Wireless Communications and Networking Conference (WCNC)*. 2019, pp. 1–6.

[193] Fasheng Zhou et al. “Edge Caching in Multi-UAV-Enabled Radio Access Networks: 3D Modeling and Spectral Efficiency Optimization”. In: *IEEE Transactions on Signal and Information Processing over Networks* 6 (2020), pp. 329–341.

[194] Juan Wen et al. “Cache-Enabled Heterogeneous Cellular Networks: Optimal Tier-Level Content Placement”. In: *IEEE Transactions on Wireless Communications* 16.9 (2017), pp. 5939–5952.

[195] Zheng Chen et al. “Cooperative Caching and Transmission Design in Cluster-Centric Small Cell Networks”. In: *IEEE Transactions on Wireless Communications* 16.5 (2017), pp. 3401–3415.

[196] Gan Zheng, Himal A. Suraweera, and Ioannis Krikidis. “Optimization of Hybrid Cache Placement for Collaborative Relaying”. In: *IEEE Communications Letters* 21.2 (2017), pp. 442–445.

[197] Cheng Zhan and Guo Yao. “SVC Video Delivery in Cache-Enabled Wireless Het-Net”. In: *IEEE Systems Journal* 12.4 (2018), pp. 3885–3888.

[198] Yongxu Zhu et al. “Content Placement in Cache-Enabled Sub-6 GHz and Millimeter-Wave Multi-Antenna Dense Small Cell Networks”. In: *IEEE Transactions on Wireless Communications* 17.5 (2018), pp. 2843–2856.

[199] Rui Wang et al. “Performance Analysis and Optimization of Caching Placement in Heterogeneous Wireless Networks”. In: *IEEE Communications Letters* 23.10 (2019), pp. 1883–1887.

[200] Leila Enamipour, Zolfa Zeinalpour-Yazdi, and Babak Hossein Khalaj. “Performance Analysis of Cache-Enabled Wireless Networks Considering Stochastic Geometry Approach”. In: *IET Communications* 13.8 (2019), pp. 1043–1050.

[201] Adrian Baddeley, Imre Bárány, and Rolf Schneider. “Spatial point processes and their applications”. In: *Lecture Notes in Mathematics: Stochastic Geometry* (2007), pp. 1–75.

[202] Sung Nok Chiu et al. *Stochastic geometry and its applications*. John Wiley & Sons, 2013.

[203] Shubin Zhang, Wen Sun, and Jiajia Liu. “An Optimized Spatially Cooperative Caching Strategy for Heterogeneous Caching Network”. In: *2019 15th International Wireless Communications Mobile Computing Conference (IWCMC)*. 2019, pp. 1685–1689.

[204] Tiankui Zhang et al. “Cache Space Efficient Caching Scheme for Content-Centric Mobile Ad Hoc Networks”. In: *IEEE Systems Journal* 13.1 (2019), pp. 530–541.

[205] Martin Haenggi. *Stochastic Geometry for Wireless Networks*. Cambridge University Press, 2012.

[206] Seong Ho Chae and Wan Choi. “Caching Placement in Stochastic Wireless Caching Helper Networks: Channel Selection Diversity via Caching”. In: *IEEE Transactions on Wireless Communications* 15.10 (2016), pp. 6626–6637.

[207] Ying Cui, Dongdong Jiang, and Yueping Wu. “Analysis and Optimization of Caching and Multicasting in Large-Scale Cache-Enabled Wireless Networks”. In: *IEEE Transactions on Wireless Communications* 15.7 (2016), pp. 5101–5112.

[208] Ying Cui and Dongdong Jiang. “Analysis and Optimization of Caching and Multicasting in Large-Scale Cache-Enabled Heterogeneous Wireless Networks”. In: *IEEE Transactions on Wireless Communications* 16.1 (2017), pp. 250–264.

[209] Jeffrey G Andrews, Abhishek K Gupta, and Harpreet S Dhillon. “A primer on cellular network analysis using stochastic geometry”. In: *arXiv preprint arXiv:1604.03183* (2016).

[210] Yong Sheng Soh et al. “Energy Efficient Heterogeneous Cellular Networks”. In: *IEEE Journal on Selected Areas in Communications* 31.5 (2013), pp. 840–850.

[211] Hakim Ghazzai et al. “Energy-Efficient Management of Unmanned Aerial Vehicles for Underlay Cognitive Radio Systems”. In: *IEEE Transactions on Green Communications and Networking* 1.4 (2017), pp. 434–443.

[212] Gunther Auer et al. “How much energy is needed to run a wireless network?” In: *IEEE Wireless Communications* 18.5 (2011), pp. 40–49.

[213] L. Breslau et al. “Web caching and Zipf-like distributions: evidence and implications”. In: *IEEE INFOCOM ’99. Conference on Computer Communications. Proceedings. Eighteenth Annual Joint Conference of the IEEE Computer and Communications Societies. The Future is Now (Cat. No.99CH36320)*. Vol. 1. 1999, 126–134 vol.1.

[214] I. Valiulahi and C. Masouros. “Multi-UAV Deployment for Throughput Maximization in the Presence of Co-Channel Interference”. In: *IEEE Internet of Things Journal* (2020), pp. 1–1.

[215] N. Zhao et al. “Joint Trajectory and Precoding Optimization for UAV-Assisted NOMA Networks”. In: *IEEE Transactions on Communications* 67.5 (2019), pp. 3723–3735.

[216] Y. Zeng, R. Zhang, and T. J. Lim. “Throughput Maximization for UAV-Enabled Mobile Relaying Systems”. In: *IEEE Transactions on Communications* 64.12 (2016), pp. 4983–4996.

[217] Y. Zeng and R. Zhang. “Energy-Efficient UAV Communication With Trajectory Optimization”. In: *IEEE Transactions on Wireless Communications* 16.6 (2017), pp. 3747–3760.

[218] Z. Yang et al. “Energy Efficient Resource Allocation in UAV-Enabled Mobile Edge Computing Networks”. In: *IEEE Transactions on Wireless Communications* 18.9 (2019), pp. 4576–4589.

[219] Xiaofang Sun et al. “Physical Layer Security in UAV Systems: Challenges and Opportunities”. In: *IEEE Wireless Communications* 26.5 (2019), pp. 40–47.

[220] Sixian Li et al. “Reconfigurable Intelligent Surface Assisted UAV Communication: Joint Trajectory Design and Passive Beamforming”. In: *IEEE Wireless Communications Letters* 9.5 (2020), pp. 716–720.

[221] Junfeng Guan et al. “3D Imaging using mmWave 5G Signals”. In: *2020 IEEE Radio Frequency Integrated Circuits Symposium (RFIC)*. 2020, pp. 147–150.

[222] Daniyal Haider, Xiaodong Yang, and Qammer Hussain Abbasi. “Post-surgical fall detection by exploiting the 5 G C-Band technology for eHealth paradigm”. In: *Applied Soft Computing* 81 (2019), p. 105537.

[223] Bahareh Gholampooryazdi and Stephan Sigg. “Walking speed recognition from 5G Prototype System”. In: *2017 IEEE International Conference on Pervasive Computing and Communications Workshops (PerCom Workshops)*. 2017, pp. 34–37.

[224] Xiaodong Yang et al. “5G-Based User-Centric Sensing at C-Band”. In: *IEEE Transactions on Industrial Informatics* 15.5 (2019), pp. 3040–3047.

[225] Hyowon Kim et al. “5G mmWave Vehicular Tracking”. In: *2018 52nd Asilomar Conference on Signals, Systems, and Computers*. 2018, pp. 541–547.